LANTHANUM DOPED DICALCIUM PHOSPHATE MIXED WITH
GRAPHENE OXIDE BONE CEMENTS AS A POTENTIAL MATERIAL IN
BIOMEDICAL APPLICATIONS

A THESIS SUBMITTED TO
THE GRADUATE SCHOOL OF NATURAL AND APPLIED SCIENCES
OF
MIDDLE EAST TECHNICAL UNIVERSITY

BY

ALI MOTAMENİ

IN PARTIAL FULFILLMENT OF THE REQUIREMENTS
FOR
THE DEGREE OF DOCTOR OF PHILOSOPHY
IN
ENGINEERING SCIENCES

SEPTEMBER 2021

Approval of the thesis:

**LANTHANUM DOPED DICALCIUM PHOSPHATE MIXED WITH GRAPHENE OXIDE BONE CEMENTS AS A POTENTIAL MATERIAL IN BIOMEDICAL APPLICATIONS**

submitted by **ALİ MOTAMENİ** in partial fulfillment of the requirements for the degree of **Doctor of Philosophy** in **Engineering Sciences, Middle East Technical University** by,

Prof. Dr. Halil Kalıpçılar
Dean, Graduate School of **Natural and Applied Sciences**       _____

Prof. Dr. Murat Dicleli
Head of the Department, **Engineering Sciences**       _____

Prof. Dr. Zafer Evis
Supervisor, **Engineering Sciences, METU**       _____


**Examining Committee Members:**

Prof. Dr. Dilek Keskin
Engineering Sciences, METU       _____

Prof. Dr. Zafer Evis
Engineering Sciences, METU       _____

Prof. Dr. Volkan Şahin
Faculty of Dentistry, Kırıkkale Uni.       _____

Assoc. Prof. Dr. Fatih Akkurt
Chemical Eng., Gazi Uni.       _____

Assist. Prof. Dr. Ammar Zeidan Ghailan Alshemary
Biomedical Eng., Karabük Uni.       _____

Date: 06.09.2021

**I hereby declare that all information in this document has been obtained and presented in accordance with academic rules and ethical conduct. I also declare that, as required by these rules and conduct, I have fully cited and referenced all material and results that are not original to this work.**

Name Last name : Ali Motameni

Signature :

# ABSTRACT

## LANTHANUM DOPED DICALCIUM PHOSPHATE MIXED WITH GRAPHENE OXIDE BONE CEMENTS AS A POTENTIAL MATERIAL IN BIOMEDICAL APPLICATIONS

Motameni, Ali

Doctor of Philosophy, Engineering Sciences

Supervisor : Prof. Dr. Zafer Evis

September 2021, 136 pages

In this thesis, mesoporous particles of β-tricalcium phosphate (βTCP, $\beta Ca_3(PO_4)_2$) and lanthanum (La) doped βTCP were synthesized by wet precipitation method attached with a microwave refluxing system. Pure dicalcium phosphate (DCP) and La modified dicalcium phosphate (La-DCP) bone cements were prepared based on acid/base reaction between βTCP (or La- βTCP) and monocalcium phosphate monohydrate (MCPM) in the presence of water. DCP bone cements were also mixed with 1.5-3.5wt.% of graphene oxide (GO). The obtained materials were characterized by XRD, FTIR, SEM, ICP-OES, BET, and helium pycnometer. The loading /releasing analysis of proteins on/from βTCP and La- βTCP disks surfaces were evaluated using Fetal bovine serum (FBS) proteins. *In vitro* cell culture studies were performed with the human osteosarcoma cell line (Saos-2). Upon incorporating $La^{3+}$ ions, expansion in lattice parameters of βTCP crystal was observed along with inhibition of growth rate. βTCP and La- βTCP materials were mesoporous in nature. Pore diameter and pore volume were expanded with the incorporation of $La^{3+}$ ions. The outcomes confirmed that all La-βTCP materials were cytocompatible, and strict

dose dependent effect of $La^{3+}$ ions was observed on cell viability and alkaline phosphatase (ALP) activity.

In DCP bone cements, the pure phase of brushite transformed into monetite with minimum addition of $La^{3+}$ ions (0.090 mole), and the plate-like crystals of brushite turned into spheroid particles. The results of *in vitro* experiments on proliferation, adhesion, and osteogenic differentiation of Saos-2 cells indicated that the addition of 0.225 mole of $La^{3+}$ ions promoted these properties compared to pure DCP. With the addition of GO to DCP bone cements, the mechanical properties of 2La-DCP cements improved. As the GO/2La-DCP bone cements were biocompatible, proliferation and differentiation properties of cells were significantly improved with the addition of GO.

# ÖZ

## KEMİK HATALARINDA DOLGU OLARAK POTANSİYEL KULLANIM İÇİN GRAFEN OKSİT / LANTHANUM KATKILI KALSİYUM FOSFAT KEMİK ÇİMENTOLARI

Motameni, Ali

Doktora, Mühendislik Bilimleri

Tez Yöneticisi: Prof. Dr. Zafer Evis

Eylül 2021, 136 sayfa

Bu tezde, β-trikalsiyum fosfat (βTCP, $\beta Ca_3(PO_4)_2$) ve lantan (La) doplanmış βTCP'nin partikülleri ıslak çöktürme yöntemi ile mikrodalga geri akış sistemini kullanarak sentezlenmiştir. Saf dikalsiyum fosfat (DCP) ve La modifiye dikalsiyum fosfat (La-DCP) kemik çimentoları, su varlığında βTCP (veya La- TCP) ile monokalsiyum fosfat monohidrat (MCPM) arasındaki asit / baz reaksiyonuna dayanarak hazırlandı. DCP kemik çimentoları ayrıca ağırlıkça% 1.5-3.5 GO ile karıştırılmıştır. Elde edilen malzemeler XRD, FTIR, SEM, ICP-OES, BET ve helyum piknometre kullanılarak karakterize edildi. βTCP ve La- βTCP partikül yüzeyleri üzerindeki yükleme/salım Fetal sığır serumu (FBS) proteinleri kullanılarak değerlendirilmiştir. Hücre kültürü çalışmaları, insan osteosarkom hücre hattı (Saos-2) ile gerçekleştirildi. $La^{+3}$ iyonlarının dahil edilmesiyle, βTCP kristalinin kafes parametrelerinde ilgili genişleme, inhibisyon büyüme oranı ile birlikte gözlendi. βTCP ve La- βTCP malzemeleri mezoporlu yapıdalar, gözenek çapı ve gözenek hacmi $La^{+3}$ iyonlarının eklenmesiyle genişletildi. Sonuçlar, tüm La-βTCP materyallerinin hücre uyumlu olduğunu onayladı ve $La^{+3}$ iyonlarının hücre canlılığı

ve alkalin fosfataz (ALP) aktivitesi üzerinde katı doza bağlı etkisi gözlendi. DCP kemik çimentolarında, minimum $La^{+3}$ iyonları (0.090 mol) ilavesiyle, bruşitin fazı monetite dönüştü ve bruşitin plaka benzeri kristalleri sferoid parçacıklara dönüştü. Saos-2 hücrelerinin proliferasyonu, adhezyonu ve osteojenik farklılaşması üzerine deneyler, saf DCP'ye kıyasla 0.225 mol $La^{+3}$ iyonu eklemenin bu özellikleri desteklediğini gösterdi. DCP kemik çimentolarına GO ilavesiyle, 2La-DCP çimentoların mekanik özellikleri GO ilavesiyle iyileştirilmiştir. GO/2La-DCP kemik çimentoları biyouyumluydu, hücrelerin proliferasyon ve farklılaşma özellikleri GO ilavesiyle önemli ölçüde iyileştirilmiştir.


**Anahtar Kelimeler:** β-trikalsiyum fosfat, Lantan, Dikalsiyum Fosfat, Grafen Oksit

To my father and son

# ACKNOWLEDMENTS

# TABLE OF CONTENTS

# LIST OF TABLES

## LIST OF FIGURES

**FIGURES**

# LIST OF ABBREVIATIONS

ABBREVIATIONS

| | | |
|---|---|---|
| AA | : | Ascorbic Acid |
| ALP | : | Alkaline Phosphatase Activity |
| ASTM | : | American Society for Testing and Materials |
| BCA | : | Bicinchoninic Acid |
| BET | : | Brunauer, Emmett and Teller |
| BHA | : | Biogenic Hydroxyapatite |
| BMP | : | Bone Morphogenetic Protein |
| BSA | : | Bovine Serum Albumin |
| C12E8 | : | Polyoxyethylene-8-Dodecyl Ether |
| CLSM | : | Confocal Laser Scanning Microscopy |
| CNT | : | Carbon Nanotube |
| CPs | : | Calcium Phosphates |
| CPCs | : | Calcium Phosphate Cements |
| CSD | : | Calcium Sulphate Dehydrate |
| CSH | : | Calcium Sulphate Hemihydrate |
| CTAB | : | Cetyltrimethylammonium Bromide |
| DAPI | : | 4′,6-diamidino-2-phenylindole |
| DCP | : | Dicalcium Phosphate |
| DCPA | : | Dicalcium Phosphate Anhydrous |
| DCPD | : | Dicalcium Phosphate Dihydrate |
| DMEM | : | Dulbecco's Modified Eagle's Medium |
| DMF | : | N,N-Dimethylformamide |
| EG | : | Ethylene Glycol |
| FBS | : | Fetal Bovine Serum |
| FDA | : | American Food and Drug Administration |
| FTIR | : | Fourier Transform Infrared Spectroscopy |
| GO | : | Graphene Oxide |

GO/ La- DCP : Graphene Oxide Reinforced La Doped Dicalcium Phosphate Cements

HA : Hydroxyapatite

ICP-OES : Inductively Coupled Plasma-Optical Emission Spectrometry

IUPAC : The International Union of Pure and Applied Chemistry

JCPDS : Joint Committee on Powder Diffraction Standards

La-DCP : Lanthanum Doped Dicalcium Phosphate

La-βTCP : Lanthanum Doped β-Tricalcium Phosphate

MC3T3-E1 : Murine Preosteoblast Cell Line

MCPM : Monocalcium Phosphate Monohydrate

MMA : Methyl Methacrylate

MPA : Monocalcium Phosphate Anhydrous

MSC : Mesenchymal Stem Cell

NR : Not Reported

OCP : Octacalcium Phosphate

OVX : Ovariectomized

P-chitosans : Phosphorylated chitosan

PBS : Phosphate Buffered Saline

PMMA :  Poly Methyl Methacrylate

pNPP : p-nitrophenyl Phosphate

rBMSCs : rat Bone Marrow Mesenchymal Stem Cells

ROB : Rat calvarial Osteoblast-like

RT : Room Temperature

SA : Sodium Alginate

Saos-2 : Human Osteosarcoma cell line

SD : Standard Deviation

SEM : Scanning Electron Microscopy

SPSS : Statistical Product and Service Solutions

SSA : Specific Surface Area

$T_i$ : Initial Setting Time

$T_f$ : Final Setting Time

| | | |
|---|---|---|
| TCP | : Tricalcium Phosphate | |
| TGA | : Thermo Gravimetric Analysis | |
| TTCP | : Tetra Calcium Phosphate | |
| UV-Vis | : Ultraviolet–Visible spectroscopy | |
| XRD | : X-Ray Diffraction | |
| αTCP | : α-Tricalcium Phosphate | |
| βTCP | : β-Tricalcium Phosphate | |

# LIST OF SYMBOLS

SYMBOLS

| | |
|---|---|
| ° | : Degree |
| °C | : The degree Celsius |
| Å | : Angstrom |
| a-axis | : lattice parameter |
| b-axis | : lattice parameter |
| c-axis | : lattice parameter |
| µL | : Microliter |
| µg | : Microgram |
| $2\theta$ | : The diffraction angle |
| $\alpha$ | : Alpha, cell angle |
| $\beta$ | : Beta, cell angle |
| $\gamma$ | : Gamma, cell angle |
| $\lambda$ | : wavelength of the X-ray |
| Ag | : Silver |
| Al | : Aluminum |
| Ba | : Barium |
| Ca | : Calcium |
| Ce | : Cerium |
| cm | : Centimeter |
| Cr | : Chromium |
| D | : Size of the crystallite size |
| Eu | : Europium |
| g | : Gram |
| G | : Graphene |
| h | : Hour |
| H | : Hydrogen |
| kg | : Kilogram |

K   : Potassium

kV   : Kilovolt

La   : Lanthanum

mA   : milliampere

Min   : Minute

Mg   : Magnesium

Mn   : Manganese

mL   : milliliter

MPa   : Megapascal

N   : Nitrogen

Na   : Sodium

Ni   : Nickel

nm   : Nanometer

O   : Oxygen

P   : Phosphorus

S   : Sulfur

Sr   : Strontium

sec   : Second

W   : Watt

Z   : Number of formula units per cell

Zn   : Zinc

## CHAPTER 1

## 1. INTRODUCTION

### 1.1. Overview

Bone, the hard tissue of the body, is a major part of the body that gives it shape, stability, and strength. Any disorder or fracture in the bone may result in a partial or severe hindrance of the body movement. However, when the bone is injured, it may undergo a self-healing process. On the other hand, if some part of the bone is lost due to accident or disease, its reconstruction is impossible. Thus, reconstruction of these types of bone defects using biodegradable or non-biodegradable biomaterials is essential. Sometimes, both can be employed in surgical applications (Honkanen et al., 2003; Kellomäki et al., 2000; Middleton & Tipton, 2000) as illustrated in Figure 1.1.
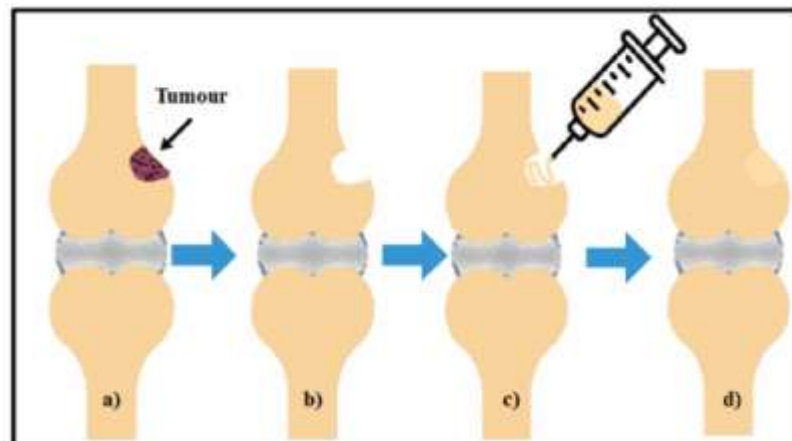


**Figure 1.1.** A schematic picture showing a) the tumour on the bone, b) bone defect after tumour removal by surgery, and (c-d) the bone defect filled by bioactive materials.

Biodegradable polymeric materials such as poly(l-lactic acid), poly(caprolactone), poly(lactic-co-glycolic acid), poly(3-hydroxybutyric acid), poly (adipic acid), poly (sebacic acid), gelatine, and chitosan have the advantage of disappearing from the body after some time and are biologically safer because they have hydrolysable chemicals  bonds like amides or esters (Feig et al., 2018; Okada, 2002). Although biodegradable polymeric materials or composites have specific properties, they are unpopular as load-bearing applications due to their weakness (Pillai, 2014). Therefore, their usage in bone defects treatment is not recommended (Song et al., 2018). In contrast to biodegradable polymers, non-biodegradable polymers have shown significant mechanical strength, so their usage in osteo-related problems is preferred (Gunatillake & Adhikari, 2016; Subramaniam & Sethuraman, 2014). Besides these polymeric materials, there are many other well-known bioceramics such as hydroxyapatite (HA), tricalcium phosphate (TCP), and dicalcium phosphate (DCP).All in pure phase form is substituted with various ions to enhance their biological and mechanical properties and is used by the orthopaedic surgeons to cure orthopaedic defects (Akram et al., 2015; Alshemary et al., 2015; Taha et al., 2017). Many researchers have been developing these biomaterials to solve trauma-based issues occurring due to accidents or diseases. Currently, they are trying to synthesize various bioactive and biocompatible materials such as HA and TCP, also focusing on developing novel materials with better mechanical strength, wear strength, and resistance towards various bacterial post-operational infections.

## 1.2. Bone Cements

Orthopedic surgeons estimate that about 30% of the population will suffer osteoporosis or osteoporotic hip fractures and 20% of the patients will hardly survive one year after the surgery. All this statistical data demonstrates a tremendous need for alternative therapies to treat the damaged or diseased bones. The mammalian hard tissue seems to be the best alternative as the major portion of it consists of 70% of Calcium phosphate (CP). To better understand this process of bone therapy, it is

crucial to understand the process of CP biomineralization, their interaction, and the biological environment of the mammalian system.

Cement is a material that binds two materials together. Bone cement provides this exact property of fixing bone defects to facilitate the living body's normal functioning. Bone cements are obtained by mixing powder form material and a liquid phase, after which they not only become hard but also stick firmly at the bone site once injected. In addition, this material has special flexibility that can be used to fix the material at the fractured site when needed. Another critical feature of these biomaterials is that they provide mechanical support to the body. Regarding the mechanical support, it is noteworthy that these cementing materials have different levels of mechanical strength. Thus, researchers in this field aim to develop higher-quality bone cements so that they not only have a longer life but also more mechanical strength, no inflammatory effect after implanted in the body, short in-situ setting time, and no post-operational viral or bacterial infection. Nowadays, various commercially available bone cements meet these qualities and are used for diversified orthopaedic surgery fields. Polymethyl methacrylate (PMMA), for example, has been applied as bone cement in joint replacements due to its good mechanical strength and efficient setting time (Deb, 2006).

Around 1870, Gluck prepared a bone cement using ivory, plaster and colophony to fix a total knee prosthesis (Ascherl, 2011). O. Rohm and Kulzer were among the pioneer scientists who utilized their potential to explore the properties and use of bone cements (Arora et al., 2013; Nottrott, 2010). They explained the polymerization process of methyl methacrylate with tertiary aromatic amine as co-initiator at ambient temperature (Kühn, 2005). In 1958, John Charnley, a surgeon, used acrylic-based bone cement for the total hip arthroplasty (Charnley, 1960),bonding PMMA with acrylic polymeric mantle to the femoral crown to adjust a metallic implant in the surgical material. It was a significant achievement in orthopedic surgery. Later, many papers were filed highlighting PMMA's potential to be used as bone cement and overcome various bone defects. In 1970, the US Food and Drug Administration

(FDA) accepted bone cement as a safe implant material for hip and knee prosthetics (Waugh, 2012). Since then, bone cements have been extensively used in orthopedic surgery, particularly in joint replacement surgery. PMMA was also utilized as dental material due to its biocompatibility, transparency, and mechanical strength (Henrichsen et al., 1952). Nevertheless, there is a growing need to explore novel bone cements for orthopedic surgical applications due to the lack of certain demerits.

Similarly, Calcium Sulphate Hemihydrate (CSH, $CaSO_4.5H_2O$) bone cements have been known for a long time and have been used to repair bone defects due to their excellent biocompatibility capacity in repairing bone defects (Kim et al., 2011). Mixing water with CSH produces Calcium Sulphate Dehydrate (CSD), which is a popular bone cement. It has good biocompatibility and fosters bone healing without any inflammatory infection. However, one major demerit of these bone cements pertains to the availability of implants of suitable size.

Owing to such emerging surgical problems, such injectable bone cements are under investigation, which are controlled in-situ after filling of the defected part of the bone. According to a survey report (Khor, 2014), modern bone cement should have the following qualities:

i.      injectability and flexibility
ii.     in-vivo setting and suitable hardening time,
iii.    ambient temperature setting,
iv.     the setting at neutral pH,
v.      no toxicity,
vi.     high porosity
vii.    biocompatibility and bioactivity

Regarding these properties, the scientist concluded that, for the time being, no biomaterial can be named as perfect hard tissue (bone) cement. Currently, the

available cements, which have debatable issues and certain restrictions, can be categorized into two: DCP cements and acrylic bone cements.

DCP cements and acrylic bone cements are summarized below based on a comprehensive review of scientific articles published in the journals indexed by Scopus from September 2000 to September 2021 (Figure 1.2). The quickly expanding number of research articles confirms how bone cements are essential in mainstream researchers because of the impact on patient needs.
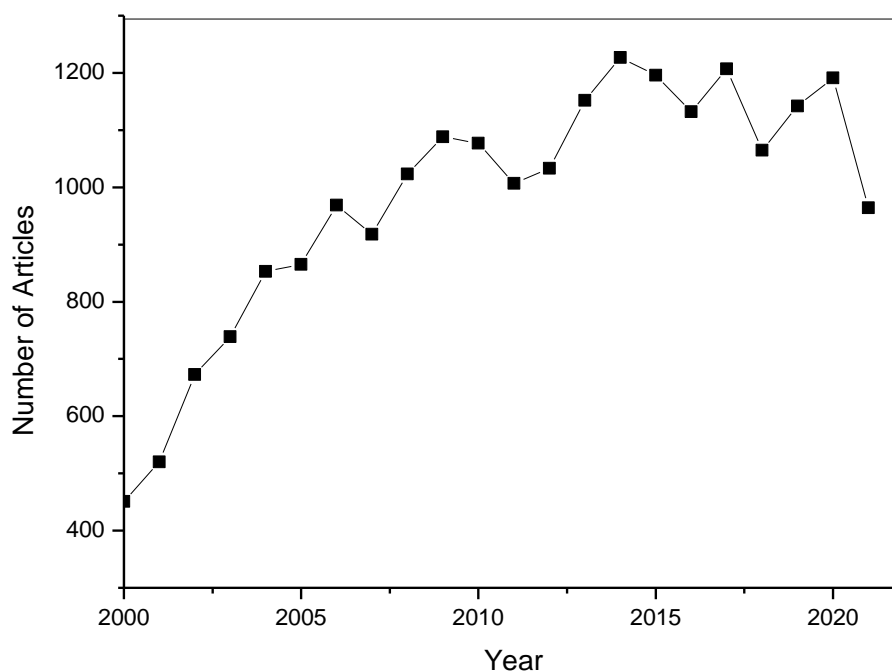


**Figure 1.2.** Annual number of articles on bone cements published in Scopus from September 2000 to September 2021.

### 1.2.1. Acrylic Bone Cements

Acrylic bone cements such as PMMA are essential materials used in joint replacement surgery. Initially, PMMA cement-like materials were prepared for dental surgery, and later on, they were found effective for joint replacement surgery. It was established that methyl methacrylate (MMA) monomers are the basic building block

units for the polymerization of acrylic bone cements (Kuehn et al., 2005). Acrylic bone cement is a mixture of solid activator (Benzoyl peroxide, PMMA, and Barium Sulphate or Zinc oxide) and liquid monomer parts (MMA, Hydroquinone, N, N, dimethyl-4-toluidine). Thus, it can be manufactured using these dense activators and liquid initiators (Figure 1.3). This reaction is exothermic, which accelerates the temperature of the system. The commercial preparation of polymethacrylates triggered the development of novel polymers further employed to treat skeletal defects. However, very high temperatures (60-120 °C) may burn the bone or the surrounding tissues, or sometimes both. Besides, unreacted monomers may be toxic, break down the bone cement, and even cause the loss of the prosthesis (Ahmari, 2010; Heini et al., 2001; Urrutia et al., 2008).



Methyl methacrylate (MMA)                    Poly(methyl methacrylate) (PMMA)
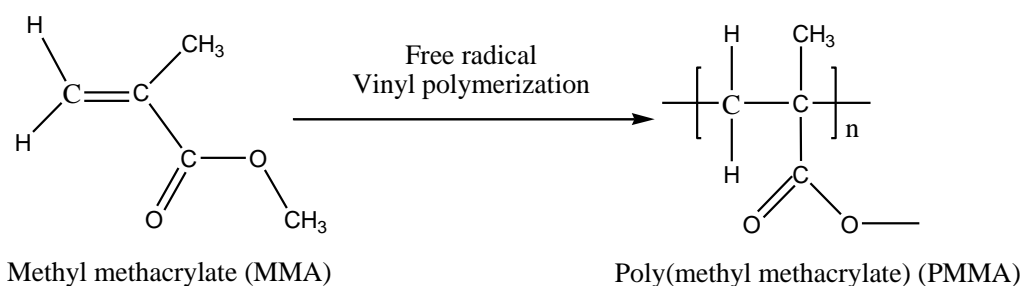
**Figure 1.3.** Scheme of the polymerization process of PMMA

Despite the few drawbacks, acrylic bone cements have been getting escalating interest due to their significant strength and support in joint replacement surgery. They have the potential to be used in a load-bearing application in bone-cement prosthesis surgery. Similarly, their mechanical properties are likely to produce favourable results overall. Furthermore, acrylic cement is effective in the captivation of artificial joints and in the affixing of the graft to the hard tissue. This bone cementing paste further facilitates plugging of the space among the living hard tissue and prosthesis. In turn, due to its elasticity, it transfers the graft load to the bone homogeneously (Lindahl et al., 2005). Nowadays, substantial efforts are paid to upgrade the properties of conventional bone cements like acrylic bone cement. Still, the use and development of DCP cements materials are also under consideration because of certain potential benefits. To name a few, they are likely to improve

mechanical strength of the bone cement, thermal stability, biological performance, and life of the cemented prosthesis.

## 1.2.2. Dicalcium Phosphate Bone Cements

DCP cement materials have been known for the last 50 years and attract the researcher's growing attention due to their wide range of applications in different fields, including biomedical engineering, chromatography, and cosmetics. Therefore, novel artificial bone cementing materials are needed to repair the bone defect resulting from trauma or accidents. Besides, due to the limited lives of implanting materials, attention has been directed towards bone tissue engineering (Hench & Polak, 2002; Kharaziha & Fathi, 2010; Sabir et al., 2009). Hence, there is a need to produce novel bone cementing materials, which may show the capability to develop a strong attachment with the living hard tissue and facilitate bone regeneration of calcified tissues rather than their replacement. This demonstrates that materials should have the capacity to promote osteogenic activity but at the same time should support bone cell proliferation. Additionally, these calcium phosphate materials should be liable to osteoclastic degradation.

Monetite cement [Dicalcium Phosphate Anhydrate (DCPA), $CaHPO_4$] is another well-known bone cement. It is gaining escalating importance due to its remarkable properties and applications in various fields: clinical fields, orthopedics, drug delivery, cancer therapy, biosensors, and craniofacial surgery. For example, monetite cement significantly shows a reduced exothermicity during its setting time (Zhou et al., 2015). In addition, it is soluble, biocompatible, biodegradable, osteoconductive, bio-resorbable, and almost identical to brushite cement in chemical composition (Dorozhkin & Epple, 2002; Higuita et al., 2016; Idowu et al., 2014; Tamimi et al., 2012a). Furthermore, in contrast to brushite cement, the monetite cement does not reprecipitate into the apatite layer, so it shows a better resorption rate (Tamimi et al., 2010; Theiss et al., 2005). Although monetite cements is a good cement material, its poor mechanical strength, compression strength, injectability behaviour, fracture

toughness, and washout resistance make it unsuitable for load-bearing surgical applications. All these deficiencies can be overcome by incorporating various ions or polymeric materials. Poor antibacterial resistance is another challenge for orthopedic surgeons injecting monetite cements into the living body. According to the related literature, monetite cements are set within the first three minutes, which does not allow enough working time, so they are not recommended as ideal cementing materials. An ideal cementing material should have at least three-eight minute setting time and about one minute cohesion time. The suggested final setting time is around 15 minutes (Carrodeguas et al., 2004; Dorozhkin, 2008). The set monetite cements have a compression strength of $8.6 \pm 3.5$ MPa and a porosity of 59% (Cox et al., 2017).

The setting time, poor mechanical properties like issues or antibacterial properties of monetite can be improved by either adjusting its composition or by incorporating various ions such as Lanthanum (La), Cerium (Ce), Silver (Ag), or Graphene oxide (GO) particles. During the last 50 years, ion substituted monetite cements have brought a substantial change to medical science by enhancing the life standard of patients using these artificial bone and dental fixtures. Incorporating such beneficial materials has markedly improved reconstructive surgery and the life quality of rehabilitated individuals.

## 1.3. Problem Statement

DCP has great potential for clinical applications with its advantageous properties. These properties include osteoconductivity, bioactivity, moldability, and injectability. Due to its great mouldability, ability to deform easily on the application, and setting at low temperature, it can be used as an alternative material for bone graft, mainly in small-scale bone defect management and load-carrying prosthetic implants (Bohner et al., 2005; Ginebra et al., 2006;  Tamimi et al., 2012b; Vahabzadeh et al., 2015a; Vahabzadeh et al., 2015b). Other important properties are its ability to be moulded upon mixing (Chow, 1999), minimal invasiveness upon injection (Xu et al.,

2006), and effectiveness as a carrier in drug and biomolecules delivery (Ginebra et al., 2006).

Despite the above stated strengths, DCP has certain limitations. For instance, it has a relatively long setting time, and poor mechanical properties and it can induce a decrease in local pH (Jang et al., 2018). Critical limitations of DCP need to be improved in order to expand their clinical use. It has been suggested that DCP trace amounts of other ions can be incorporated or carbonaceous materials can be added.

## 1.4. Objectives of This Thesis

The main objective of this thesis is to investigate and improve the microstructural, mechanical, and biological properties of DCP cements using $La^{3+}$ ions as dopant and GO as an additive.

The specific objectives are summarized as follows:

1.  To synthesize the pure phase of β-Tricalcium phosphate (β-TCP) and $La^{3+}$ doped β-TCP powders based biomaterials using microwave-assisted precipitation method, to characterize the above-mentioned β-TCP and La-βTCP materials utilizing X-ray diffraction (XRD), Fourier transform infrared (FTIR), scanning electron microscope (SEM), inductively coupled plasma optical emission spectroscopy (ICP-OES), Brunauer–emmett–teller (BET), and helium pycnometer techniques and to evaluate the impact of the addition of La ions on microstructure analysis of βTCP, loading /release capacity of fetal bovine serum (FBS) proteins, degradation behavior of βTCP over 21 days in Phosphate-buffered saline (PBS), osteoconductive and osteogenic behavior of human osteosarcoma cell line (Saos-2).

2.  To optimize the right amount of ingredients used to prepare the pure phase of DCP cement with pH equal or near to 7, to synthesize DCP cements from

the corresponding β-TCP (or La- βTCP) precursors,  to characterize the obtained cements utilizing XRD, FTIR and SEM, TGA and ICP-OES techniques, and to evaluate the impact of the addition of La ions on microstructure analysis of βTCP, loading /release capacity of FBS proteins, degradation behavior of βTCP over 21 days in Phosphate-buffered saline (PBS), setting time and mechanical properties of DCP bone cements, osteoconductive and osteogenic behavior of Saos-2 cell line.

3. To evaluate the impact of GO substitution up to the physicochemical properties, setting time, mechanical properties, loading /release capacity of FBS proteins, osteoconductive and osteogenic properties of La-DCP cements.

## 1.5. Significance of the Study

The practical significance of the study is that synthesis of new bone cement materials proposed in this thesis endeavours to produce Lanthanum doped Dicalcium phosphate mixed with Graphene oxide bone cements. These newly developed bone cements are expected to have superior mechanical and biological properties compared to the existing bone cements.

# CHAPTER 2

# 2. LITERATURE REVIEW

## 2.1. Dicalcium Phosphate Cements

DCP cements are bone filling materials and manifest close resemblance with the human hard tissue because CP is the major mineral part of the mammalian bones (Yoshikawa & Myoui, 2005). DCP cements offer numerous advantages due to their excellent osteoconductivity, biocompatibility, biodegradability, injectability, and potential to fill the produced cavities in hard tissues (bones or teeth) which further may facilitate the process of bone regeneration phenomenon as well as self-hardening at room temperature (RT) (Habraken et al., 2016; Mestres & Ginebra, 2011; O'Neill et al., 2017).

DCP cements have been attracting growing attention because of their utilization as injectable pastes to fill bone imperfections, cracks, or discontinuities (Barralet et al., 2002; LeGeros, 2002). The clinical applications of DCP cements further increased when the self-setting of these materials was upgraded around the 1980s (O'Neill et al., 2017). DCP cements undoubtedly have excellent osteoconductivity and are used in low load-bearing applications to treat bone defects due to their weak mechanical strength and brittle behaviour (Deb, 2006). Additionally, monetite and brushite are allotropic forms of DCP based cements and are applied as a paste, but their setting and hardening times are different. In short, their mechanical strength and fracture toughness lower than the human hard tissue make them unsuitable for load-bearing applications. Besides, DCP based cements are costly, time-consuming, and difficult to synthesize. Furthermore, existing bone cements like α-Tricalcium phosphate (α-TCP), β-TCP and tetra calcium phosphate (TTCP) can only be synthesized at high temperatures, and sintering at these high temperatures results in hard and dense

samples. Dense materials need fine grinding, and in this process, some impurities are also incorporated in the powder, reducing their *in vivo* absorption.

### 2.1.1. Dicalcium Phosphate Dehydrate

Dicalcium Phosphate Dehydrate (DCPD, $CaHPO_4 \cdot 2H_2O$, Figure 2.1) cements are known as brushite. It is biologically present in nature and found naturally in the biological living system. They occur as pathological calcification in crystalluria, chondrocalcinosis, dental calculi, and few carious lesions. Although they occur naturally in the living bodies, they can also be synthesized using CP cements. In 1987, the first brushite cement was obtained by Lemaitre and his colleagues (Lemaitre et al., 1987). Under physiological circumstances, brushite cement is metastable and, at the same time, acidic, which makes it readily resorbable in the biological system compared to apatite based CP cements (Constantz et al., 1998; Elliott, 1994). The acidic nature of brushite cement presents because it can only be precipitated out in an acidic medium (at pH lower than 6), which usually changes after the setting of the cement (Ferna et al., 1999). The setting time of brushite cement is very short, and the reaction is exothermic because it warms the brushite cement before the final setting (Hofmann et al., 2006). Brushite cement has been receiving massive recognition because of its quick setting time, brittleness, and low strength (Approximately around 15-52 MPa) (Engstrand., 2014).
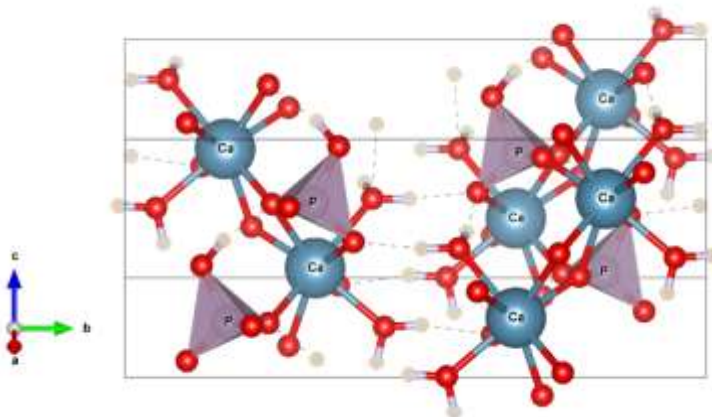


**Figure 2.1.** Brushite crystal lattice plotted using VESTA software.

12

In a typical chemical reaction, synthesized biomaterials are mixed manually or mechanically with several CP based cements with a liquid phase. Owing to a change in pH, two types of cements are produced. The product produced around a pH of 4.2 is named HA, whereas brushite is obtained in other cases (Chow, 1991; Mirtchi et al., 1989).

Researchers prepare brushite cements considering acid-base reaction as the basic tool to synthesize this class of materials. Brushite is usually produced by mixing β-TCP and Monocalcium phosphate monohydrate (MCPM) (Roy et al., 2012). Generally, β-TCP is frequently used as a reactant due to its good solubility.

## 2.1.2. Dicalcium Phosphate Anhydrous

Monetite cement is slightly acidic, capable of self-hardening, and is mainly in use to repair mammalian skeletal (Chow & Takagi, 2001; Tas, 2008; Xu & Simon, 2004). For many years due to its better self-hardening ability, people have been using it in toothpaste, chewing gums, and as emulsifies (Francis & Rahman, 2016).

DCP cements have been attracting the attention of the researchers as they can be utilized as tableting agents in pharmaceutical factories, in some tubes of toothpaste and also in bone regeneration applications (Dorozhkin, 2016; Švecová & Bartůněk, 2018). They are chemically similar to mammalian hard tissues, and due to their osteoconductive ability, they are suggested to be used for orthopedic based defects (Jokić et al., 2011; Oguchi et al., 1995). However, some CP cements or HA have limitations like limited biosorption, which restricts the *in vivo* regeneration process of human bones (da Silva et al., 2001; Sheikh et al., 2017). Additionally, monetite cement has engendered growing attraction due to its rapid in-vivo resorption, which is significantly more efficient than HA (Tamimi et al., 2008b).

The monetite phase of DCP cements has better resorption time in contrast to HA, or TCP. Besides this, nanosized monetite particles have better mechanical strength due

to their dense nature (Hong et al., 2017; Tamimi et al., 2012b). Additionally, applications of nanosized monetite cement in the water purification industry and the purification of nucleic acids from plants are promising (Hong et al., 2017; Shen et al., 2016).

## 2.1.2.1. Chemical and Physical Structure of Monetite Cement

Monetite cement structure exists as triclinic and according to standard protocol lattice parameters, of a=6.910 Å, b=6.627 Å, c=6.998 Å, $\alpha$=96.34°, $\beta$=103.82°, and $\gamma$=88.33° at 25°C, with Z=4, as shown in Figure 2.2. It manifests triclinic-pinacoidal assembly in which $CaHPO_4$ chains are bonded through three hydrogen bonds and calcium-oxide bonds (Tortet , 1997).
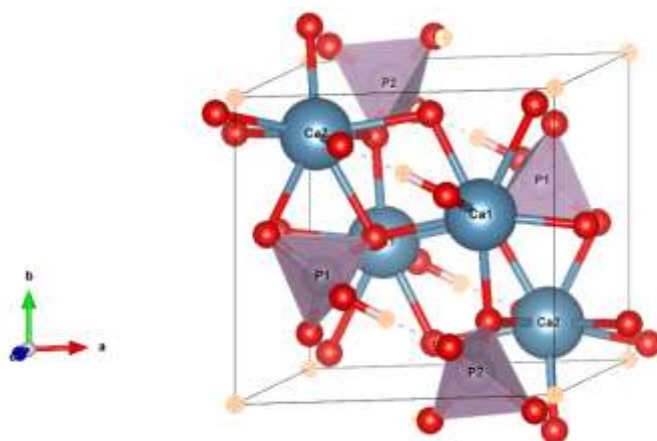


**Figure 2.2.** Monetite crystal lattice plotted using VESTA software.

Brushite cements are considered to be effective osteoconductive materials which are bioresorbable and to have great potential for bone regeneration. However, it can be converted into monetite cement by autoclaving, and dehydration caused by heating treatment changes its physical properties. This change in physical characteristics improves its *in vivo* biosorption behaviour (Tamimi et al., 2012a). In the last few years, several studies have been conducted to compare the chemical, physical, and biological properties of monetite cement with those of brushite cement to explore

14

which one is preferable for bone regeneration (Klammert et al., 2009; Kraus et al., 2012; Tamimi et al., 2012a). Even though brushite and monetite cements have the same chemical formulas except water of crystallization and the same calcium to phosphate ratio (Ca/P = 1), their behaviour towards *in vivo* degradation are different. The degradation rate of monetite cement is more favorable than that of brushite for new bone formation (Kraus et al., 2012).

The related literature demonstrates that brushite cement can be transformed into monetite cement through heating activity. As a result of its various physicochemical properties, monetite cement undergoes certain changes (Sheikh et al., 2017). These changes usually occur under dry conditions, which further affect its resorption and bone formation (Sheikh et al., 2017). In different studies, it has been observed that monetite grafts possess high-level porosity and specific surface area. Similarly, the compressive strength of monetite cement is reduced by around 50% due to the heating of brushite.

### 2.1.2.2. Methods to Synthesize Monetite Cement

Monetite cement can be synthesized by reacting in-situ phosphoric acid ($H_3PO_4$) and calcium hydroxide ($Ca(OH)_2$) simultaneously during PLA electrospinning (Touny & Bhaduri, 2010). Mixing concentrations of both $Ca(OH)_2$ and setting solution can be calculated according to the Ca/P molar concentrations of the ultimate product. Monetite cement can be prepared by the following reaction (Eq. 2.1).

$$Ca(OH)_2 \ + \ H_3PO_4 \ \rightarrow \ CaHPO_4 \ + \ 2H_2O \qquad\qquad Eq.\,2.1$$
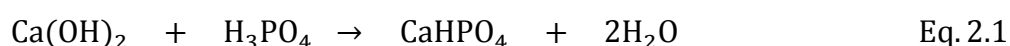
Svecova and Bartunek reported the preparation of monetite cement through a facile method (2018). In this method, $H_3PO_4$, $Ca(OH)_2$, ethanol, and water were employed, and all the contents were homogenized using an ultrasound treatment. In another study, monetite cement was synthesized using a thermal method (Karimi et al., 2017). Others suggest that monetite cement can be synthesized by just doing

15

modifications in the precipitation conditions of brushite cement (Aberg et al., 2010; Bohner & Gbureck, 2008). Similarly, in another method, it was reported that brushite cement was kept in an acidic medium (Low pH). In aqueous-deficient conditions, monetite cement can be prepared (Alkhraisat et al., 2008). Following the same method with a little addition of metallic ions disrupts the formation of brushite cement and ensures monetite cement formation (Tamimi et al., 2008a).

Tokuoka et al. (2006) successfully synthesized monetite particles in agglomerated form using aqueous solutions of both triethyl phosphate and Ca-nitrate in the presence of cetyltrimethylammonium bromide (CTAB) by reacting the two solutions at ambient temperature for 24 h. In 2005, Chen et al. synthesized monetite cement using a unique membrane micro-dispersion method. Their investigation employed aqueous solutions of sodium dodecyl Sulphate containing calcium acetate as a water phase, whereas the mixture of butanol-phosphoric acid as an oil phase. Yet in another research, Wei et al. (2007) described the formation of spheres, mono-dispersed nano-fibres, and packs of nano-wires of monetite cement using reverse micelles solutions water and cyclohexane. Cuneyt Tas (2009) successfully synthesized monetite cement having sub-micrometre and nanosheets morphology at RT by shaking precipitated $CaCO_3$ in ethanol solution in the presence of phosphoric acid.

In another study, either CTAB or polyoxyethylene-8-dodecyl ether (C12E8) surfactants or n-pentanol as co-surfactant were introduced to set up a microenvironment to synthesize well-crystallized monetite cement. Cama et al. (2014) described the development of monetite particles without the need for hydrothermal treatment by a simple route and using a concentrated solution of sodium chloride in the mixture of β−TCP and MCPM. Where monetite cement can be synthesized using inorganic materials simultaneously, it can also be synthesized using natural resources like eggshells or any calcium-rich natural source. Zhou et al. (2015) reported on the preparation of monetite cement using eggshells through microwave irradiation. Some research have also revealed that monetite cement can be synthesized by the hydrothermal conversion of brushite cement (Gbureck et al.,

2007; Tamimi et al., 2008b). As regards monetite in clinical applications, it was synthesized using a novel solvent exchange technique, and the results were promising (Nishad et al., 2017). Besides the above-stated methods, monetite has also been synthesized through other techniques like hydrothermal, sonochemical, solvent extraction, reverse micelles, microwave-assisted, precipitation from microemulsion, and by electrodeposition methods (Bonfield et al., 1998; Karimi et al., 2017; Kong et al., 2005; Ma et al., 2006; Nishad et al., 2017; Wei et al., 2007). Synthesis methods of monetite cements are summarized in Table 2.1.

### 2.1.2.3. Setting Time and Injectability Behaviour of Monetite Cement

Setting time is perhaps the most important feature of all cementing materials as it directly controls setting properties, physical and biological properties, and strengthens tough cement time (Chow, 2009). It simply means the time required for the cement to become hard enough to show strong resistance to the applied force after being injected into the patient's body (ASTM, 2008). Setting time is also critical in that cement should not deform after injection because, in this case, cracks would form which means cement is in poor quality (Driessens et al., 1998). Nowadays, various efforts are paid to shrink the setting time of the cement materials from days to hours and minutes. Certain factors facilitate rapid kinetics and reduce the setting time. Some are the high surface area of the particles, particles size, higher setting temperature, high solid/liquid ratio, low crystallinity of the cementing material, and the liquid and solid composition (Müller et al., 2007). Although researchers endeavor to lessen the setting time, shorter setting time is not always beneficial. Sometimes, a shorter setting time may be a drawback before the doctors complete their surgical procedures. Therefore, cement with a suitable setting time is preferable for the surgical tasks (Dagang et al., 2007).

Similarly, along with setting time, monetite cement injectability behaviour also has prime importance in orthopedic surgical measures. Injectability means injection force applied to a syringe used to deliver the cementing material into the patient's body

17

(Bohner, 2010). During these surgical processes, commonly invasive techniques like vertebroplasty and kyphoplasty are adopted to apply monetite cement in root canal obturation with a narrow space (Sahin, 2018).

**Table 2.1.** Methods, raw materials, and preparation protocol of monetite cements.

| Method | Raw Materials | | | Notes | Particles | | Refs |
|---|---|---|---|---|---|---|---|
| | Ca- source | P- Source | Additives | | Shape | Size (µm) | |
| Sonochemical | CaCl$_2$ | NaH$_2$PO$_4$ | EG, DMF | • The solution mixture was sonicated using high-intensity ultrasonic radiation for various lengths of time (10-60 min) at 25°C. <br> • The products were separated, washed, and dried at 50°C /1 h. | plate-like | 0.21 | (Baradaran et al., 2013) |
| Wet precipitation | Ca(NO$_3$)$_2$·4H$_2$O | (NH$_4$)$_2$HPO$_4$ | AgNO$_3$ | • The solution mixture was stirred at 110°C/2 h. | block-like | NR | (Chen et al., 2016) |
| | Ca(OH)$_2$ | H$_3$PO$_4$ | NR | • The precipitation was kept under stirring for 5 min, and then the filter cake was dried overnight at 90°C. | plate-like | NR | (Duncan et al., 2014) |
| | Ca(OH)$_2$ | H$_3$PO$_4$ | NaHCO$_3$ | • Heat-treated in 1200W microwave for 1 min and obtained dry powder. | NR | NR | (Lin et al., 2014) |
| | CaCO$_3$ | H$_3$PO$_4$ | NR | • The solution mixture was kept under reflux in an oil bath at | plate-like | 1-2 | (Mulongo-Masamba et al., 2016) |

**Table 2.1.** (Continued).

| Method | Raw Materials | | | Notes | Particles | | Refs |
|---|---|---|---|---|---|---|---|
| | Ca- source | P- Source | Additives | | Shape | Size (μm) | |
| | | | | 85°C/24 h. The white precipitate dried overnight at 60°C. | | | |
| | $Ca(OH)_2$ | $H_3PO_4$ | lactic acid | • The pH of the solution was 3.7 | plate-like | 8×4×2 | (da Silva et al., 2001) |
| | $CaCl_2$ | $(NH_4)_2HPO_4$ | CTAB | • Free of CTAB, the precipitation process of monetite occurs within 12 h.<br>• In the presence of CTAB surfactant, clear and transparent solutions are obtained after an ageing process of two weeks.<br>• The obtained residue is heated and dried in an oven at 100°C/ 24 h. | fiber boundless | 0.1 | (Wei et al., 2007) |
| | $CaCl_2·2H_2O$ | $Na_2HPO_4$ | silk sericin | • Silk sericin+ $Na_2HPO_4$ was stirred for 8 h, then added to $CaCl_2·2H_2O$ and stirred for three h. | NR | NR | (Vedakumari et al., 2020) |
| | $Ca(NO_3)_2.4H_2O$ | $(NH_4)_2HPO_4$ | NR | | NR | 0.7 | (Sych et al., 2015) |

**Table 2.1.** (Continued).

| Method | Raw Materials | | | Notes | Particles | | Refs |
|---|---|---|---|---|---|---|---|
| | **Ca- source** | **P- Source** | **Additives** | | **Shape** | **Size (µm)** | |
| | $Ca(NO_3)_2.$ $4H_2O$ | $(NH_4)_2HP$ $O_4$ | BHA | • The monetite was mixed with different fractions of BHA, then the composites were sintered in a muffle furnace at 800°C/2 h. | NR | 0.14 | (Sych et al., 2014) |
| | $Ca(NO_3)_2.$ $4H_2O$ | $(NH_4)_2HP$ $O_4$ | NR | • The solution mixture was stirred and heated at 90°C/2 h under nitrogen atmosphere. <br> • The milky suspension was aged for 24 h. <br> • The resultant gel-like paste was oven-dried at 100°C/ 24 h. | rods | Width:0. 020- 0.080 Length: 0.2 to 0.6 | (Abdel-Fattah et al., 2008) |
| | $Ca(OH)_2$ | $H_3PO_4$ | lactic acid, $Sr(OH)_2·8$ $H_2O$ | • The prepared samples were rinsed with water and dried at 60°C for 10 min. | rhombohedr al crystal | NR | (da Rocha et al., 2019) |
| | $Ca(NO_3)_2.4$ $H_2O$ | $H_3PO_4$ | NR | • The pH was maintained at 3.5 <br> • The obtained residue was washed with acetone and air-dried for 12h. | strip-like | 0.2 | (Nishad et al., 2017) |

**Table 2.1.** (Continued).

| Method | Raw Materials | | | Notes | Particles | | Refs |
|---|---|---|---|---|---|---|---|
| | **Ca- source** | **P- Source** | **Additives** | | **Shape** | **Size (μm)** | |
| | | | | • The samples were dried overnight at 600°C. | | | |
| | β-TCP + MCPM | | $Sr(NO_3)_2$ | • The addition of 0.75 mole $Sr^{2+}$ ions enhanced the formation of the monetite phase. | plate-like | NR | (Taha et al., 2017) |
| Hydrothermal | $CaCO_3$ | $H_3PO_4$ | $Fe(NO_3)\cdot9 H_2O$ | • The solution mixture was poured into a Teflon-lined autoclave and then heated under autogenous pressure at 180°C for two weeks. | NR | NR | (Ouerfelli & Zid, 2016) |
| Thermal conversion | | | | • The synthetic brushite phase is heat-treated in the air using three different heating methods: thermal X-ray powder diffraction, TGA, and a muffle furnace with an adjustable heating rate. | NR | NR | (Dosen & Giese, 2011) |
| | | | | • The synthetic brushite powder was transformed into monetite by hydrothermal conversion using an | needle-like | NR | (Idowu et al., 2014) |

**Table 2.1.** (Continued).

| Method | Raw Materials | | | Notes | Particles | | Refs |
|---|---|---|---|---|---|---|---|
| | Ca- source | P- Source | Additives | | Shape | Size (µm) | |
| | | | | autoclave at 121°C, 100% humidity for 30 min. | | | |
| | | | | • The Monetite particles were obtained via thermal conversion of brushite cement granules. The brushite cements were autoclaved at sterilizing conditions (121°C, 100% humidity and 15 psi, for 20 min). | spaced microcrystal | 0.5-2.0 | (Torres et al., 2015) |
| | | | | • Monetite phase was prepared via heat treatment of brushite in an autoclave at 121°C and 100% humidity for 20 min. | irregular microstructure | NR | (Tamimi et al., 2010) |

Refs= References, EG= ethylene glycol, N,N-dimethylformamide (DMF), SA=Sodium Alginate, CTAB = cetyltrimethylammonium bromide, BHA= Biogenic hydroxyapatite, NR= Not reported.

DCP cements usually show relatively low shear viscosity, but with time, they become elastic and viscous. Although the growth rate, shear viscosity, and elasticity of DCP cements are low, the conventional cements and their behaviours can be ascribed to the rapid rate of dissolution and crystallization (Sahin, 2018). Various studies found that DCP cements must respond gradually to give proper time for their appropriate injectability and avoid being washed out. Furthermore, its preliminary setting time is significant, which further allows its proper shaping and setting. Usually, eight minutes of primary setting time and 15 minutes of ultimate setting time are recommended for the applications of CP cements in orthopedic surgical processes (Eliaz & Metoki, 2017).

In setting time and injectability of monetite cement, the stability of monetite is also essential. In this connection, acidic pH is favorable as in the acidic environment; monetite precipitate out easily and get stable (Drouet, 2013). A significant issue researchers have to deal with is the porosity of monetite. A scholar of master of dental science synthesized monetite by autoclaving the brushite, enhancing the porosity of the material from 23% (brushite) to 30% (monetite) (Aati, 2017). However, the synthesized product was poor in strength, and its setting time was not up to the required norm, either. In another study, setting time was increased by using some additives such as citric acid and tartaric acid (Barralet et al., 2004).

Monetite cement is considered more useful in the bone regeneration process than brushite cement, which tends to precipitate as insoluble HA and show rapid replacement by bone (Tamimi et al., 2012b). In contrast to brushite cement, monetite cements exhibit less solubility, so they do not easily transform to HA. Thus, monetite manifests excellent resorbable behaviour characteristics *in vivo* settings and is considered a beneficial matrix for bone tissue engineering (Tamimi et al., 2012a; Tamimi et al., 2010).

### 2.1.2.4. Mechanical Properties of Monetite Cement

Mechanical properties such as compression strength, fracture toughness, flexural strength, and fatigue have a pivotal role in using monetite cement in various applications, particularly during surgery (Fu et al., 2013). Usually, bioceramics are not mechanically strong enough to be used in load-bearing applications. According to a study, the poor tensile strength of monetite cement should be improved using various substituents because poor tensile strength makes it difficult to be used in load-bearing surgical applications (Nien & Huang, 2010). Because brushite and monetite are different in their water content, they show differences in their physical properties. Monetite prepared through the autoclaving of brushite cement is markedly different in its specific surface area, porosity, and density (Tamimi et al., 2012a). Some attempts were made to increase the surface area and porosity of the monetite by about 50% and 5%, respectively, by autoclaving of brushite cement (Alshaaer et al., 2011; Bohner & Gbureck, 2008). However, autoclaving did not seem to improve the mechanical properties of monetite (Tamimi et al., 2012a). Because of weak mechanical properties, monetite can be recommended as an injectable cement for bone void fillers. A complete list of mechanical properties and setting times of monetite cements is given in Table 2.2, along with the cement system additives used.

### 2.1.2.5. Biological Properties of Monetite Cement

DCP cements have short term biological properties, including their dissolution behaviour, resorption, osteointegration, and biocompatibility. For example, resorption properties depend on the solubility of constitutive phases. Resorption of cements in the body might follow two possible mechanisms: active resorption and passive resorption. Active resorption path is interceded by various cell activities of osteoclasts, macrophages, and many different cells.

**Table 2.2.** Setting time, total porosity, and mechanical properties of monetite cements.

| Composition | Additives* | Setting Time (min) | | Total porosity (%) | Compressive Strength (MPa) | Refs |
|---|---|---|---|---|---|---|
| | | Initial setting time | Final setting time | | | |
| Monetite | - | - | - | 71.70 | 5.70 | (Tamimi et al., 2012a) |
| Monetite | - | - | - | --- | 4.40 | (Tamimi et al., 2012b) |
| Monetite | - | - | - | 71.00 | - | (Tamimi et al., 2010) |
| Monetite | - | - | - | 29.00 | - | (Cama et al., 2017) |
| Monetite | 1wt% ZnO | - | - | 27.00 | - | (Cama et al., 2017) |
| Monetite | - | 8.00 | 36.00 | - | 11.40 | (Boroujeni et al., 2013) |
| Monetite | 2wt% CNT | 4.00 | 26.00 | - | 17.90 | (Boroujeni et al., 2013) |
| Monetite | - | - | - | 56.00 | 7.90 | (Sheikh et al., 2017) |
| Monetite | - | - | - | 46.00 | 14.00 | (Sheikh et al., 2017) |
| Monetite | 5wt % P-chitosan | 17.00 | 80.00 | - | 23.43 | (Boroujeni et al., 2014) |
| Monetite | - | 3.00 | 11.50 | - | 8.00 | (Zhou et al., 2015) |
| Monetite | 50wt % SiO2 | 3.50 | 9.00 | - | 20.00 | (Zhou et al., 2015) |
| Monetite | - | 19.00 | 58.00 | - | 2.05 | (Desai et al., 2007) |
| Monetite | - | 8.83 | 15.33 | - | 19.70 | (Koju et al., 2018) |
| Monetite | 10wt % $BaTiO_3$ | 7.58 | 13.67 | - | 19.65 | (Koju et al., 2018) |
| Monetite | - | - | - | 41.5 | 0.60 | (Sych et al., 2015) |
| Monetite | 5wt% SiO2 | - | - | 43.5 | 16.40 | (Sych et al., 2015) |
| Monetite | - | - | - | 38.5 | 0.60 | (Sych et al., 2014) |
| Monetite | 25wt% BHA | - | - | 40.2 | 32.00 | (Sych et al., 2014) |
| Monetite | - | 0.48 | 6.90 | 24.9 | 15.6 | (Cox et al., 2017) |
| Monetite | 2wt% Alginate | 1.21 | 7.00 | 30.5 | 7.90 | (Cox et al., 2017) |
| Monetite | Glycerol + 2wt% Alginate | 60.70 | 1355 | 59.1 | 8.60 | (Cox et al., 2017) |
| Monetite | 10wt% Ag | - | - | - | 123 | (Chen et al., 2016) |
| Monetite | 7.4wt% Sr | 10 | 16 | 20.9 | 15 | (Taha et al., 2017) |

*(Minimum amount of additives), CNT (Carbon nanotube), P-chitosans (phosphorylated chitosan)

Impassive resorption can be controlled by employing chemical hydrolysis or chemical dissolution in the body fluids (Dorozhkin, 2008). Although the resorption level of HA is minimal, monetite has better resorption ability (Touny & Saleh, 2018).

Moreover, it was confirmed that monetite cement has better bioresorbability and biocompatibility (Higuita et al., 2016; Idowu et al., 2014; Tamimi et al., 2014). According to the previous studies, brushite cement resorbs rapidly and transmutes into a stable apatite phase after *in vivo* implantation (Dorozhkin, 2013). Moreover, monetite prepared by the autoclaving technique discharges ions more slowly than brushite and does not change into unsolvable HA *in vivo*. On intravenous grafting, monetite resorbs rapidly than brushite (Gbureck et al., 2007; Tamimi et al., 2008b; Tamimi et al., 2006).

It was also reported that monetite cement has a higher level of osteoconductivity and resorbability *in vivo* and, thus, is considered as an excellent matrix for bone tissue engineering (Tamimi et al., 2012a; Tamimi et al., 2010). This presents a major advantage as the release of orthophosphoric acid during the degradation of brushite to apatite may cause inflammation in the tissues, which may be dangerous for the patients (Constantz et al., 1998).

However, monetite has the potential to exhibit a better rate of degradation and does not change into the apatite layer rapidly, which ensures an increase in bone formation (Boroujeni et al., 2014; Cama et al., 2013; Kruppke et al., 2016; Sheikh et al., 2017; Tamimi et al., 2010). The biological performance of the monetite can also be enhanced using calcium extracting from natural sources, such as eggshells, as the calcium extracted from natural materials has similar mechanical strength and biological characteristics (Boroujeni, 2012).

Cytocompatibility and biodegradation rate of monetite are also critical in augmenting cell viability and biodegradation. It was found that 20% incorporated BT- monetite

has the potential to show better cell viability and biodegradation rate when implanted in the living system (Koju et al., 2018).

## 2.1.2.6. Effect of Substitution on the Properties of Monetite Cement

Various cementing materials such as brushite, monetite, and MCPM have been receiving growing attention due to their potential to treat different osteo-oriented disorders such as osteoporosis, osteoarthritis, dental, and maxillofacial surgical challenges. Although monetite can harden in-situ and has superior mechanical properties, because of its mechanical strength, setting time and capability limitations, and the defective place needs further improvement for invasive surgery. In this regard, there is an increasing demand to synthesize unique phase pure, ion substituted composite materials to overcome current challenges. Doping of trace elements in monetite can be a good opportunity to meet the challenges of orthopedic experts. Strontium (Sr) can improve bone development rapidly, and it is naturally present in hard tissues (around 1wt%) (Aati, 2017). According to previous studies, the substitution of $Sr^{2+}$ ions in monetite may upgrade the mechanical strength and its dissolution rate (Huang et al., 2014; Romieu et al., 2010).

Osseous materials are generally recommended to treat the defective parts of the living body in orthopedic surgery (Wang et al., 2007). However, various complications are associated with monetite materials, which limits their long-term applications in orthopedic or dentistry. Substituting some of the ions such as $Sr^{2+}$, $Ba^{2+}$, $Zn^{2+}$, $Cr^{3+}$, $Mg^{2+}$, $Eu^{3+}$ or some polymeric substances in the monetite is suggested to sort out some deficiencies including poor compression strength, fracture toughness, low biodegradability, injectability, and setting time problems. For example, the compression strength (an improvement in Young's modulus) of the monetite cement can be increased up to 100% by substituting 5% chitosan in it (Planell, 2009). Similarly, in 2013, Boroujeni et al. synthesized the multi-walled carbon nanotubes (CNT) incorporated monetite cement as a bone defect repair material. The results confirmed that CNT incorporated monetite has the necessary characteristics and bears

28

appropriate setting time, which is the primary requirement for surgical procedures. Moreover, 1wt% incorporation of multi-walled CNT helped shorten the monetite setting time and enhanced its compression strength from 11.1 MPa to 21.6 MPa. In another study, monetite incorporated with Silica ($SiO_2$) was synthesized using microwave-assisted technique (Luchini, 2012).

The incorporation of $SiO_2$ improved the compression strength (40-60 MPa). In this research, the effect of nano-sized $SiO_2$ on the setting ability of the material, diametral tensile strength, and morphology of the cement was also studied. Various studies regarding the substitutions of different ions or composite materials in the monetite have confirmed the physical, chemical, and biological properties of monetite. Any biomaterial, once injected into the body, should allow cellular ingrowth, which is essential to resorb the newly formed tissues and support new bone growth. Zinc ($Zn^{2+}$) ions, for example, showed a potential for promoting and sustaining bone growth *in vivo* and *in vitro* (Ito et al., 2002; Ovesen et al., 2001; Qiao et al., 2014). Cama et al. (2017) synthesized $Zn^{2+}$ incorporated monetite and reported its role in the differentiation of mesenchymal stem cells (Cama et al., 2017).

This study confirmed that $Zn^{2+}$ incorporated in β-TCP did not hinder monetite precipitation and $Zn^{2+}$ ions entered the β-TCP crystal lattice differently over the monetite counterpart (according to XRD results). The results further confirmed the discharge of $Zn^{2+}$ ions from 0.004 to 1.35 mM, and further up-gradation in cell proliferation was observed after 7 to 14 days. This study also found that various concentrations of $Zn^{2+}$ ions had different biological responses, such as favoring the cell growth and inhibiting the osteogenic differentiation (Cama et al., 2017). Similar to bone surgical studies, teeth surgical studies need attention. It is essential to protect the adjoining teeth in dental refurbishment work when removing the filling mass from the mouth. Monetite doped with different amounts of Europium ($Eu^{3+}$) ions acted as a fluorescent material for dental renewal studies (Chen et al., 2018b). The results confirmed that $Eu^{3+}$ doped monetite showed two moderate bands around 699 and 593 nm and powerful fluorescent peaks at 616 nm. They further ensured that $Eu^{3+}$

substituted cement is the potential material fluorescent representative for dental restorations. Kaygili et al. (2017) prepared the $Ni^{2+}/Al^{3+}$, $Ni^{2+}/Mn^{2+}$ and $Al^{3+}/Mn^{2+}$ co-substituted monetite cements and undoped monetite through a wet chemical technique.

XRD results demonstrated that the dopants have a positive effect on the structure of monetite and its lattice parameters. Medvecky et al. (2018) described the formulation of a new toothpaste composed of a mixture of bioactive TTCP/monetite and fluoride, which manifested worthy dentine mineralization prospective under demineralization cycling analogous two-commercial toothpaste. This study revealed that almost all available toothpaste could stimulate superficial micro hardness recovery than saliva treated dentine samples and reduce the numerous open dentin tubules. However, the newly formulated fluoride toothpaste showed significant stability. The bioactivity property of the CP cements is an important parameter that is always considered before injecting them into the living system. The bioactivity of the CP cements coating can be controlled using different precipitation protocols and by the addition of various ions of $Zn^{2+}$, $Sr^{2+}$ and $Mg^{2+}$ into their crystal lattice. In recent years, the replacement of $Sr^{2+}$ ions into the CP cements has attracted escalating attention because of their exceptional potential in enhancing new bone development.

Concerning this behaviour of $Sr^{2+}$ ions, a study probed into the effect of $Sr^{2+}$ ions on CP structure using the chemical deposition technique (da Rocha et al., 2019). This work introduced a novel path to synthesize $Sr^{2+}$ doped CP coatings on metallic substances containing 5, 10, and 15 mol% $Sr^{2+}$ concentrations by the chemical method. The results showed that 5% Sr-monetite formulation could be the best alternative for HA coating due to its improved biological performance. However, in another study, with the addition of melt-derived 45S5 bioactive glass, a tetra calcium phosphate/nano-monetite composite was fabricated (Stulajterova et al., 2017).

A study focused on *in vitro* mesenchymal stem cell (MSC) response after synthesizing of the composite cement. The phase composition and compression

strength of the cement were also studied. In addition, a study observed the straight influence of released Ca and Si ions on the in-situ expansion of surface texture with analogous morphology on proliferation mesenchymal stem cells along with pH changes. It concluded that an increase took place in the compression strength and setting time after adding 15 wt.% bioglass. Similarly, a change in morphology was detected on inducting bioglass, which was beneficial for cell adhesion and proliferation.

So far, numerous studies have been conducted to develop a suitable bioceramic that can meet all the criteria for hard tissue replacement material. To this end, a team of researchers synthesized $BaTiO_3$ substituted monetite, which was expected to enhance the electrochemical effect of the material due to the piezoelectric nature of the $BaTiO_3$ (Koju et al., 2018). This study was unique because the increased electrochemical character of the monetite could be beneficial to promote fracture healing at the defective site and bone integration with the implant. It is a well-known fact that the bioceramic materials like monetite, brushite, HA, or TCP have poor mechanical strength, poor biodegradability rate, and weak biological performance. All these characteristics of the monetite can be upgraded using various ions like $Mg^{2+}$, $Sr^{2+}$, $Zn^{2+}$, chitosan, and CNT. The influence of CNT doping in the monetite cement was also studied, and the results confirmed that substitution of CNT and chitosan enhances both the mechanical and biological performance of the monetite and, at the same time, broadens their scope for orthopedic and dentistry applications (Boroujeni, 2012).

Recently, applications of rare earth elements in orthopedic fields have received significant attention. Lanthanum (La) is an important rare earth element that has been widely utilized in clinical applications (Yu et al., 2017). In 2005, the use of $La^{3+}$ ions in the form of lanthanum carbonate ($La_2(CO_3)_3$) for hemodialysis patients was approved by the U.S. Food and Drug Administration (FDA), although it was used as phosphate binders (Qazi & Martin, 2008). $La^{3+}$ ions were also used as a tracer to study tight junctions in epithelia by transmission electron microscopy (Nilsson et al.,

2006). Dawei et al. reported that $La^{3+}$ ions at a concentration of $1x10^{-5}$ mol/L significantly increased the alkaline phosphatase activity of Rat calvarial osteoblast-like cells (ROB cells) up to 3 folds (Dawei et al., 2007) and significantly inhibited the bone resorption (Zhang et al., 2003). In general, $La^{3+}$ ions are known as Ca-substituting ions in apatite (Lou et al., 2015). The incorporation of $La^{3+}$ ions in HA improves both the physicochemical and biological properties of HA. $La^{3+}$ doped HAs were synthesized by solid-state reaction, and it was observed that incorporation of $La^{3+}$ ions stabilized its apatite structure (Serret et al., 2000). Furthermore, it was demonstrated that adding $La_2O_3$ into $B_2O_3$-HA composites enhanced particle growth and increased tensile strength with no toxic effect on the human osteosarcoma cell line (Saos-2) (Khoshsima et al., 2018). In another study, $La_2O_3$ augmented the compression strength and microhardness in the bioceramics (Oktar et al., 2006).

Some recent studies confirmed that doping of various biocompatible oxides such as graphene oxide (GO), zirconia ($ZrO_2$), or $La_2O_3$ improves the mechanical properties and biological behaviours of DCP cements (Aissa et al., 2009; Liu et al., 2014; Suchanek & Yoshimura, 1998). Furthermore, $La_2O_3$ is non-toxic and has the capability of improving the biological properties of biomaterials (Gerber et al., 2012). Similarly, $La^{3+}$ has a wide range of biomedical applications, and its incorporation in the apatite cements may enhance its flexural strength and alkaline phosphatase activity (Guo et al., 2009; Yu et al., 2017). In short, rare earth elements such as $La^{3+}$, $Ce^{3+}$, and $Eu^{3+}$ have the potential to be used in biomedical applications (Pazarlioglu & Salman, 2019; Willbold et al., 2015).

Moreover, GO was found to be highly attractive due to its electrical, thermal, and mechanical properties (Dikin et al., 2007; Liang, Neophytou et al., 2008). Graphene can be used as a filling material in the nanocomposites to introduce super mechanical and optical properties (Ishigami et al., 2007). Graphene composites are also promising in emerging fields such as biosensors, blood-compatible bio-composites, and biocompatible gels (Choi et al., 2010; Lu et al., 2008). GO-based composites were synthesized and found reliable in various biological solutions and used for

32

hydrophobic drugs (Bai et al., 2010). Some other GO composites were found to possess antibacterial, specific targeting capability, mild cytotoxicity, and anti-thrombogenic characteristics with improved cell adhesion behaviour  (Cai et al., 2011; Meng et al., 2010; Zhou et al., 2009). Additionally, GO-based composites are reported to promote beneficial biomedical applications due to their exceptional mechanical and biocompatible properties (Hu et al., 2010; Li et al., 2014b).

Briefly, GO-based materials are attributed to the development of next-generation of biocomposites and biosensors. This fascinating character of GO may be the result of its good water dispersibility, high affinity for various biomolecules, and biocompatibility (Lee et al., 2016). These properties demonstrate that many novel biological sensing materials with improved setting time, superior mechanical properties, and excellent clinical applications can be synthesized.

# CHAPTER 3

# 3. MATERIALS AND METHODS

## 3.1. Materials and Chemicals

Calcium nitrate tetrahydrate ($Ca(NO_3)_2.4H_2O$) (Merck, Germany), diammonium hydrogen phosphate (($NH_4)_2HPO_4$) (Merck, Germany), and Lanthanum (III) nitrate hexahydrate ($La(NO_3)_3 \cdot 6H_2O$) (Merck, Germany) were used as sources of $Ca^{2+}$, $(PO_4)^{3-}$ and $La^{3+}$ ions, respectively. Ammonium hydroxide ($NH_4OH$) (Merck, Germany) was used to adjust the pH value. Monocalcium phosphate monohydrate (MCPM) powder (Sigma Aldrich, USA) was used as the main material to prepare DCP. Graphite powder (Ave. size: 3 μm, Ege Nanotek, Turkey), potassium permanganate ($NH_4OH$) (Merck, Germany), sulfuric acid ($H_2SO_4$) (Merck, Germany), phosphoric acid ($H_3PO_4$) (Merck, Germany), and hydrogen peroxide ($H_2O_2$) (Merck, Germany) were used to prepare Graphene oxide (GO).

## 3.2. Sample Preparation

### 3.2.1. Preparation of Pure and La Doped β-Tricalcium Phosphate

βTCP and La-βTCP powders were synthesized by microwave-assisted wet precipitation method. About (9-x M) of $Ca(NO_3)_2.4H_2O$ and $La(NO_3)_3 \cdot 6H_2O$ (x M) were dissolved in 200 mL of distilled water (dH₂O) and stirred until they completely dissolved to form solution A. (6M) of (($NH_4)_2HPO_4$) was dissolved in 200 mL of dH₂O and stirred until it dissolved forming solution B. Then, solution B was added dropwise (using separation funnel) into solution A under vigorous stirring for 30 min at room temperature (RT). The pH of the precipitated slurry was maintained at 7 by the addition of $NH_4OH$ as needed. The reaction mixture was loaded in a round bottom

35

flask (500 mL) and heated under microwave irradiation for five minutes in an 800W household microwave (SAMSUNG, MS23F301EAW). The precipitated slurry was collected by means of a filtration process, washed with $dH_2O$, then dried in an oven at 80°C for overnight, and finally calcined in a muffle furnace at 1000°C for two hours. All groups are listed in Table 3.1.

**Table 3.1.** The nominal composition of βTCP and La- βTCP samples.

| Samples ID | Chemical formula $Ca_{9-x}La_x (PO_4)_6$ | Reactants (M) | | |
|---|---|---|---|---|
| | | $Ca^{2+}$ | $(PO_4)^{3-}$ | $La^{3+}$ |
| βTCP | $Ca_9(PO_4)_6$ | 9.00 | 6.00 | 0.0 |
| 1La- βTCP | $Ca_{8.910}La_{0.09} (PO_4)_6$ | 8.910 | 6.00 | 0.090 |
| 2La- βTCP | $Ca_{8.775}La_{0.225} (PO_4)_6$ | 8.775 | 6.00 | 0.225 |
| 3La- βTCP | $Ca_{8.550}La_{0.45} (PO_4)_6$ | 8.550 | 6.00 | 0.450 |

### 3.2.2. Preparation of Pure DCP and La Doped DCP Cements

Initially, β-Tricalcium phosphate (βTCP) and La doped βTCP samples were synthesized in the lab as described in Section 3.2.1. DCP cements were prepared by mixing βTCP (or La- βTCP) with MCPM powder (Sigma Aldrich, USA); then, the powder mixture was mixed with (0.8 mL) of water. The resulting mixture was blended until a homogenized paste was obtained. The cement formation reaction of this process is given in Equation (3.1) (Saleh et al., 2016):

$$Ca_3(PO_4)_2 + Ca(H_2PO_4)_2 \cdot H_2O + 7H_2O \rightarrow 4CaHPO_4 \cdot 2H_2O \qquad \text{Eq. 3.1}$$
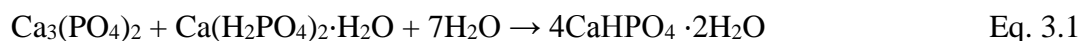
The amounts of reactants used to synthesise DCP and La doped DCP bone cements are reported in Table 3.2.

36

**Table 3.2.** The nominal composition of DCP and La- DCP samples.

| Sample ID | Reactants | | |
|---|---|---|---|
| | Powder Phase (Grams) | | Liquid Phase (mL) |
| | βTCP (or La- βTCP) | MCPM | $H_2O$ |
| DCP | 1.00 | 0.50 | 0.80 |
| 1La- DCP | 1.00 | 0.50 | 0.80 |
| 2La- DCP | 1.00 | 0.50 | 0.80 |
| 3La- DCP | 1.00 | 0.50 | 0.80 |

### 3.2.3. Production of Graphene Oxide from Graphite Particles

The tour method was used to produce GO from graphite powder (Marcano et al., 2010). The graphite powder (3 g) was mixed with potassium permanganate (18 g) in a glass beaker. A concentrated sulfuric acid and phosphoric acid (75%) solution was prepared in a 9:1 volume ratio and added into the powder mixture while stirring. An increase in the solution temperature up to 45ºC was observed, after which the temperature was set to 50ºC and the solution was stirred for 12 hours. Consequently, the colour of the solution turned from greenish to purple-brown, and heating was stopped. Ice cubes prepared from 400 mL of $dH_2O$ were added into a stirring solution, and when the ice melted, 3 mL of hydrogen peroxide solution was added into the mixture. In this step, the colour of the solution immediately turned into light yellow, indicating the formation of GO. The formed go particles were washed with $dH_2O$, HCl (30%) and $dH_2O$ orderly by precipitating with centrifugation (5000 g for 8 min). As the last step, GO nanoparticles were produced by separating GO flakes through homogenization at 12000 rpm.

### 3.2.4. Graphene Oxide/ Doped Calcium Phosphate Cement Composites

Based on the obtained results, the 2La- βTCP sample was selected to prepare to GO/DCP composites. 2La- DCP material was mixed with different fractions of GO to obtain GO/ doped DCP. The sample ingredients are described in Table 3.3.

**Table 3.3.** The chemical composition of La-DCP and GO/La- DCP samples.

| Sample ID | Reactants (Grams) | | | |
|---|---|---|---|---|
| | βTCP | MCPM | GO | $H_2O$ |
| La-DCP | 1.00 | 0.5 | 0 | 0.800 |
| 1GO/La- DCP | 1.00 | 0.5 | 0.0225 (1.5wt.%) | 0.812 |
| 2GO/La- DCP | 1.00 | 0.5 | 0.0375 (2.5wt.%) | 0.820 |
| 3GO/La- DCP | 1.00 | 0.5 | 0.0525 (3.5wt.%) | 0.828 |

### 3.3. Characterizations

### 3.3.1. X-Ray Diffraction Analysis

The purity and development of phases in the powders were identified using an X-ray diffractometer (XRD, Rigaku Ultima IV) that operated at 40 kV and 30 mA. Utilising CuKα radiation, diffraction patterns were taken in a 2θ range from 5° to 90° with a step size of 0.02° and scan speeds of 1s/step. The crystallinity noted by Xc corresponds to the fraction of crystalline βTCP phase in the investigated volume of powdered sample by using $Xc = 1 - V_{300/0210}/I_{0210}$, where $I_{0210}$ is the intensity of (0 2 10) reflection of βTCP structure and $V_{300/0210}$ is the intensity of the hollow between the (3 0 0) and (0 2 10) reflections. The crystallite size was calculated using the Debye–Scherrer equation, based on the diffraction plane of (0 2 10), as described in Equation (3.2).

$$x = \frac{0.9\lambda}{\beta \cos \theta}$$

Eq. 3.2

38

where $x$ = Crystallite size (nm), $\lambda$ = wavelength of the X-ray, $\beta$ = full width of the line at half of its maximum intensity in radians (FWHM) at (0 2 1 0) reflection, $\theta$ = diffraction angle.

### 3.3.2. Fourier Transform Infrared Spectroscopy

Presence of functional groups was confirmed using Fourier Transform Infrared Spectroscopy (FTIR, Bruker IFS66/S). All spectra were recorded in the scanning range of 4000-400 $cm^{-1}$ in transmission mode.

### 3.3.3. Scanning Electron Microscopy

The surface topologies and grain sizes were examined through scanning electron microscopy (SEM). To evaluate the particle size distribution, the size of the particles was measured in 100 random locations in SEM images using the image analysis software Image J (National Institutes of Health, USA). All samples were coated by Au prior to SEM imaging.

### 3.3.4. Inductively Coupled Plasma - Optical Emission Spectrometry

Inductively coupled plasma-optical emission spectrometry (ICP-OES, Perkin Elmer Optima 4300DV, USA) was used to determine the chemical compositions of the materials. Approximately 500 mg of sample was decomposed overnight in a mixture of 10 mL of concentrated nitric acid ($HNO_3$) and hydrochloric acid (HCl) at a ratio of 1:3. Then, the solution underwent several dilutions before injected inside analyzing chamber of ICP-OES.

### 3.3.5. Helium Pycnometer

Bulk density of powders was estimated using a Helium pycnometer (Ultrapycnometer 1000, Quantichrome Corporation, USA). In this device, gas displacement was used to measure volume accurately.

### 3.3.6. Brunauer-Emmett-Teller (BET) $N_2$ Absorption

The specific surface area (SSA), pore size distribution, and pore volume of the sample powders were measured using Brunauer, Emmett and Teller (BET-Multiple point, Quantachrome Corporation – Autosorb 6, USA).

### 3.3.7. Thermogravimetric Analysis

The thermogravimetric analysis (TGA) was carried out under a nitrogen atmosphere (Perkin Elmer Pyris 1) from RT to 950 ℃. Depending on the temperature, changes in the sample weights were monitored to study the thermal stability of the prepared materials.

### 3.3.8. Diffuse Reflectance UV-Vis Spectroscopy

The absorption spectra of GO/La doped DCP composites were recorded on Varian Cary 100, UV-Vis-NIR spectrophotometer within a 200-800 nm spectral range with the resolution of about 0.2 nm.

### 3.4. Analysis of Physical and Mechanical Properties

### 3.4.1. Bone Cement Setting Time Measurements

The setting time of cements paste was measured using the instruments and procedure specified in ASTM C266-15. The cement paste was obtained by mixing 1 gram of

β-TCP (or La-βTCP) with 0.5 grams of MCPM. The powders were mixed manually using a mortar pestle to obtain a homogeneous phase; then, about 0.8 mL of $H_2O$ was added to the powders mixture to prepare cement paste. The cement paste was moulded in Teflon rings (14 mm diameter and 5 mm height). The setting time tests were conducted at RT using a 113 g Gillmore needle with a tip diameter of 2.12 mm to measure the initial setting time ($T_i$) and a 453.5 g Gillmore needle with a tip diameter of 1.06 mm to measure the final setting time ($T_f$). Four samples per group were used.

### 3.4.2. Compressive Strength Tests

The DCP bone cement pastes were prepared and placed into cylindrical moulds (12 mm in height and 6 mm in diameter). The compressive strength was measured according to the ASTM F451-15 (F451-16, 2016). Briefly, the casted samples were removed from the containers, dried up at RT, then polished with 600 grit SiC papers to provide a smooth and flat surface. The compressive strength of specimens was measured using a Universal Instron testing machine (Instron 5565A, USA) at a cross-head speed of 4 mm/min until failure. The tests were performed in triplicate.

### 3.5. *In Vitro* Dissolution Behaviour

*In vitro* dissolution test was conducted using phosphate-buffered saline (PBS, pH 7.4) with 0.01% sodium azide (Sigma, USA). About 0.15 g  powder was immersed in 15 mL of PBS and incubated for different time intervals (1, 3, 7, and 14 days) at 37ºC. At the end of each interval, the samples were centrifuged at 12000 rpm for 20 minutes, and the supernatant was collected. The release profile of Ca, P and La ions in PBS media was alayzed using ICP-OES. Supernatant pH values were recorded using a pH meter (Thermo Orion 3 Star, Thermo Scientific, USA). The experiments were conducted in triplicate.

## 3.6. *In Vitro* Protein Adsorption and Desorption

The powder samples were weighted (0.15 g) and transferred into 15 mL falcon tubes. They were rinsed and wetted in PBS (pH:7.4, 0.1% Sodium azide) and centrifuged at 12000 rpm for five minutes to settle down. Supernatants were removed, and powder samples were immersed in Fetal bovine serum ((FBS), Thermo fisher scientific, USA) (1 mL) solution prepared PBS dilution (1:9, FBS: PBS). After a 24 hour incubation period, FBS solutions were collected and analysed for protein content with bicinchoninic acid ((BCA), Sigma, USA) protein assay. For protein desorption study, incubation media was exchanged to PBS (pH:7.4, 0.1% Sodium azide), and protein desorption from powder samples was detected with BCA assay after the 24 hour incubation period. Protein concentrations were determined from a previously plotted calibration curve with known concentrations of protein (Bovine serum albumin) solutions. The experiments were carried out in triplicate.

## 3.7. *In Vitro* Cell Culture Experiments

*In vitro* cell viability, Alkaline phosphatase (ALP) activity, and cell adhesion studies were conducted with Human osteosarcoma cell line (Saos-2) (ATCC, USA). Cell growth was maintained in Dulbecco's modified Eagle medium (DMEM, Merck, Germany) supplemented with FBS (10%) and penicillin-streptomycin (1%) (Invitrogen, USA), with incubation in a $CO_2$ incubator (Shel Lab, USA) at 37°C. DCP bone cement groups were cast into a disc shape for cell viability test and extract preparation. The cement discs were sterilized by incubation in ethanol solution (70%) followed by UV irradiation (254 nm)  for 30 minutes for each side. According to the International Standard for Biological Testing of Medical Devices, extracts of the cement discs were prepared in growth or differentiation medium at 0.20 g/mL concentration (Tsukimura et al., 2009). The extracts of the groups were obtained by incubating discs in media at 72 h for 37°C. The prepared extracts were diluted with media to obtain different extract concentrations.

### 3.7.1. Indirect Cell Viability

Indirect cell viability of disc groups (entire materials) was compared with Alamar Blue assay after incubating Saos-2 cells in extract media for 1, 4, and 7 days. Alamar Blue solution (10% v/v) was prepared by diluting in DMEM without phenol red. After incubations, media was discarded from wells, and wells were rinsed with PBS. Alamar Blue solution (100 µL/well, 96 well plates) was added, and the well plate was incubated for four hours in the dark at 37°C. Then, Alamar Blue solutions of each well were transferred to a new plate, and a microplate reader (Biotek Instruments Inc., µOuantTM, USA) was used to measure the optical densities of wells at 570 and 600 nm wavelengths. After rinsing with PBS, extract media of wells were replenished for further incubation.

### 3.7.2. Direct Cell Viability

A direct cell viability study was performed by incubatingSaos-2 cells directly on DCP bone cement discs' surface. Cement discs were cast to fit in 48 well plates. Cells were seeded onto the disc's surface ($2\times10^4$ cells/disc) in a drop of media (50 µL). After two hours of incubation for initial attachment at 37°C, media were completed to 500 µL for incubation through 1, 4, and 7 days. After the first day of incubation, discs were transferred into a new plate in order to separate the cells that proliferated on discs from those that proliferated on the cell culture plate. Alamar Blue assay was conducted at each incubation time point to compare the cell viability among groups with the method described in Section 3.7.1. Indirect Cell Viability. Alamar Blue solution was applied at 500 µL/well since 48 well plates were used for direct cell viability.

### 3.7.3. Alkaline Phosphatase Activity

The osteogenic medium was prepared for Alkaline Phosphatase Activity (ALP) test by dissolving ascorbic acid (AA) (50 µg/mL), β-glycerophosphate (10 mM), and

dexamethasone ($10^{-8}$ M) in a growth medium. In order to compare the ALP activity of Saos-2 cells, extract media of cement groups were prepared in an osteogenic medium as described in the previous section '*In Vitro* Cell Culture Studies,' and cells were incubated in these extracts for 7 and 14 days. At the end of the incubation periods, ALP activities of cells were measured by preparing cell lysates in PBS. Briefly, wells were rinsed with PBS, and the culture plate was incubated for 30 minutes at -80°C and 30 minutes at 37°C. The same freeze-thawing cycle was repeated after adding 500 µL of PBS in wells, and cell lysate was obtained as it dissolved in PBS. To determine the ALP activity, 75 µL of cell lysates were incubated with 75 µL of p-nitrophenyl phosphate (pNPP) substrate and 25 µL of $MgCl_2$ (10 mM, catalyst) in 96 well plates in the dark for one hour at 37°C. After incubation, the optical density of wells was measured at 405 nm wavelength. The ALP activity was determined from the calibration curve plotted with known amounts of p-nitrophenol. Specific ALP activity (nmol/µg protein/min) was calculated after BCA assay detecting protein contents in cell lysates. BCA assay was conducted according to the method described in Section 3.6. *In vitro* Protein Adsorption and Desorption Experiments.

### 3.7.4. Confocal Laser Scanning Microscopy Analysis

Cell morphology was determined by confocal laser scanning microscopy (CLSM, Leica DM2500, Germany) seven days after incubation with cement extract groups. The cement extract groups with 0.2 g/mL concentration were selected based on cell viability results for confocal imaging. After seven days of growth, cells were fixated (4% paraformaldehyde, 15 min) and incubated with Triton X-100 solution (0.1% (v/v) in PBS, 5 min) before cell staining. Alexa Fluor 488 phalloidin solution (1%) was prepared in 0.1% BSA solution and incubated for one hour with cells to stain cytoskeletons. Cell nuclei were stained with DAPI (1 µg/mL, 10 min, 37°C). Fluorescence of excitation at 488 nm for Alexa Fluor 488 phalloidin (green) and at 650 nm for DAPI (red) were used for the analysis.

## 3.8. Statistical Analysis

Statistical data analysis was performed and analysed with a one-way analysis of variance with Tukey's post hoc test for multiple comparisons using SPSS software (SPSS 22 Software Program, USA). Differences were considered significant at $p \leq 0.05$.

# CHAPTER 4


# 4. RESULTS AND DISCUSSION


## 4.1. Preparation and Characterizations of Lanthanum Doped βTCP Materials

XRD patterns of βTCP and La$^{3+}$ doped βTCPs calcined at 1000 ºC for two hours are illustrated in Figure 4.1. All XRD patterns show characteristic diffraction lines of βTCP, which is confirmed against a standard phase of βTCP (JCPDS No: 09-0169). No other CP phases could be detected, which confirms the phase purity of βTCP. Furthermore, the peaks apparent in the sharp or narrow shape demonstrated the high crystallinity nature of βTCP powder. With the incorporation of La$^{3+}$ ions, line shifting, peak broadening, and peak intensity changes were observed. Shifting peaks lower than 2θ was attributed to the replacement of smaller size Ca$^{2+}$ ion (0.099 nm) with larger size La$^{3+}$ ion (0.106 nm), which caused an expansion in lattice parameters of βTCP along with a and c axis (Table 4.1) (Geng et al., 2016). It might also be attributed to the greater structural strain and smaller particle size in the La-βTCP than in the pure βTCP (Gamal et al., 2013; Ofudje et al., 2019). Broadening of the peaks was assigned to small crystallite size and lattice micro-strain (Gencalp & Saklakoglu, 2017). Previous studies attributed the broadening and shifting of the peaks to the reduction in the crystallite size and expansion in the lattice disorder (Alshemary et al., 2019) (Table 4.1). Furthermore, a reduction in peak intensities indicates the diminution of the crystallinity degree (Alshemary et al., 2019).
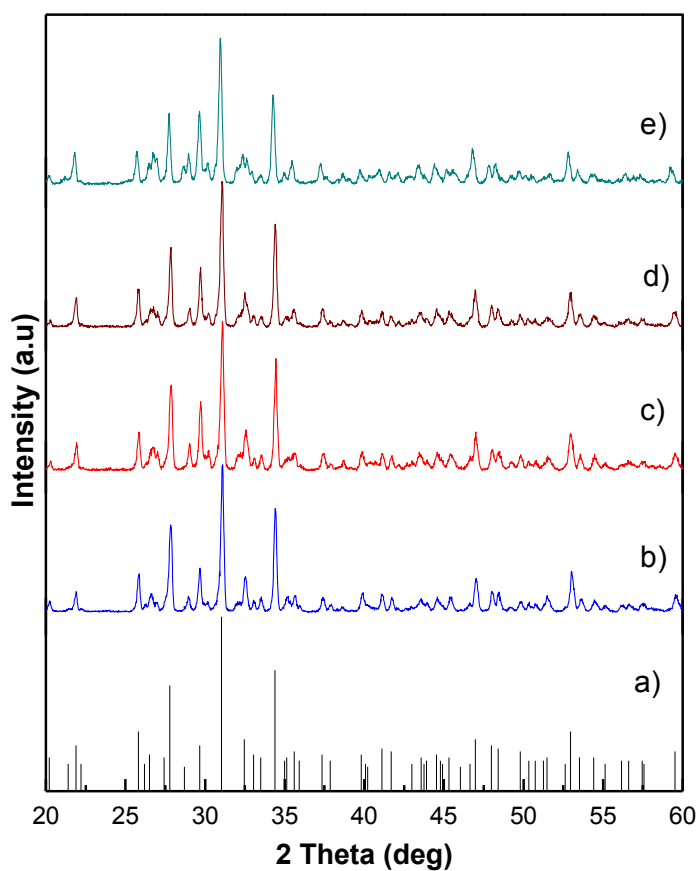
**Figure 4.1.** XRD patterns of βTCP and La$^{3+}$ doped βTCP, calcined at 1000ºC for 2 h, a) βTCP (JCPDS No: 09-0169), b) βTCP, c) 1La-βTCP, d) 2La-βTCP, e) 3La-βTCP.

**Table 4.1.** Degree of crystallinity and lattice parameters of βTCP and La$^{3+}$ doped βTCP, calcined at 1000ºC for 2 h.

| Sample ID | Lattice parameters | | | | Crystallite size (nm) by XRD | Particle size (nm) by SEM |
|---|---|---|---|---|---|---|
| | a (Å) | c (Å) | V (Å)$^3$ | Crystinallity (%) | | |
| JCDPS (βTCP) | 10.412 | 37.318 | 3503.6 | ---- | ---- | ---- |
| βTCP | 10.413 | 37.312 | 3503.9 | 99.97 | 45.85 | 830 |
| 1La- βTCP | 10.416 | 37.366 | 3510.8 | 96.97 | 42.04 | 1001 |
| 2La- βTCP | 10.424 | 37.382 | 3517.4 | 97.57 | 42.46 | 730 |
| 3La- βTCP | 10.455 | 37.443 | 3544.4 | 95.81 | 11.47 | 680 |

48

The chemical nature of βTCP indicates that it has the ability to undergo cationic substitution with Ca ions, and the dopant will be hosted in one of five crystallographic sites of Ca, the preferential occupancy determined based on charge and ionic sizes of dopant (Meenambal et al., 2014). For instance, monovalent ions ($Na^+$ and $K^+$) have ionic charges lower than $Ca^{2+}$ ions, and they prefer to occupy at the Ca (4) site (Matsumoto et al., 2010; Meenambal et al., 2014). The occupancies of divalent ions ($Cu^{2+}$, $Zn^{2+}$, and $Mg^{2+}$), which hold smaller ionic size, took place at site Ca (5), while substitution of bigger sized ($Sr^{2+}$) resulted in their preferred occupancy at the Ca (4) site (Enderle et al., 2005; Kannan et al., 2011; Kawabata et al., 2011; Meenambal et al., 2014). The case of trivalent confirmed that the bigger ions ($Nd^{3+}$, $La^{3+}$) tend to occupy the Ca (3) site (Bessière et al., 2012; Meenambal et al., 2014). In this study, it is believed that $La^{3+}$ ion doping into the crystal structure of βTCP takes place at site Ca (3), giving rise to the formation of La-βTCP.

It is well known that the substitution of divalent $Ca^{2+}$ ions by trivalent $La^{3+}$ ions requires charge neutrality. Two competing mechanisms have been proposed for charge compensation. First, the substitution of $Ca^{2+}$ ions by $La^{3+}$ ions must be balanced by rises of negative charge through $OH^-$ to $O^{2-}$ ion transformation. This mechanism, however, is not applicable. It is possible in the case of HA, whereas the chemical structure of βTCP has no $OH^-$ group. Secondly, cationic vacancies (□) generated due to the charge difference between the $Ca^{2+}$ and $La^{3+}$ ions are suggested. The existence of vacancy maintains charge neutrality (Alshemary et al., 2015). The latter is thought to be more appropriate to describe the charge compensation for this study.

FTIR spectrum of βTCP and $La^{3+}$ doped βTCP materials sintered at 1000ºC for two hours are displayed in Figure 4.2, and the band assignment are given in Table 4.2 (Destainville et al., 2003; Pham Minh et al., 2013). The absorption bands related to the stretching mode of $PO_4^{3-}$ group ($\vartheta 2$) were seen at 460 cm$^{-1}$ and 498 cm$^{-1}$. The bands at 541 cm$^{-1}$, 607 cm$^{-1}$, 666 cm$^{-1}$ were associated with the bending mode of the $PO_4^{3-}$ group ($\vartheta 4$). The bands at 725 cm$^{-1}$ and 1210 cm$^{-1}$ were assigned to P–O–P

stretch and P=O stretch mode of $P_2O_7$ groups, respectively (Destainville et al., 2003; Pham Minh et al., 2013). Two more peaks at 937 $cm^{-1}$ and 971 $cm^{-1}$ were attributed to the $PO_4^{3-}$ group ($\vartheta 1$). Furthermore, other two peaks detected at 1012 $cm^{-1}$ and 1105 $cm^{-1}$ were attributed to the $PO_4^{3-}$ group ($\vartheta 3$). No bands were located at 755 $cm^{-1}$, 880 $cm^{-1}$, 961 $cm^{-1}$, 1410 $cm^{-1}$ or 1455 $cm^{-1}$, which confirmed that the prepared materials were free from the carbonate group (Gibson & Bonfield, 2002). No peaks for the hydroxyl group ($OH^-$) were observed at 630 $cm^{-1}$ or 3500 $cm^{-1}$, which indicated that the prepared materials were free from HA phase (Jaber et al., 2018). Similarly, no peaks were detected between 1387 $cm^{-1}$ and 1389 $cm^{-1}$, demonstrating that the obtained materials were free from $-NO_3^-$ groups from the synthesis starting material (Ofudje et al., 2019). Increased incorporation of $La^{3+}$ ions caused expansion in the band area, which might be attributed to the decreased crystallinity, which was also observed in the XRD analysis (Table 4.1).

Frequencies of bands of $PO_4^{3-}$ groups shifted to lower wavenumber values with the increasing amount of $La^{3+}$ in βTCP structure. Fowler, who discusses this behaviour, asserts that the frequencies of $PO_4^{3-}$ groups decrease nearly linearly with increasing a-axis dimension (as cited in Bigi et al., 1997).
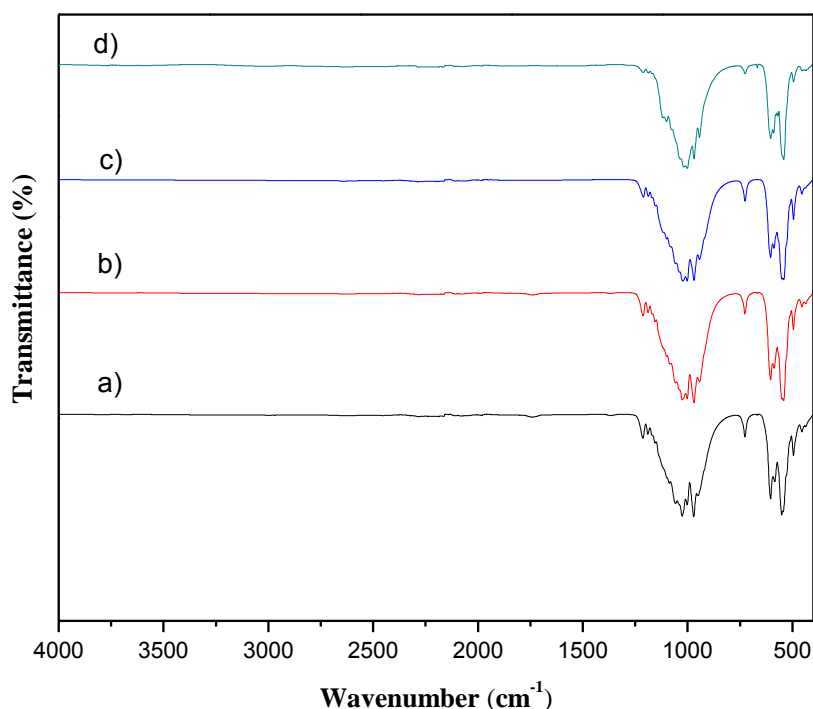
**Figure 4.2.** FTIR spectrum of βTCP and La$^{3+}$ doped βTCP, calcined at 1000ºC for 2 h, a) βTCP, b) 1La-βTCP, c) 2La-βTCP, d) 3La-βTCP.

**Table 4.2.** Band assignments for βTCP and La$^{3+}$ doped βTCP materials (Destainville et al., 2003; Pham Minh et al., 2013).

| Wavenumber (cm$^{-1}$) | Band assignment |
|---|---|
| 460-498 | Stretching mode of PO$_4^{3-}$ group ($\vartheta2$) |
| 541-607-666 | Bending mode of the PO$_4^{3-}$ group ($\vartheta4$) |
| 725-1210 | Stretching modes of P–O–P and P=O in P$_2$O$_7$ group |
| 937-971 | Stretching mode of PO$_4^{3-}$ group ($\vartheta1$) |

Microstructures of the βTCP and La$^{3+}$ doped βTCP materials calcined at 1000ºC are shown in Figure 4.3. All prepared samples showed that the particles were present in the form of irregular, spherical and tightly packed agglomerates, demonstrating that the incorporation of La$^{3+}$ ions had no noticeable effect on the morphology of βTCP particles, which was previously shown by Jadalannagari et al. (2014). The growth rate of βTCP particles was diminished by the increasing amount of La$^{3+}$ ion content in the sintered composites. However, the average particle size estimated from the

51

SEM micrographs was higher than the size determined by the Scherrer equation (Table 4.1). This mismatch between SEM micrographs and Scherrer equation was ascribed to particles coalescence leading to agglomerated particles. This grain growth could result from either superficial diffusion or gaseous phase transport (Senamaud et al., 1997).
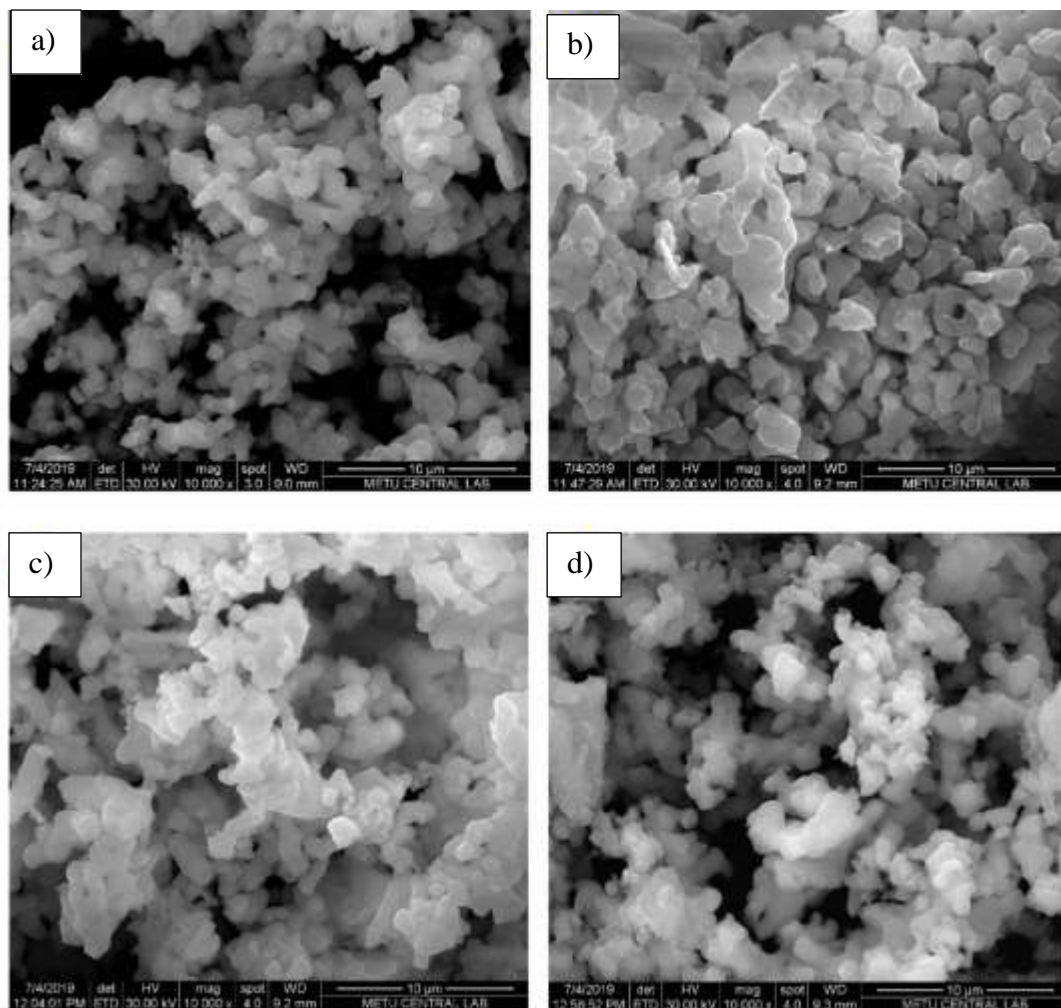


**Figure 4.3.** SEM micrographs of a) βTCP, b) 1La-βTCP, c) 2La-βTCP and d) 3La-βTCP.

The Ca/P ratio is a crucial parameter in osteochondral scaffold design (Boushell et al., 2017). Ca/P, La/(La+Ca), and (Ca+La)/P ratios of the βTCP and La$^{3+}$ doped βTCP materials were calculated and summarized in Table 4.3. The results showed that the La$^{3+}$ ions had been successfully doped into the crystal lattice of βTCP. According to

the amount of $La^{3+}$ in the samples, the Ca/P ratio of 1.39 for βTCP was lower than the standard value of 1.50 for βTCP. This reduction in Ca/P ratio could be attributed to the formation of $P_2O_7$ (Figure 4.2) (Berzina-Cimdina & Borodajenko, 2012). The La/(La+Ca) ratio was higher than the expected value and could be attributed to charge compensation. The proposed mechanism (ii) replaced 3 atoms of $Ca^{2+}$ ions by 2 atoms of $La^{3+}$ ions, resulting in a reduction in $Ca^{2+}$ ions more than the calculated value. The (Ca+La)/P molar ratio increased upon increased $La^{3+}$ ions doping into βTCP, but this relation is not linear due to preferential sputtering of $Ca^{2+}$ ions compared to $La^{3+}$ ions deriving from different atomic weight (Graziani et al., 2018). Overall, the (Ca+La)/P molar ratio was in the range of 1.31-1.62. However, this range was recognized for optimal osteoblast viability and promoted alkaline phosphatase activity in osteoblasts.

**Table 4.3.** Chemical composition of βTCP and La- βTCP materials measured by ICP-OES.

| Sample ID | Theoretical ratios | | Measured ratios by ICP-OES | |
|---|---|---|---|---|
| | La/(La+Ca) | (Ca+La)/P | La/(La+Ca) | (Ca+La)/P |
| βTCP | 0 | 1.50 | 0 | 1.39 |
| 1La- βTCP | 0.010 | 1.50 | 0.064 | 1.51 |
| 2La- βTCP | 0.025 | 1.50 | 0.108 | 1.62 |
| 3La- βTCP | 0.053 | 1.50 | 0.170 | 1.58 |

The textural characteristics of the βTCP and La-βTCP materials were examined using $N_2$ adsorption-desorption isotherms. Based on IUPAC classification, isotherms for all prepared materials are of type IV, and capillary condensation is accompanied by the narrow hemispherical meniscus, indicating that all the samples have mesoporous nature (Goh et al., 2014) (Figure 4.4). The amount of $N_2$ adsorbed increased with the addition of $La^{3+}$ ions, indicating an expansion in pore size (Table 4.4). The Specific surface area (SSA) for pure βTCP was about 4.751 $m^2/g$, which is higher than SSA of βTCP (~0.739 $m^2/g$) synthesis using the heating and quenching method (Gallinetti et al., 2014) (Table 4.4). However, SSA was reduced gradually as the amount of $La^{3+}$

increased in βTCP structure. Fluctuations in SSA values were observed, which could be ascribed to the differences in the particle size, porosity, pore size distribution, shape, and size (Amador & Martin de Juan, 2016) as well as to particles' coalescence (Senamaud et al., 1997).
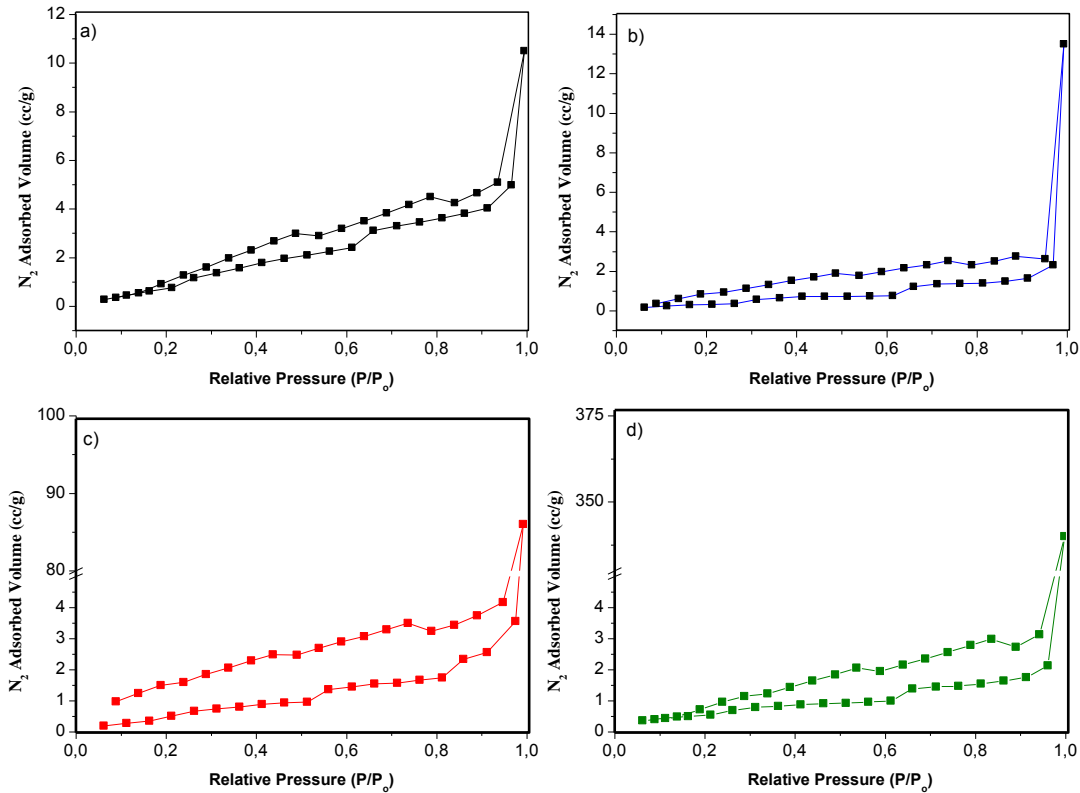


**Figure 4.4**. $N_2$ adsorption-desorption isotherm, a) βTCP, b) 1La-βTCP, c) 2La-βTCP and d) 3La-βTCP.

The pore volume and pore size increased gradually with the incorporation of $La^{3+}$ ions in βTCP structure (Table 4.4).  CP materials with mesoporous nature have become more attractive and frequently used for various medical applications (Wijesinghe et al., 2018).

The bulk density of βTCP and La-βTCP materials was also measured using a helium pyrometer (Table 4.4). It was deduced that the bulk density of βTCP was lowered than the theoretical value (3.14 $g/cm^3$). The same observation was reported by Unosson et al. ( 2015). The incorporation of $La^{3+}$ ions revealed a slight reduction in

bulk density mainly due to increased nonuniformity of particle packing (Galakhov et al., 1993) or possibly due to the coarse (Kim et al., 2014).

**Table 4.4.** Textural parameters obtained by $N_2$ adsorption measurement.

| Sample ID | Surface area ($m^2$/g) | Pore Volume ($cm^3$/g) | Pore Size (Å) | Bulk Density (g/ $cm^3$) |
|---|---|---|---|---|
| βTCP | 4.751 | 0.0185 | 22.51 | 1.3851 |
| 1La- βTCP | 1.372 | 0.0219 | 25.21 | 1.4467 |
| 2La- βTCP | 3.546 | 0.1374 | 44.38 | 1.3891 |
| 3La- βTCP | 2.038 | 0.5345 | 3808 | 1.3479 |

*In vitro* dissolution behaviour of pure and La doped βTCP materials was investigated in PBS solution at 37ºC for 14 days (Figure 4.5). The leaching of $Ca^{2+}$ ions from pure and La doped βTCP is shown in Figure 4.5 (A). After 14 days of incubation in PBS, the maximum leaching amount of $Ca^{2+}$ was up to 2.11 mg/L for pure βTCP. Compared to pure βTCP, doped βTCP showed a relatively low concentration of $Ca^{2+}$ leaching. The lowest amount of $Ca^{2+}$ release was observed from 3La-βTCP (1.15 mg/L), perhaps due to the slower dissolution of samples resulting from the increased structural stability of the lattice (Li et al., 2009), which indicates that the partial incorporation of $La^{3+}$ ions in the lattice causes chemical interactions and hence diminishes species mobility (Senamaud et al., 1997). Li et al. demonstrated that the inclusion of $Mg^{2+}$ ions into βTCP lattice improved structural stability and resulted in a lower solubility rate than pure βTCP. Furthermore, La- βTCP'ssurface area turned out to be lower than pure βTCP (Table 4.3), lowering its dissolution rate (Smolen et al., 2013). The release profile of $La^{3+}$ ions was illustrated in Figure 4.5 (B). As expected, the maximum amount of La was observed for 3La- βTCP at about 33 µg/L after 14 days of incubation in PBS. However, this concentration has a toxic effect based on previous studies (Balusamy et al., 2015).

The relationship between the soaking time in PBS and pH for all samples is shown in Figure 4.5 (C). The pH value decreased gradually by about 0.1 units with an

increasing incubation period for all the samples. This decline in the pH value was more evident for La doped βTCP materials than the βTCP material, which was ascribed to low release of $Ca^{2+}$ from La- βTCP, whereas $Ca^{2+}$ ion has the ability to make an ionic exchange with $H^+$ of PBS solution (Alshemary et al., 2015).
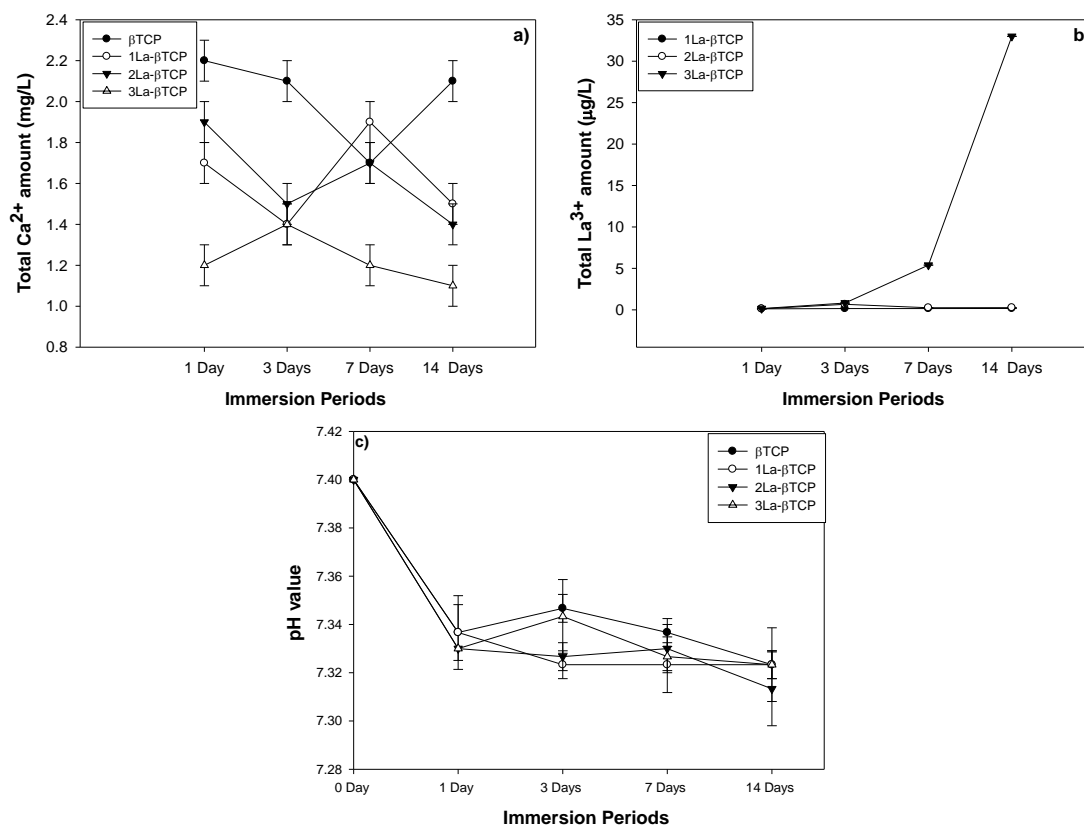


**Figure 4.5.** a) cumulative releases of $Ca^{2+}$, b) cumulative releases of $La^{3+}$ and c) changes in pH of PBS with immersion periods for La- βTCP series.

Protein adsorption is one of the first *in vivo* responses after implantation of a biomaterial in the human body (Felgueiras et al., 2018). The type and amount of adsorbed proteins on the surface play an important role in cell-material interactions. Therefore, investigation of the interaction between proteins and bioceramic surface has crucial importance for several biomedical applications (Yu & Chen, 2015). This thesis investigates protein (FBS) adsorption and desorption on and from βTCP and La-βTCP particles after 24 hours of incubation in FBS solution, and the results are presented in Figure 4.6. After the incubation period, the total FBS adsorbed on βTCP particles was 7.5 µg/mL. This adsorbed amount was reduced to 2.9 µg/mL with an

addition of minimum concentration of $La^{3+}$ ions (1La-βTCP). This reduction could be due to the shrinkage in the surface area (Table 4.4). Furthermore, protein adsorption increased in parallel to increasing La doping concentration in La- βTCP series, and it was measured as 6.65 µg/mL for 3La- βTCP. Previously, the protein adsorption capacity of βTCP was reported to be higher than hydroxyapatite (Wang et al., 2014). In the study by Ling-Ling et al., protein adsorption of βTCP from FBS stock solution (0.25% ) was reported to be around 18%. Also, in this study, protein adsorption of the βTCP group was at similar levels (20.39 ± 5.49) after a 24 hour incubation (Ling-Ling et al., 2010). The study of Ellingsen and Pinholt (1995) proposed that, when titanium implants were pre-treated with La, adsorption of human serum proteins increased due to increased positive charge with $La^{3+}$ ions. The desorption rate of FBS from pure βTCP disc surface was 2.93 µg/mL. The desorption rate decreased with increasing La into βTCP, whereas the minimum FBS desorption rate from 3La- βTCP disc surface was 2.44 µg/mL. This behaviour could be attributed to electrostatic forces between La- βTCP and FBS molecules.

The viability of Saos-2 cells treated with βTCP and La-βTCP materials was studied using the indirect method over seven days of incubation at 37ºC. Extracts from the βTCP and La-βTCP materials were collected, and the concentration of the stock solution was equal to 0.20 g/mL. Then, serial dilutions were made 0.10 g/mL, 0.05 g/mL, 0.025 g/mL, and 0.0125 g/mL, respectively. The diluted extracts were cultured with Saos-2 cells, and the samples were incubated over 1, 4, and 7 days of incubation periods at 37ºC (Figure 4.7). On the first and fourth days of incubation, the cell viability of 0.20 g/mL concentration of βTCP and La-βTCP materials was similar or slightly higher than the control media group, indicating that none of the groups have a toxic effect on Saos-2 cells. On day four of incubation periods, 2La-βTCP and 3La-βTCP groups showed 37.2±1.2% and 37.5±0.5% cell viability. They were strikingly higher than those of the pure βTCP and control media at 0.0125 g/mL concentration, suggesting that $La^{3+}$ ions doping can improve cell viability at specific concentrations.

**Figure 4.6.** Protein a) adsorption and b) desorption on/from βTCP and La$^{3+}$ doped βTCP after 24 h incubation periods.

The viability of Saos-2 cells treated with βTCP and La-βTCP materials was studied using the indirect method over seven days of incubation at 37°C. Extracts from the βTCP and La-βTCP materials were collected, and the concentration of the stock solution was equal to 0.20 g/mL. Then, serial dilutions were made 0.10 g/mL, 0.05 g/mL, 0.025 g/mL, and 0.0125 g/mL, respectively. The diluted extracts were cultured with Saos-2 cells, and the samples were incubated over 1, 4, and 7 days of incubation periods at 37°C (Figure 4.7). On the first and fourth days of incubation, the cell viability of 0.20 g/mL concentration of βTCP and La-βTCP materials was similar or slightly higher than the control media group, indicating that none of the groups have

a toxic effect on Saos-2 cells. On day four of incubation periods, 2La-βTCP and 3La-βTCP groups showed 37.2±1.2% and 37.5±0.5% cell viability. They were strikingly higher than those of the pure βTCP and control media at 0.0125 g/mL concentration, suggesting that $La^{3+}$ ions doping can improve cell viability at specific concentrations.

Conformably through the incubation period, the 3La-βTCP group at 0.0125 g/mL concentration tended to have significantly higher cell viability of Saos-2 cells among other groups. With a prolonged culture period (seven days), the Alamar blue reduction per cent of βTCP, 1La-βTCP and 2La-βTCP groups, at 0.025 g/mL concentrations were about 45.1±1.8%, 42.6±1.4%, and 41.6±1.4%, respectively. At 0.0125 g/mL concentrations, they were about 43.2±1.0%, 44.3±1.0%, and 43.9±0.6%, respectively. They showed significantly higher cell viability than the control media group (34.2±1.3%). The 3La-βTCP group with the highest $La^{3+}$ concentration supported the highest cell viability (65.4±4.8%) after seven days of incubation at 0.0125 g/mL concentration among all samples. The study conducted by Von Rosenberg and  Wehr (2012) investigated the impact of $La^{3+}$ salts on bone metabolism and found that $La^{3+}$ salts enhance osteoblast activity, resultinhg in higher serum osteocalcin, and improved bone mineral density in osteoporotic OVX rats(Von Rosenberg & Wehr, 2012). The physicochemical characteristics of $La^{3+}$ ions were reported to be similar to $Ca^{2+}$ ions (Liu et al., 2015).
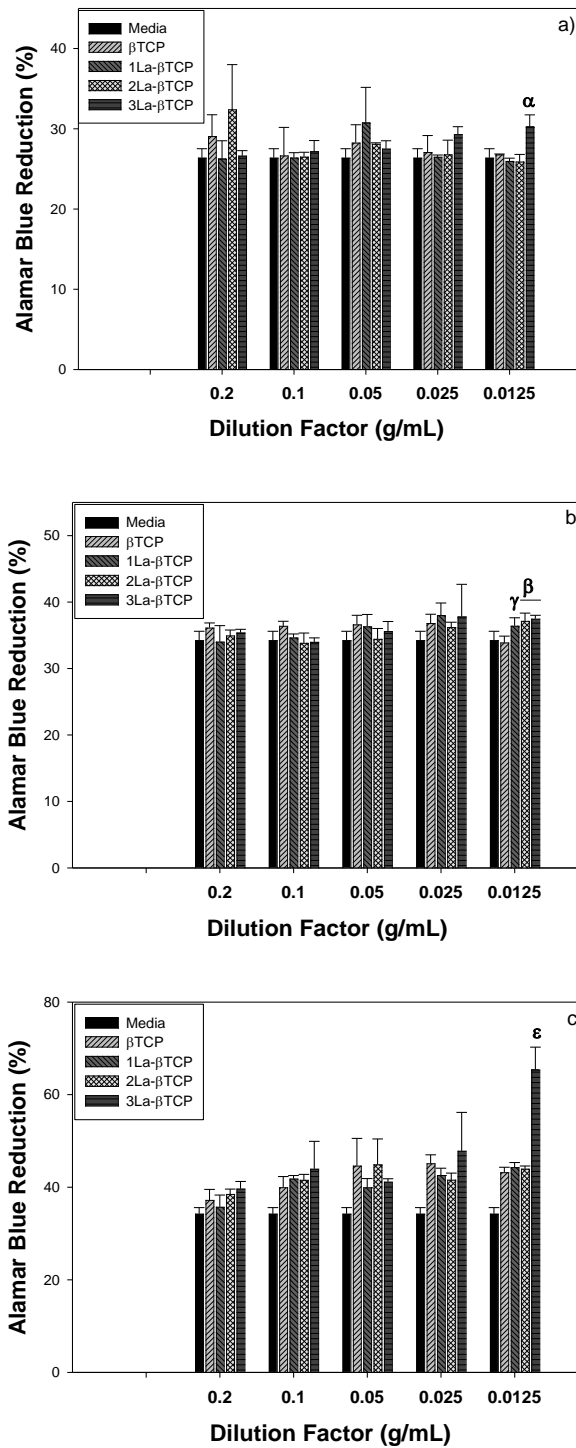
**Figure 4.7.** Alamar Blue cell viability assay of Saos-2 cells cultured with different dilutions of βTCP and La-βTCP materials extracts after a)1, b) 4, and c) 7 days of incubation. Values are means ± SD (n=4); $p^\alpha < 0.05$, $p^\gamma < 0.05$, $p^\beta < 0.05$ and $p^\varepsilon < 0.05$ were considered.

60

Furthermore, lanthanides enhanced osteoblast proliferation while suppressing osteoclast differentiation (Dang et al., 2019). This positive effect of La ions was reported to be strictly dose-dependent. It is considered as beneficial at low concentrations, while it can be toxic at high concentrations (Pagano et al., 2015). When La containing Ca-P particles interacted with bone marrow stromal cells at low concentrations ($10^{-9}$ M), cell viability increased, while at higher concentrations ($10^{-5}$ M), cell viability was suppressed (Bai et al., 2018). In the study of Liu et al., the proliferation rate of murine preosteoblast cell line (MC3T3-E1) was highest at the lowest $LaCl_3$ concentration, which was below the control group at $LaCl_3$ concentration higher than 1 µM (Liu et al., 2012). Also, an optimum concentration of $Ca^{2+}$ and $La^{3+}$ ions was reported to induce the proliferation of rBMSCs (Peng et al., 2019). Similarly, in this study, enhanced cell proliferation for seven days was achieved at 0.0125 g/mL extract concentrations of the 3La doped group. When the ion leaching experiment results were observed, the 3La-βTCP group showed the highest $La^{3+}$ release through 14 days of incubation, which was slightly lower than $Ca^{2+}$ release of other groups (Figure 4.5).

The La-βTCP and 2La-βTCP materials showed low release of La ions over 14 days of incubation. Through seven days of incubation, cell viability did not increase by the released amount of La in 0.2 g/mL extract of 3La-βTCP group. This result corresponds to studies that pointed to the dose dependent effect of La ions on cell viability (Bai et al., 2018; Liu et al., 2012; Pagano et al., 2015; Peng et al., 2019). When the extract of 3La-βTCP group was diluted 16-fold (0.0125 g/mL), the positive effect of released La ions on cell viability was obvious. Therefore, the concentration of released La ions was optimum at 0.0125 g/mL dilution, and the dose-dependent effect of La was observed for this dose.

Alkaline phosphatase activities of Saos-2 cells incubated with different concentrations of βTCP, and La-βTCP material extracts are presented in Figure 4.8. ALP assay was applied after seven and 14 days of incubation, while regular osteogenic media was used as control. After seven days of incubation, the ALP

activity of 1La-βTCP, 2La-βTCP, and βTCP groups were higher than that of 3La-βTCP and control groups in all concentrations except 0.0125 g/mL. In the concentration group 0.0125 g/mL, the ALP activity of 1La-βTCP and βTCP were about 6.5±0.6 and 6.2±0.5 nmol/µg/min, respectively. However, they were still statistically higher than 3La-βTCP (5.1±0.4 nmol/µg/min) and control groups (4.2±0.7 nmol/µg/min). The ALP activity decreased upon increasing of La in βTCP, which increased (3La-βTCP) in all concentrations after seven days of incubation. At higher La doping (3 La), the osteogenic activity of cells was less than it is in other groups. This might be due to the decreased release of Ca and P from βTCP and the less enhancing effect on ALP activity, or due to the higher proliferative effect of this dose on cells at this incubation period. With the extension of the incubation period from seven to 14 days, the ALP activity of all groups decreased to similar levels, and some were even less than the control group. However, at 0.05 g/mL concentration, the ALP activity of the 3La-βTCP group was about 0.14±0.01 nmol/µg/min and was higher than other groups; 1La-βTCP (0.11±0.01 nmol/µg/min), βTCP (0.1±0.01 nmol/µg/min) and control groups (0.12±0.01 nmol/µg/min). Similarly, at 0.0125 g/mL concentration, the ALP activity of the 3La-βTCP group was significantly higher than 1La-βTCP at this time point.
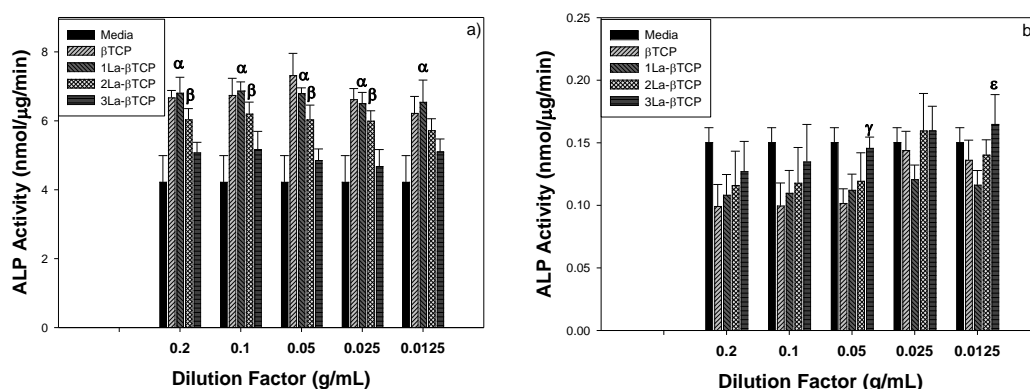


**Figure 4.8.** Alkaline phosphatase activity of Saos-2 cells was incubated with different concentrations of βTCP and La-βTCP materials extracts after a) 7 and b) 14 days of incubation. Values are means ± SD (n=4); $p^{\alpha} < 0.05$, $p^{\gamma} < 0.05$, $p^{\beta} < 0.05$ and $p^{\varepsilon} < 0.05$ were considered.

La ions and La bearing compounds were known to promote differentiation and induce osteogenic activity (Dang et al., 2019). In the study of Hu et al., osteogenic differentiation of BMSCs was reported to be enhanced by La through the Wnt/$\beta$-catenin signalling pathway, leading to increased alkaline phosphatase, osteocalcin, and collagen I gene expression (Hu et al., 2018). The osteogenic differentiation effect of La ions was also reported to be dose-dependent. The study of Liu et al. reported that ALP activity level of murine preosteoblast cell line (MC3T3-E1) was highest at the lowest $LaCl_3$ concentration and decreased with increasing $LaCl_3$ concentration (Liu et al., 2012). The osteogenic differentiation of cells was also observed to be affected by the concentration of $Ca^{2+}$. However, an increased concentration of $Ca^{2+}$ can lead to apoptosis. The optimum balance between $Ca^{2+}$ and $La^{3+}$ ions will improve osteogenic differentiation (Peng et al., 2019).

In order to observe the morphology of Saos-2 cell after incubation with the 0.0125 g/mL extract concentrations, cells were investigated under laser scanning confocal microscopy after seven days of incubation (Figure 4.9). In all groups, cells displayed a healthy morphology and adhered to the plate surface. Different doping concentrations of La did not show any effect on cell morphology. All groups possessed healthy cell growth with good spreading and population.
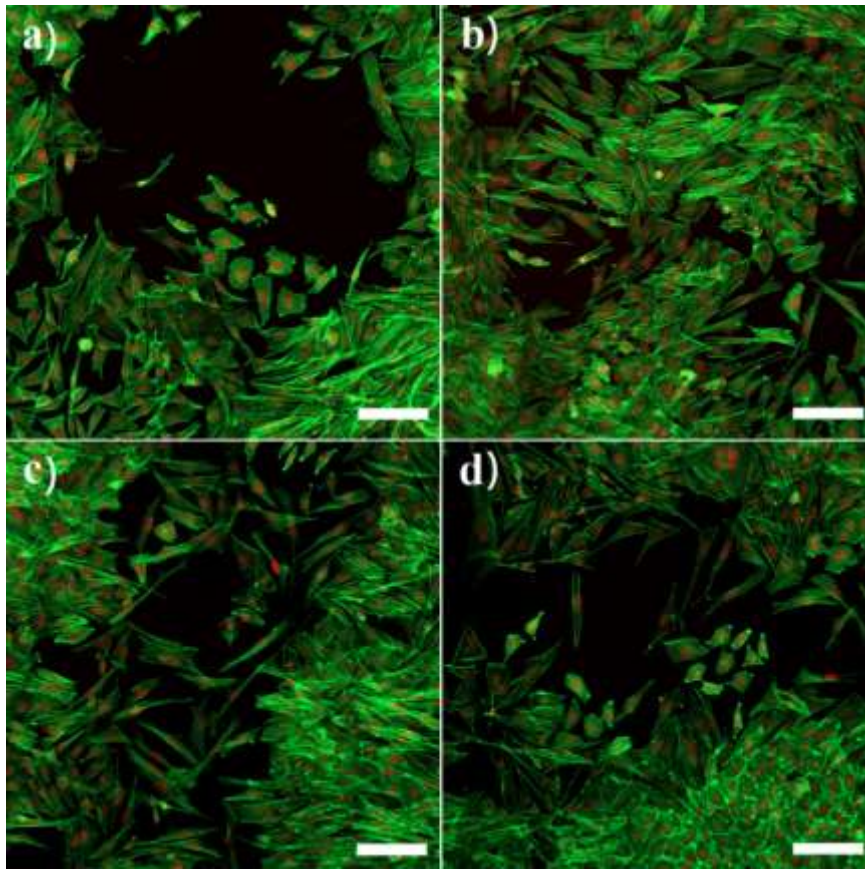
**Figure 4.9.** Laser scanning confocal microscopy analysis of Saos-2 cells that incubated with group extracts (0.0125g/mL) after 7 days of incubation. a) βTCP, b) 1La-βTCP, c) 2La-βTCP and d) 3La-βTCP. Scale bar represents 100 μm in length. Green and red colours on the images are representing FITC and Draq5 staining, respectively.

## 4.2. Preparation and Characterizations of Lanthanum Doped Dicalcium Phosphate Cements

The pre-optimization of the chemical contents of βTCP, MCPM, and $H_2O$ used to prepare DCP cements (different groups), and experiment conditions of pH results of these groups are summarised in Table 4.5.

**Table 4.5.** DCP cement ingredients and related pH values.

| Sample ID | Cement Ingredients | | | pH Value |
|---|---|---|---|---|
| | βTCP (g) | MCPM (g) | Water (mL) | |
| 1T1M | 1.00 | 1.00 | 0.80 | 3.5 |
| 1T0.75M | 1.00 | 0.75 | 0.80 | 4 |
| 1T0.5M | 1.00 | 0.50 | 0.80 | 7 |
| 1T0.25M | 1.00 | 0.25 | 0.80 | 7 |
| 1T | 1.00 | 0 | 0.80 | 7 |
| 1M | 0 | 1.00 | 0.80 | 2.5 |

About 1.0g of βTCP, known as basic material (Huan & Chang, 2009), was mixed with different fractions of MCPM, known as acidic material (Huan & Chang, 2009); then, the powder was combined with 0.8 mL of water to obtain salt of DCP cement.

In this research, DCP cement phases (Brushite or Monetite) were identified according to the standard peaks of Brushite (JCDPS NO: 09-0077), and Monetite (JCDPS NO: 09-0080) (Figure 4.10), and the acidic behaviour (pH value) was assessed after soaking the specimens in PBS for 24 hours (Table 4.5). The DCP cement phase (monetite) was performed by mixing 1.0g of βTCP with 1.0g of MCPM (Sample ID: 1T1M, Figure 4.10), but the obtained monetite phase showed acidic behaviour with pH: 3.5, which could be due to some amount of MCPM that did not react with βTCP (Huan & Chang, 2009). When the amount of MCPM was reduced to 0.75g (Sample ID: 1T0.75M), no change in the monetite phase was observed, and the acidity decreased as pH increased to 4 (Figure 4.10, Table 4.5).
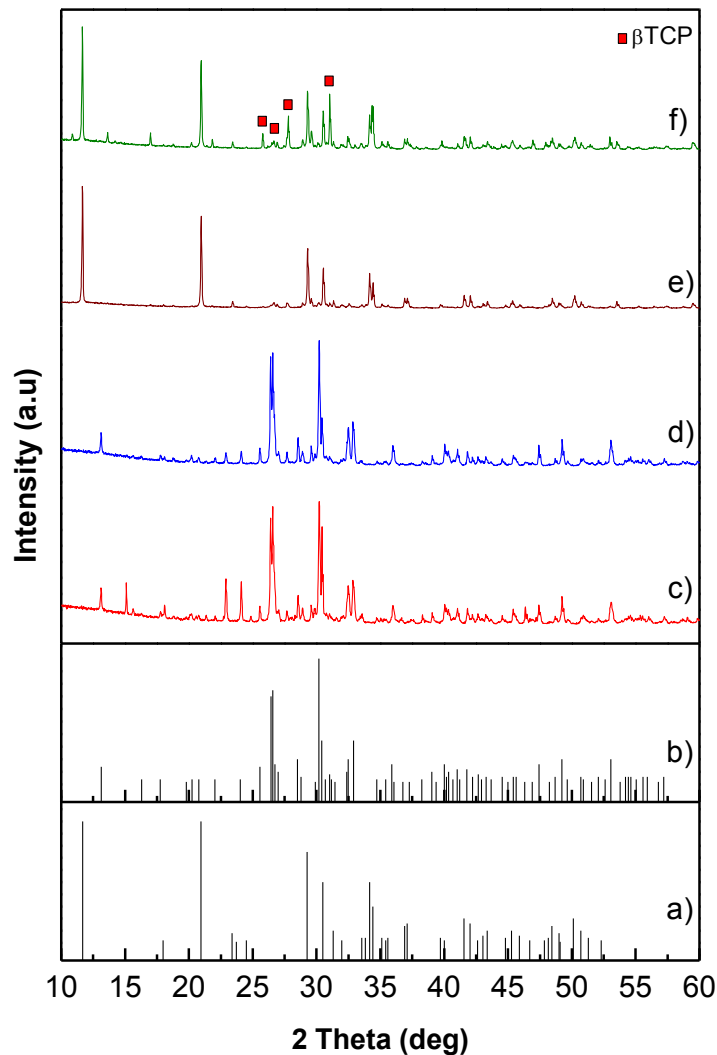
**Figure 4.10.** XRD spectra of samples prepared at RT: a) JCDPS NO: 09-0080 (Monetite), b) JCDPS NO: 09-0077 (Brushite), c) 1T1M, d) 1T0.75M, e) 1T0.5M, f) 1T0.25M.

To further increase the pH value, the amount of MCPM was reduced to 0.5g (Sample ID: 1T0.5M); the obtained DCP cement was a pure phase of brushite, and the acidity was equal or near to 7. To obtain optimum conditions with less amount of chemical ingredients, the amount of MCPM was reduced to 0.25g (Sample ID: 1T0.25M). The brushite phase was presented as the main phase along with some peaks that belonged to βTCP (JCDPS NO: 09-0169).

This outcome confirmed that some amount of βTCP did not react with MCPM and existed as a second phase and the acidity was equal or near to 7. Based on this optimizations, 1.0g of βTCP, 0.5g of MCPM and 0.8 mL of water formed pure phase of brushite cement resulted in pH value close to 7, and these contents were considered as an optimum condition. X-ray diffraction of DCP and La doped DCP cement are displayed in Figure 4.11. DCP was predominantly composed of the crystalline brushite phase (JCDPS NO: 09-0077). No other phases such as monetite was detected along with the brushite phase, which confirmed the phase purity of DCP cement. With incorporation of $La^{3+}$ ions into DCP cement, the cement phase transformed from brushite to monetite (JCDPS NO: 09-0080) cement. Taha et al. (2017) suggested some causes that may be responsible for monetite formation as the main setting product; the authors ascribed it to an excess of acidity in the cement paste with higher addition of $Sr^{2+}$ ions. Luo et al. (2017) approved that the addition of citric acid increased the monetite ratio. Incorporation of citric acid (0.1M ) is sufficient to kinetically favour monetite phase over brushite phase (Sahin & Çiftçioğlu, 2014).

Another study conducted by Ren at el. confirmed that addition of amelogenin protein endorsed the phase transformation from brushite to monetite. The researchers claimed that amelogenin protein speeds up dehydration of brushite crystals (Ren et al., 2016). An increase in $La^{3+}$ ion amount into DCP cement structure resulted in inhibition in the peaks intensity and shrinkage along with *a* axis and expansion along with *b* and *c* axis of DCP cement lattice structure (Table 4.6). These fluctuations in lattice parameters were presumably due to the replacement of smaller size of $Ca^{2+}$ ion (0.099 nm) with the larger size of $La^{3+}$ ion (0.106 nm) and indicate the incorporation of La into the DCP lattice.
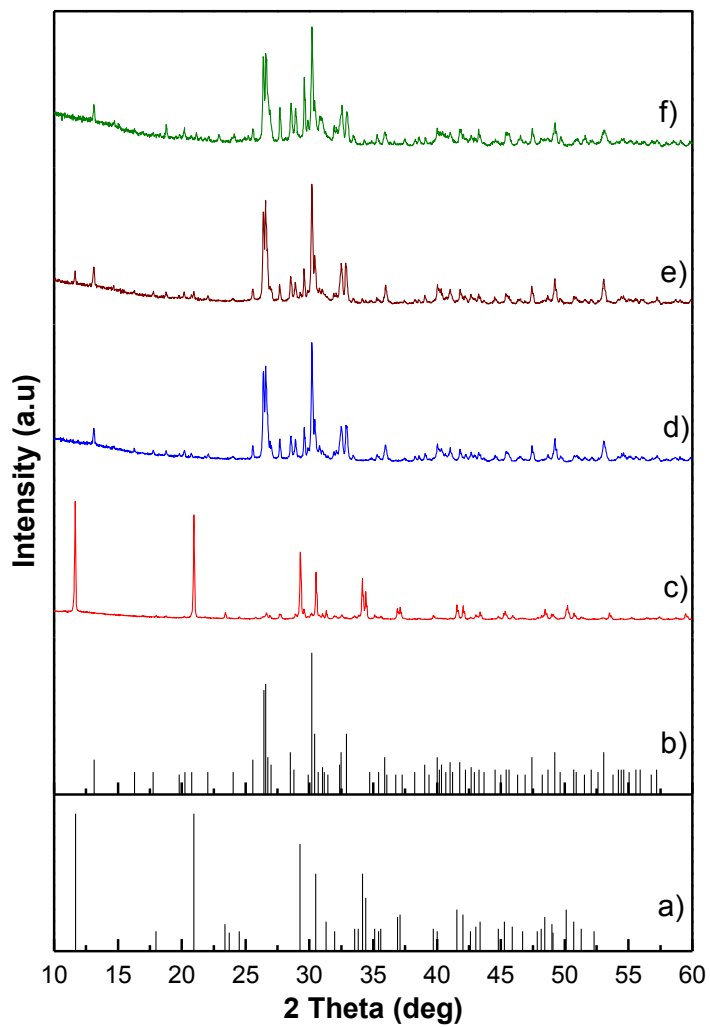
*Figure 4.11. XRD patterns of DCP and La-substituted DCP bone cements, a) JCDPS NO: 09-0077, b) JCDPS NO: 09-0080, c) DCP, d) 1La-DCP, e) 2La-DCP, f) 3La-DCP.*

**Table 4.6.** Lattice parameters of DCP and La-substituted DCP bone cements.

| Sample ID | Lattice parameters | | | |
|---|---|---|---|---|
| | a (Å) | b (Å) | c (Å) | V (Å)$^3$ |
| JCDPS (Brushite) | 6.363 | 15.190 | 5.815 | 493.93 |
| DCP | 6.365 | 15.190 | 5.814 | 493.76 |
| JCDPS (Monetite) | 6.906 | 8.577 | 6.634 | 309.40 |
| 1La- DCP | 6.906 | 8.574 | 6.635 | 309.17 |
| 2La- DCP | 6.908 | 8.573 | 6.637 | 309.47 |
| 3La- DCP | 6.900 | 8.580 | 6.639 | 309.03 |

FTIR spectra of pure DCP and La doped DCP bone cements are shown in Figure 4.12. Two broad doublets were detected at 3537 cm$^{-1}$, 3481 cm$^{-1}$, 3277 cm$^{-1}$ and 3158 cm$^{-1}$ in the spectrum of pure DCP cements, demonstrating that two kinds of H$_2$O molecules exist in the unit cell (Cama et al., 2011). Three absorption bands at 1210 cm$^{-1}$, 1135 cm$^{-1}$, and 1057 cm$^{-1}$ were assigned to the stretching mode of P=O. The asymmetric stretching vibrations of P–O–P led to absorptions at 985 cm$^{-1}$, 872 cm$^{-1}$, and 792 cm$^{-1}$. Furthermore, P-O bending was recorded at 661 cm$^{-1}$, 577 cm$^{-1}$ and 522 cm$^{-1}$ (Taha et al., 2017). With incorporation of La$^{3+}$ ions into DCP structure, the absorption bands attributed to water molecules were observed to have disappeared, confirming the transformation of brushite phase (CaHPO$_4$·2H$_2$O) to monetite phase (CaHPO$_4$), as approved by XRD analysis (Figure 4.11).

The absence of absorption in the area 3560-3150 cm$^{-1}$ suggested that the chemical compositions of 1La, 2La, 3La- DCP were free of water molecules, confirming the obtained materials were a pure phase of monetite (CaHPO$_4$). Furthermore, with an increasing La$^{3+}$ ions amounting into DCP structure, the sharpness of PO$_4^{3-}$ vibrational bands diminished, proposing a distortion of the structure, andchanging the particular geometric linkage of the CaP associated bonds due to the existence of La$^{3+}$ ions (Taha et al., 2017).
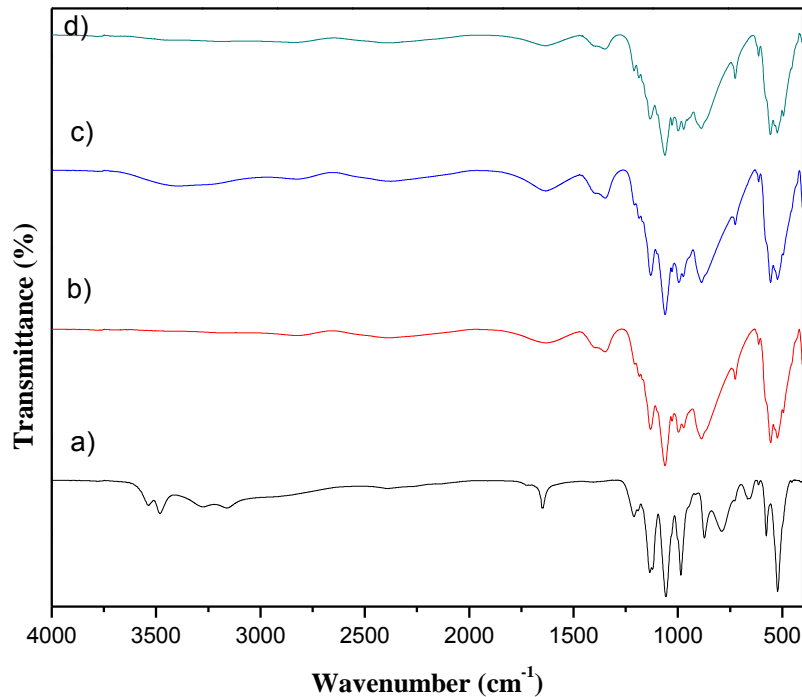
**Figure 4.12.** FTIR spectra of DCP and La doped DCP bone cements. a) DCP, b) 1La-DCP, c) 2La-DCP, d) 3La-DCP.

The SEM images of DCP and La doped DCP bone cements are presented in Figure 4.13. Micrographs of pure DCP showed densely packed plate-like crystals that were packed in multiple layers. Their dimensions ranged from 0.5 to 2 μm while some particles appeared as clusters of smaller particles. In previous studies, similar observations have been made for a pure phase of brushite (Brundavanam et al., 2014; Taha et al., 2017; Toshima et al., 2014), which is consistent with the results of the XRD analysis. However, the plate-like crystals did not show a particular direction, suggesting a further or fewer isotropic behaviour (Taha et al., 2017). Upon addition of $La^{3+}$ ions, the parallelogram shapes of brushite were completely transformed into small spheroid particles, the same trend as the conversion of brushite to monetite in XRD and FTIR analysis. With an increasing amount of $La^{3+}$ ions, a reduction of the mean particle sizes of monetite from 188 μm for 1La-DCP to 107 μm for 3La-DCP was recognized. The incorporation of higher amount of $La^{3+}$ ions inhibited the growth of monetite particles.
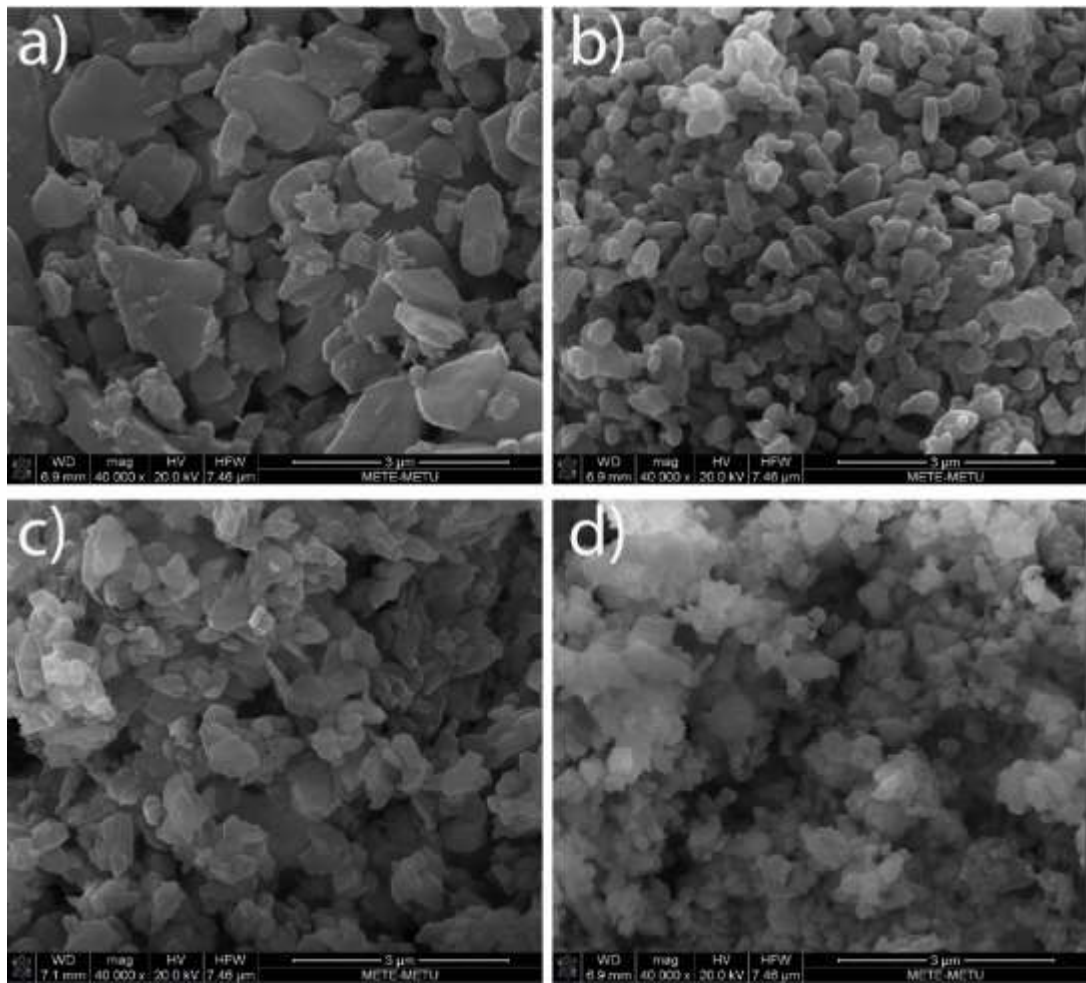
**Figure 4.13.** SEM micrographs of DCP and La doped DCP bone cements, a) DCP, b) 1La-DCP, c) 2La-DCP, d) 3La-DCP.

The setting time of bone cement is considered as one of the most important parameters that should meet the design prerequisites of surgical operations. Among these requirements, the initial preparation time ought to be sufficient for the forming and filling process. After the filling process, the cement paste should be left until it hardens.

During the setting time, it is not advisable to apply any kind of mechanical stress as it can cause cracks and negatively affect the mechanical properties later. Therefore, the shortest possible time that the bone cement needs to harden after placement is important, or else the operation could bedelayed. Previous studies concluded that the initial setting time (eight minutes) and a final setting time (<15 min) are more

favoured for orthopaedic applications (Driessens et al., 1998; Komath et al., 2000). The initial and final setting times of DCP and La doped DCP at RT are presented in Figure 4.14 (a). Initial and final setting times for DCP (brushite phase) were 9.5 min and 84.5 min, respectively. The final setting time of DCP cements paste significantly exceeded the preferred range ($< 15$ min). However, a long setting time may be disadvantageous in certain situations because of the risk of washing out (Sahin, 2018).

Furthermore, a gradual and significant reduction in initial and final setting time for DCP was observed with the addition of La ions. This could be attributed to the formation of monetite phase (Figure 4.11). However, the setting time of the La-DCP cement paste further decreased with increasing $La^{3+}$ concentration in DCP, which might be due to the reduction in the particle size (Khashaba et al., 2010).

The compressive strength results of pure DCP and La substituted DCP bone cements that were moulded to obtain cylindrical forms are illustrated in Figure 4.14 (b). The compressive strength of the pure DCP bone cement was about 7.9 MPa, which is comparable to values reported by Tamimi et al ( 2012a). After adding a minimum amount of $La^{3+}$ ions (0.090 mole, 1La-DCP), the compressive strength declined to about 6.7 MPa. This result was related to brushite phase transformation to monetite, where the latter possesses a compressive strength lower than brushite phase, as measured and discussed by Tamimi et al (2012b). After increasing the substitution amount of $La^{3+}$ ion to about 0.225 mole (2La-DCP), the compressive strength value was raised to about 9.6  MPa. Oktar et al. (2006) attributed this improvement in mechanical properties to densified cement matrix, which strongly influences the regime of cement microstructure.

The researcher concluded that the addition of $La_2O_3$ resulted in improvement in microhardness and compressive strength of HA-$La_2O_3$ composites. Shin-Ike et al. demonstrated that incorporation of $La_2O_3$ led to improvement in bending and tensile strengths of HA (Shin-Ike et al., 1989). It was also confirmed that the addition of

La$_2$O$_3$ into HA-ZrO$_2$ composites boosted the diametral tensile strength of the composites (Khoshsima et al., 2016). The compressive strength dropped to about 6.9 MPa with increasing of the doping amount of La$^{3+}$ ions to about 0.450 mole (3La-DCP). The mechanical analysis manifests that the compressive strength of pure DCP and La-DCP bone cements matches to that of human cancellous bone (5-10 MPa) (Xu et al., 2014).
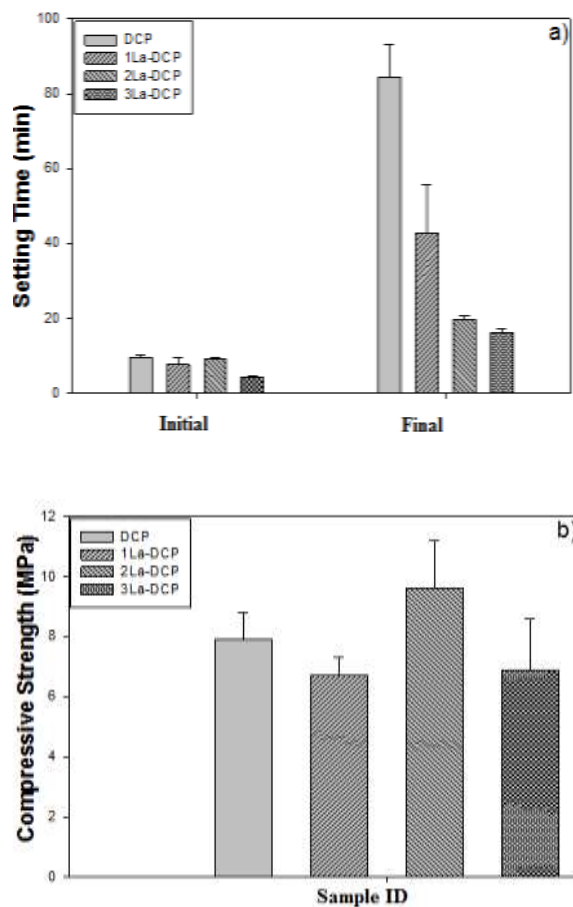


**Figure 4.14.** a) Setting time, b) Compressive strengths of DCP and La doped DCP bone cement (values are mean ±SD; n = 4).

The *in vitro* dissolution behaviour of DCP and La-DCP materials in PBS medium was investigated by the leaching behaviour of ions (Ca$^{2+}$, P$^{5+}$ and La$^{3+}$) and pH variation as shown in Figure 4.15 (a-c). As can be seen, the pure DCP dissolves at a lower rate than other materials. With the addition of La$^{3+}$ ions, the degradation rate of DCP bone cements gradually increased. In contrast, the previous research claimed

that incorporation of $La^{3+}$ ions diminished the degradation rate of β tricalcium phosphates (βTCP) (Motameni et al., 2020) and addition of $La^{3+}$ ions reduced degradation rate of HA (Guo et al., 2009). This enhancement in the degradation rate of La-DCP materials could be traced to factors such as differences in the composition and the physical properties of the materials (Gbureck et al., 2007; Tamimi et al., 2012b; Yousefi et al., 2014). Overall, all cement samples showed faster release of ions ($Ca^{2+}$ and $P^{5+}$) within the first day, which continued as slow release followed by a stable release rate at the incubation period, 7-14 days. This change in the release profile of ions could be attributed to the deposition of different phases of CP. It was reported that incubated DCP cements in PBS transformed to octacalcium phosphate (OCP) or HA depending on chemical composition of cements and aging conditions (Bannerman et al., 2016).

Surprisingly, the leaching amount of $La^{3+}$ ions was so low that (lower than 0.03 mg/L) ICP-OES could not detect it. This could be due to the chemical interaction between $La^{3+}$ ions and $H_2PO_4^-$ of PBS, resulting in precipitated and highly insoluble Lanthanum(III) phosphate ($LaPO_4$) salt, as shown in the Equation 4.1 (Aissa et al., 2009 ; Schaad et al., 1994).

$$La^{3+} + H_2PO_4^- \rightarrow LaPO_4 + 2H^+ \hspace{3cm} Eq.\,4.1$$

The deposited $LaPO_4$ material can be considered a beneficial additive. The previous studies suggested that it could support osteoblast (bone-forming cell) adhesion (Ergun et al., 2009) and have better machinability (Ghosh et al., 2016). The pH value decreased upon increase in the immersion time (Fig. 4.15(c)), which could be related to the release of two protons for each $La^{3+}$ ion as displayed in Equation 4.1.

The ability of a biomaterial to interact with proteins is crucial since a healthy cell-biomaterial interaction depends on the amount and type of protein adsorbed onto the material surface (Yu & Chen, 2015). Adsorption and desorption of serum proteins on/from DCP and La doped DCP over 24 hour incubation sets are presented in Figure

4.16. The total amount of proteins adsorbed on the surface of DCP disc was about 1.04 μg/mL.
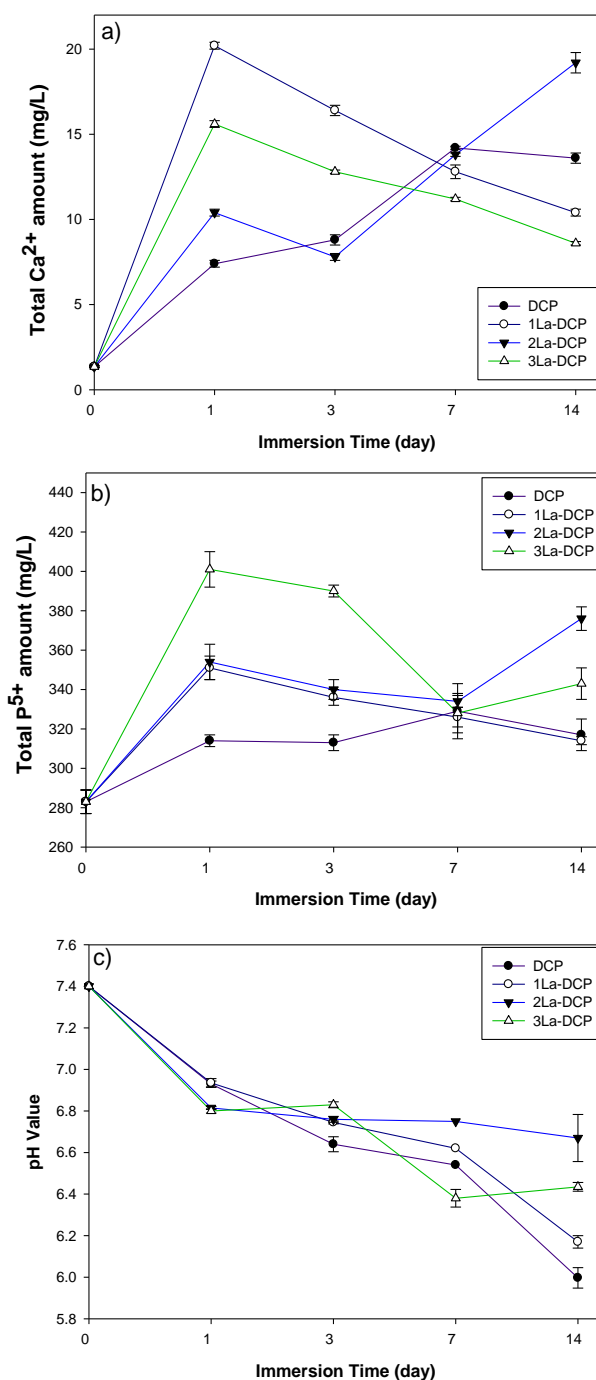


**Figure 4.15.** a) Total $Ca^{2+}$ amount, b) Total $P^{5+}$ amount, and c) pH value of PBS for various immersion period.

This amount increased gradually upon the increase in $La^{3+}$ ions amounting into DCP structure, and the amount of protein adsorbed on 2La-DCP and 3La-DCP disc surfaces were significantly higher than the protein adsorption amounts on DCP and 1La-DPC groups, and this behaviour could be due to the lower particle size of La doped DCP than pure DCP (Figure 4.13). Smaller particle size revealed a greater surface area. Higher surface promoted the contact of the material particles with the solvent and hence increased the adsorption ratio (Bavnhøj et al., 2019). After a desorption study of 24 hours, the groups with higher protein adsorption (2La-DCP and 3-La-DCP) showed a lower rate of protein desorption. 2La-DCP and 3-La-DCP groups lost approximately $47.8 \pm 14.4$ % and $61.8 \pm 10.1$ % of the proteins adsorbed. Meanwhile, the DCP group had the highest protein dissolution rate, up to $73.4\pm19.6$ % of the adsorbed proteins. Protein desorption from the 1La-DPC group ($66.8 \pm 10.1$ %) was slightly lower than the DCP group. Among the groups, the interaction behaviour of 2La-DCP group with proteins was the most desirable in terms of material-cell interaction, with high protein adsorption and low desorption.

*In vitro* cell culture analysis using Saos-2 cells cultured with the prepared bone cement was performed using direct and indirect methods. Saos-2 cells' viabilities in the presence of extracts of all groups of bone cements were compared in Figure 4.17. Different extracts were prepared by serial dilution of original extract (0.20 g/mL) of DCP and La doped DCP bone cement, and cell viability was evaluated by Alamar Blue assay on the first and fourth days. After one day of incubation, the viability of cells cultured with the extracts of 2La-DCP was significantly higher than other groups at 0.20 g/mL and 0.10 g/mL concentrations. When the extract concentrations were reduced to 0.025 g/mL, cell viability cultured with pure DCP bone cement extract was slightly higher than 3La-DCP. With a prolonged immersion period, after four days, the cell viability of La-DCP group cultured at concentration range of 0.20-0.05 g/mL was higher than pure DCP. Along with reducing the concentration of extracts to 0.025 g/mL, the number of cells increased, and the results showed the highest cell viability with 2La-DCP and 3La-DCP cement among other groups.
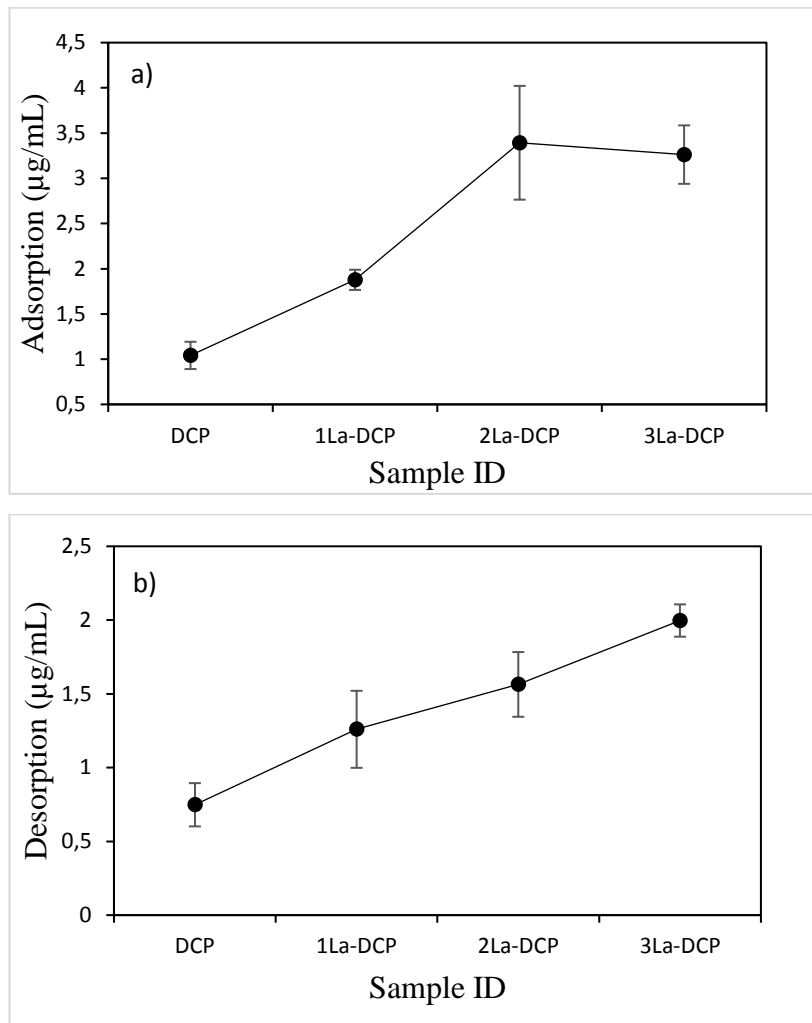
***Figure 4.16.*** *a) Adsorption and b) desorption amounts of proteins on cement groups after 24h of immersion in PBS.* Denklemi buraya yazın.

Cell viability results support that there is an optimal La concentration range that enhances cell viability. Above the optimum concentration, cell viability decreased most similarly to La-TCP cell viability results. After one day of incubation, the amount of released ions at lower extract concentrations was not enough to trigger a noticeable difference in cell viability. However, as the incubation time increased, extract with low ion concentration started to create a difference in cell viability. After four days of incubation, the highest cell viability was obtained at the lowest extract concentration for groups with the lowest La doping (1La-DCP and 2La-DCP).

Previously, a high concentration of La was reported to create cytotoxicity, and the enhanced cell viability was strictly concentration dependent (Pagano et al., 2015). The study of Bai et al.(2018) showed that the viability of bone marrow stromal cells decreased when they interacted with La bearing calcium phosphate particles at high concentrations ($10^{-5}$ M) while cell viability was enhanced at lower concentrations ($10^{-9}$ M). In another study, low concentration of $LaCl_3$ improved the proliferation rate of murine pre-osteoblast, while higher concentrations above 1 µM suppressed the proliferation (Liu et al., 2012). The results of the extraction test confirmed that La doping at a specific concentration could support higher cell viability with an optimum range of La release.
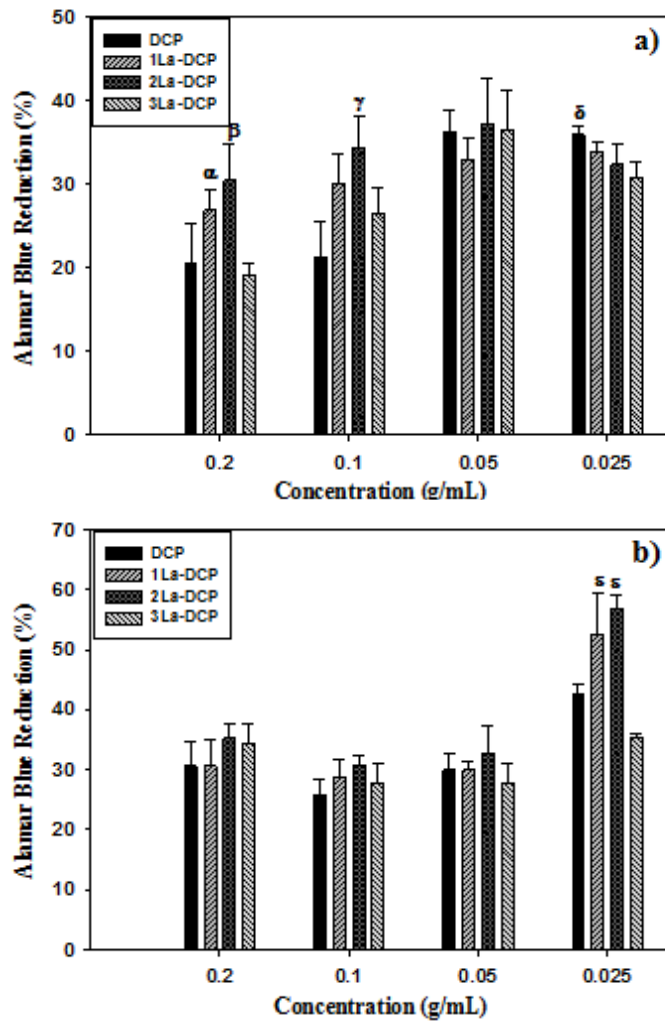
**Figure 4.17.** Percent Alamar Blue reduction of Saos-2 cells subjected to DCP and La doped DCP powder extracts with different concentrations at a) 1 and b) 4 days. For 1La-DCP, α states P<0.01 with respect to 3La-DCP at 0.20 g/mL concentration after 1 day of incubation. For 2La-DCP, β states P<0.05 with respect to DCP and 3La-DCP groups at 0.20 g/mL concentration after 1 day of incubation. For 2La-DCP, γ states P<0.05 with respect to DCP at 0.10 g/mL concentration after 1 day of incubation. For DCP, δ states P<0.01 with respect to 3La-DCP at 0.025 g/mL concentration after 1 day of incubation. For 1La-DCP and 2La-DCP, ε states P<0.05 with respect to other groups at 0.025 g/mL concentration at 4 days.

Direct contact cell viability experiment was conducted on the prepared disc groups with Alamar Blue assay (Figure 4.18(a)). Saos-2 cells were seeded on bone cement discs, and cell viability of groups was compared on days 1, 4, and 7. After one day of incubation, cell viability on the DCP disc only was slightly higher than La bearing groups, and cell viabilities of La doped DCP groups were similar. After four days of

incubation, the effect of La doping was revealed with higher cell viability on 1La-DCP and 2La-DCP groups. The cell viability was higher on DCP discs with lower La doping, and the DCP group with highest La doping (3La-DCP) showed lower cell viability than pure DCP. Cell viability of groups decreased more in a seven day period than in a four day period. However, cell viability of the middle two groups (1 and 2 La-DCP) was still higher than the DCP and 3La-DCP groups. This reduction in the cell viability could be due to the initial confluences reached at some areas on discs after cell seeding (Khoshsima et al., 2018).

The direct contact cell viability assay results also supported the dose-dependent effect of La on Saos-2 cell viability as DCP groups with low La doping supported higher cell viability than DCP disc with high La doping. The ions like calcium, released alongside La from DCP, could have also affected the cell viability. Study of Peng et al. (2019) showed that an optimum concentration balance of $Ca^{2+}$ and $La^{3+}$ ions can enhance bone mesenchymal stem cell proliferation. La is also called the "bone-seeking" element since physicochemical characteristics of La ions are similar to those of Ca (Liu et al., 2015).

ALP activity of cells seeded on disc samples was investigated, and the results are presented in Figure 4.18(b). After both incubation periods, the highest ALP activity was achieved by Saos-2 cells incubated on 2La-DCP disc group. The high viability sustained with 2La-DCP disc group could have also supported higher ALP activity. $La^{3+}$ salts known to enhance osteoblast activity with higher osteocalcin expression are linked to increased bone mineral density (Von Rosenberg & Wehr, 2012).
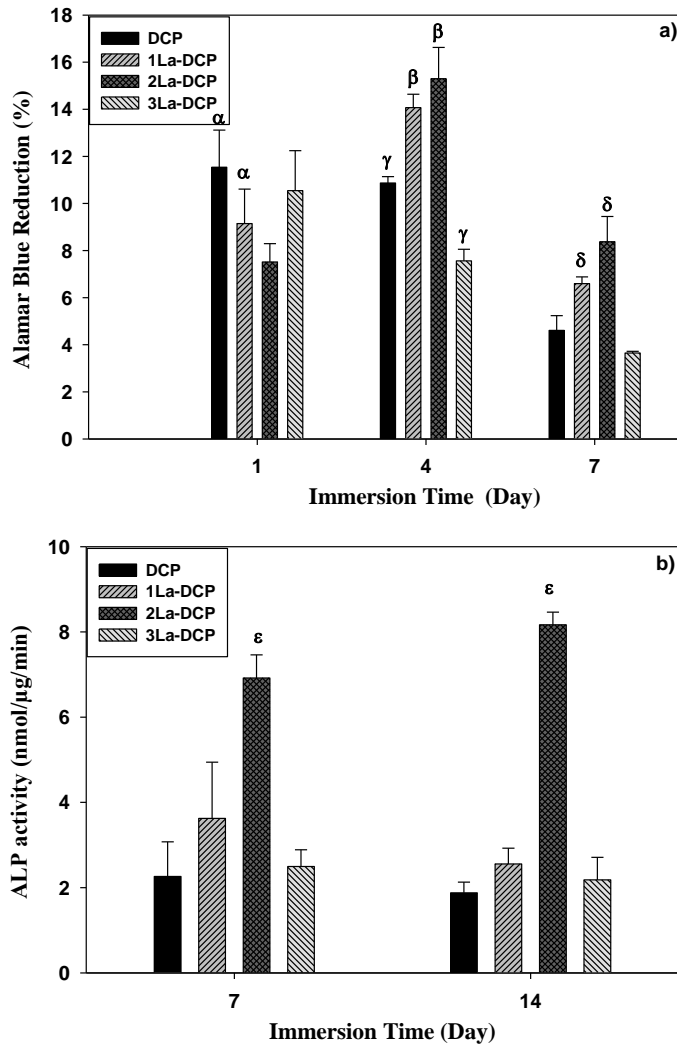
**Figure 4.18.** a) Percent Alamar Blue reduction of Saos-2 cells on DCP and La doped DCP discs surface after 1, 4 and 7 days of incubation. For 1La-DCP, $\alpha$ states $P<0.05$ with respect to DCP after 1 day of incubation. For 1La-DCP and 2La-DCP, $\beta$ and $\delta$ states $P<0.01$ with respect to other groups at 4 and 7 days. For 3La-DCP, $\gamma$ states $P<0.01$ with respect to DCP after 4 days of incubation. b) Normalized ALP activity of Saos-2 cells seeded on bone cement disc groups at 7 and 14 days. For 2La-DCP, $\varepsilon$ states $P<0.01$ with respect to other groups at 7 and 14 days.

The presence of La element was known to trigger osteogenic differentiation and activity (Dang et al., 2019). Previous studies have shown that La acts through Wnt/$\beta$-catenin signalling a pathway and enhances ALP, osteocalcin, and collagen I gene expression of bone mesenchymal stem cell (Hu et al., 2018). The effect of La on ALP activity was reported to be dose-dependent on murine pre-osteoblast cell line, and the highest ALP activity was achieved at lower La concentrations (Liu et al., 2012). The

results of the ALP activity showed that an optimum concentration of La doping was needed to promote the ALP activity of Saos-2 cells. The 2La-DCP disc group was able to improve both cell viability and ALP activity, which shows that La doping concentration of 2La-DCP group sustained La release in a preferable way.

CLSM images of Saos-2 cells subjected to extracts of DCP and La-DCP bone cements (at concentration 0.20 g/mL) for seven days are presented in Figure 4.19(a-d). After incubation with extracts, no distinct negative effect was observed on cell morphologies, and all the groups showed healthy and well spread morphology. The extracts with increasing La doping concentration did not create any adverse effect on cells. Image J software was used to calculate the average cell spreading areas for groups (Figure 4.19(e)). Spreading areas of cells incubated with 2La-DCP and 3La-DCP were slightly higher, but still, spreading areas of cells did not differ in a statistically significant way.
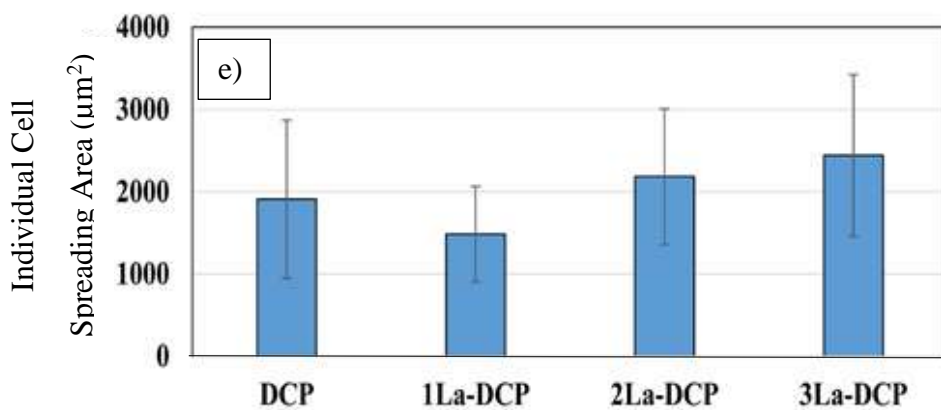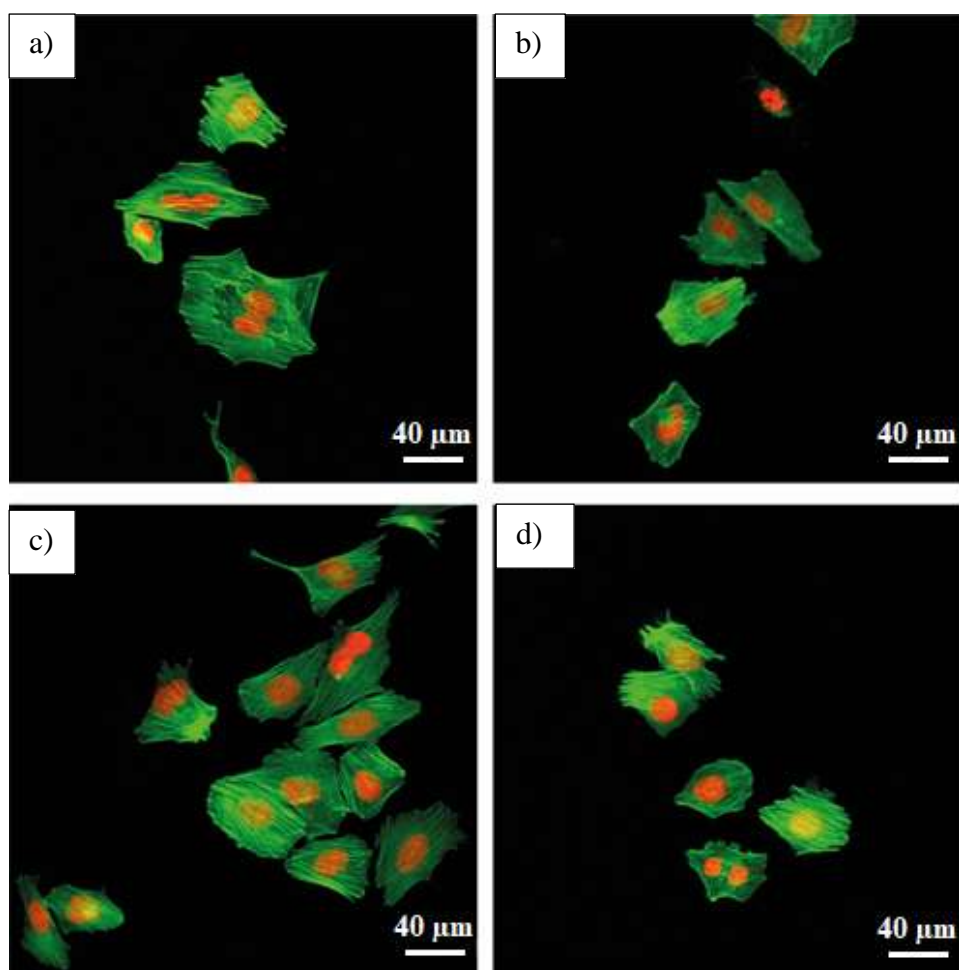
**Figure 4.19.** CLSM analysis of Saos-2 cells subjected to extracts of (0.20 g/mL) a) DCP, b) 1La-DCP, c) 2La-DCP and d) 3La-DCP for 7 days. Fluorescence of excitation at 488 nm for Alexa Fluor 488 phalloidin (green) and at 650 nm for DAPI (red) was used (Scale bar: 40 µm), e) Individual cell spreading areas of Saos-2 cells subjected to extracts for 7 days.

## 4.3. Preparations and Characterizations of Graphene Oxide Reinforced La Doped Dicalcium Phosphate Cements

Phase pure GO particles were synthesized through Tour method and later on fully characterized using XRD, FTIR, TGA and SEM techniques (Figure 4.20). XRD pattern (Fig. 4.20 (a)) exhibited the presence of sharp and intense peaks around 10.52° corresponding to Miller reflection plane (001) which further confirmed the synthesis of phase pure GO particles and this result is consistent with the previous studies (Ban et al., 2012; Hsiao et al., 2010; Soomro et al., 2019). However, a small peak can be seen around 20.1° which confirms that synthesized GO is not completely interposed (Hsiao et al., 2010). At the same time, a tiny peak around 45.26° exhibiting the occurrence of short-range order in the layers of stacked GO (Stobinski et al., 2014). FTIR spectrum of GO (Fig. 4.20 (b)) displayed the appearance of C-H =C-H and C=C bands at 568, 870 and 1622 cm$^{-1}$. Another bunch of oxygen containing functional groups (C–O ($\upsilon$C–O), C–O–C ($\upsilon$C–O–C), C–OH ($\upsilon$C–O–H) bands in GO were observed at 1036, 1157 and 1381 cm$^{-1}$.

FTIR spectrum also shows the presence of C=O bands along the sheet edges and on the basal plane of GO sheets around ($\upsilon$C=O at 1729 cm-1) and a broad band in the range of 3000 3500 cm$^{-1}$ corresponding to O-H functional groups (Ossonon & Bélanger, 2017). Moreover, FTIR results also have revealed that many oxygen-containing functional groups are present in the GO sample after the oxidation phenomenon (Sharma et al., 2017). Surface morphology of GO was investigated using SEM, which confirmed large lamellar grains with tens of micrometres in size (Fig. 4.20(c)). Similarly, it can also be seen from the SEM micrographs that they show packing of thin sheets with relatively flat surfaces on the top and can be peeled off (Serodre et al., 2019). Besides this, to reveal the thermal stability behaviour of GO, TGA technique was utilized and the results have been described in Fig. 4.20(d). It can easily be seen from the decomposition behaviour of GO that the first major weight loss (about 58%) is appearing in the range of 30 -300°C and this loss in weight can be ascribed due to the absorbed and latter water molecules. Where the second

weight loss (10 %) was seen in the range of 300°C to 400°C and it could be the result of decomposition of oxygen containing functional groups. A slight loss in the weight was observed around 400°C which was attributed to unstable carbon held in the CO and $CO_2$ structures (Sharma et al., 2017).
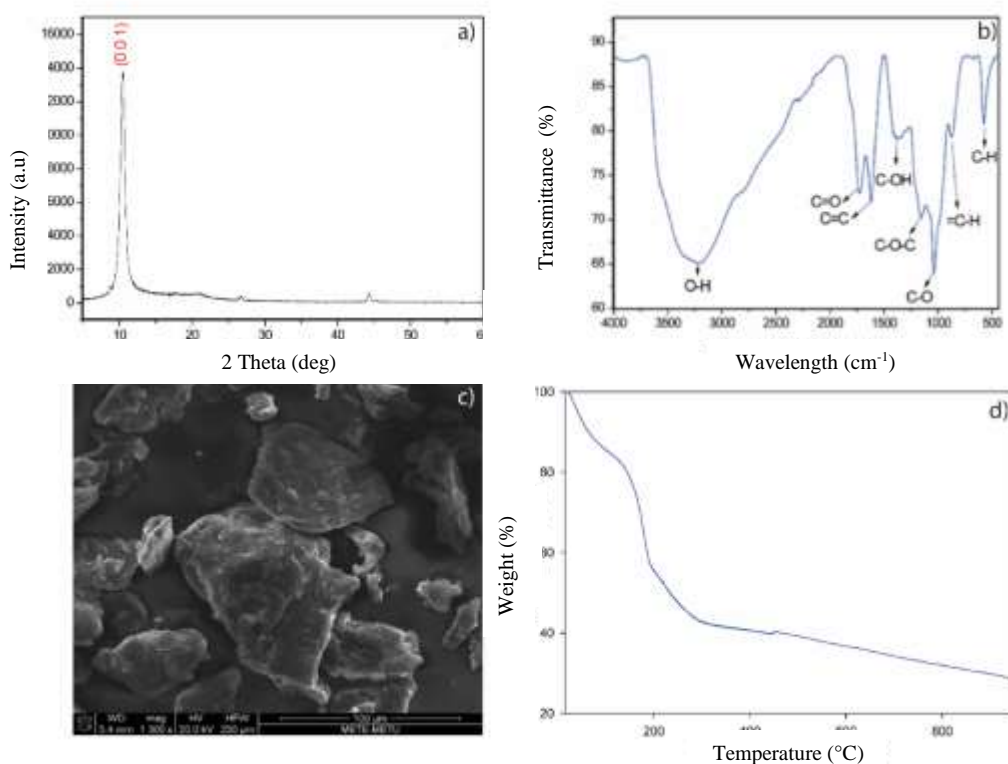


**Figure 4.20.** a) XRD pattern, b) FTIR spectra, c) Micrograph image and d) TGA analysis of GO synthesized using Tour method.

Figure 4.21. illustrates the XRD patterns of La-DCP and GO substituted La-DCP. Results showed that La-DCP XRD patterns are in good agreement with monetite crystal (JCPDS No: 09-0080). Where an appearance of a small peak at 11.60° (corresponds to diffraction plane 020) was detected as brushite peak (JCPDS No: 09-0077). However, an addition of GO showed no appearance of any peak around 10.52° (corresponding (001) plane) which means that no substitution of GO has been seen and it could be due to small amount of GO (Zeng et al., 2015). It has also been inferred that the disappearance of GO peak may result from exfoliation of steady stacks of GO sheets (Li et al., 2014a; Xu et al., 2008). However, increased substitution of GO showed shifting of the XRD peaks (Table 4.7) which resulted in

an increase in the degree of crystallinity and development of brushite phase gradually according to increasing concentration of GO. This significant effect of GO increasing the degree of crystallinity and formation of either brushite or monetite is not clear. Based on the assumption of previous observations, this behaviour could be assigned to the strong hydrogen bonding interactions that may occur between GO nanosheets and monetite crystals (Chen et al., 2018a; Iacoboni et al., 2019).
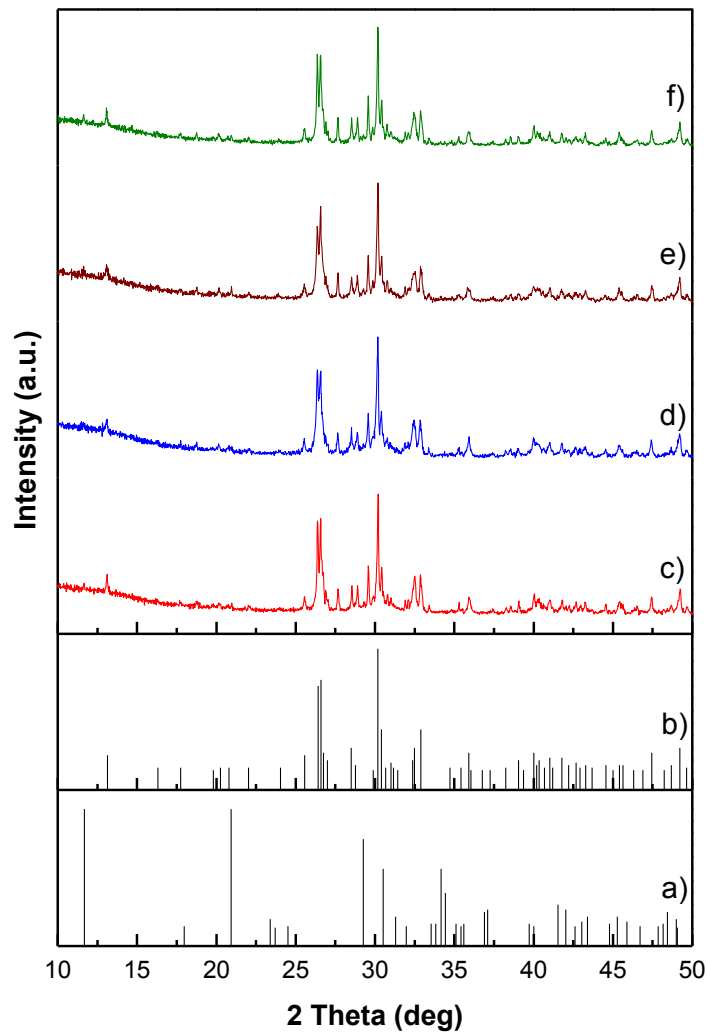


**Figure 4.21.** XRD pattern of La-DCP and GO/La-DCP cements, a) JCDPS NO: 09-0077, b) JCDPS NO: 09-0080, c) 2La-DCP, d) 1GO/2La-DCP, e) 2GO/2La-DCP, f) 3GO/2La-DCP.

**Table 4.7.** Lattice parameters and degree of crystallinity of La-DCP and GO/La-DCP comments.

| Sample ID | Lattice parameters | | | | Degree of crystallinity |
|---|---|---|---|---|---|
| | a (Å) | b (Å) | c (Å) | V (Å$^3$) | |
| Monetite (09-0080) | 6.906 | 8.577 | 6.634 | 309.4 | ---- |
| 2La-DCP | 6.919 | 8.580 | 6.640 | 308.9 | 80 |
| 1GO/2La- DCP | 6.927 | 8.603 | 6.659 | 309.2 | 84 |
| 2GO/2La- DCP | 6.923 | 8.610 | 6.656 | 309.35 | 88 |
| 3GO/2La- DCP | 6.912 | 8.589 | 6.646 | 309.27 | 93 |

The FTIR spectra of GO/La-DCP cements (Figure 4.22) displayed two absorption bands around 522 and 555 cm$^{-1}$ attributed to the bending mode of O-P-O (H). Another FTIR band found around 891 cm$^{-1}$ was assigned to the stretching mode of P-O (H) bond and similarly another band was observed at 997 cm-1 and was related to stretching of P-O bond. Besides this, three other FTIR bands can be seen around 1061, 1136, and 1185 cm$^{-1}$ and were accredited to the stretching mode of P-O bond. Where a broad band can be observed in the range of 1338-1400 cm$^{-1}$ and was described as the bending mode of P-O-H bond. Similarly, band at 1640 cm$^{-1}$ which may be due to the bending mode of H-O-H and rotation of residual water was observed (Tortet et al., 1997). Results further confirmed that incorporation of GO substance, showed an elongation and an increase in the sharpness of the HPO$_4$ $^{-1}$ FTIR bands which can be due to increased degree of crystallinity of the synthesized material (Table 4.7).
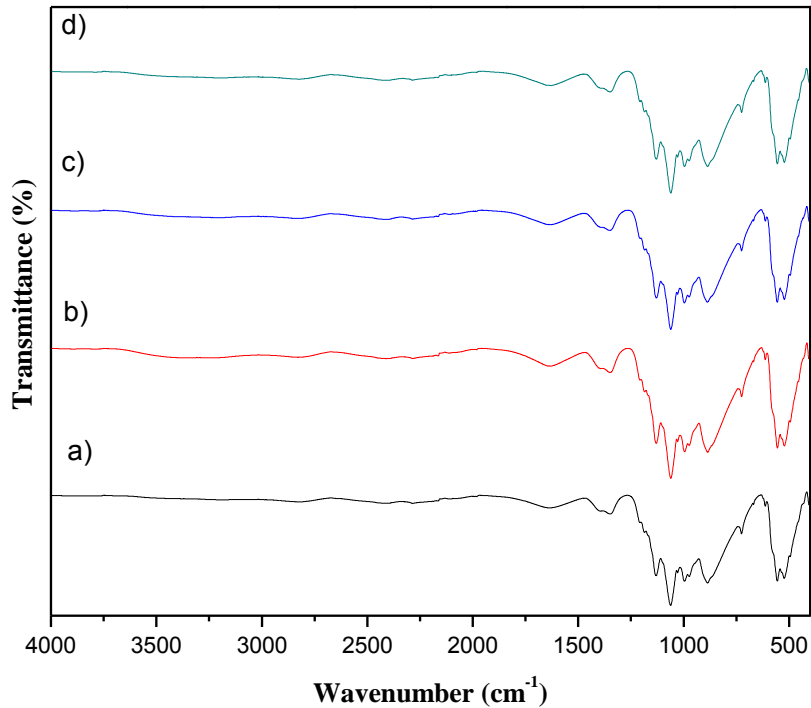
**Figure 4.22.** FTIR spectra of 2La-DCP and GO/2La- DCP samples, a) 2La-DCP, b) 1GO/2La-DCP, c) 2GO/2La-DCP, d) 3GO/2La-DCP.

SEM micrographs of La-DCP and GO/La-DCP bone cements are presented in Figure 4.23. showed the formation of agglomerated and irregular shapes, dominating the elongated particles. Monetite cement using brushite phase upon heating for 20 min in an autoclave at 121°C and the prepared monetite phase showed the formation of agglomerated and irregular microstructures (Tamimi et al., 2010). Besides this, no remarkable change in the morphology of the synthesized sample was observed upon substitution of GO. However, GO in the monetite cement manifested an increase in the particle size (240-520 nm) and crystallinity degree of 3GO/2La-DCP.
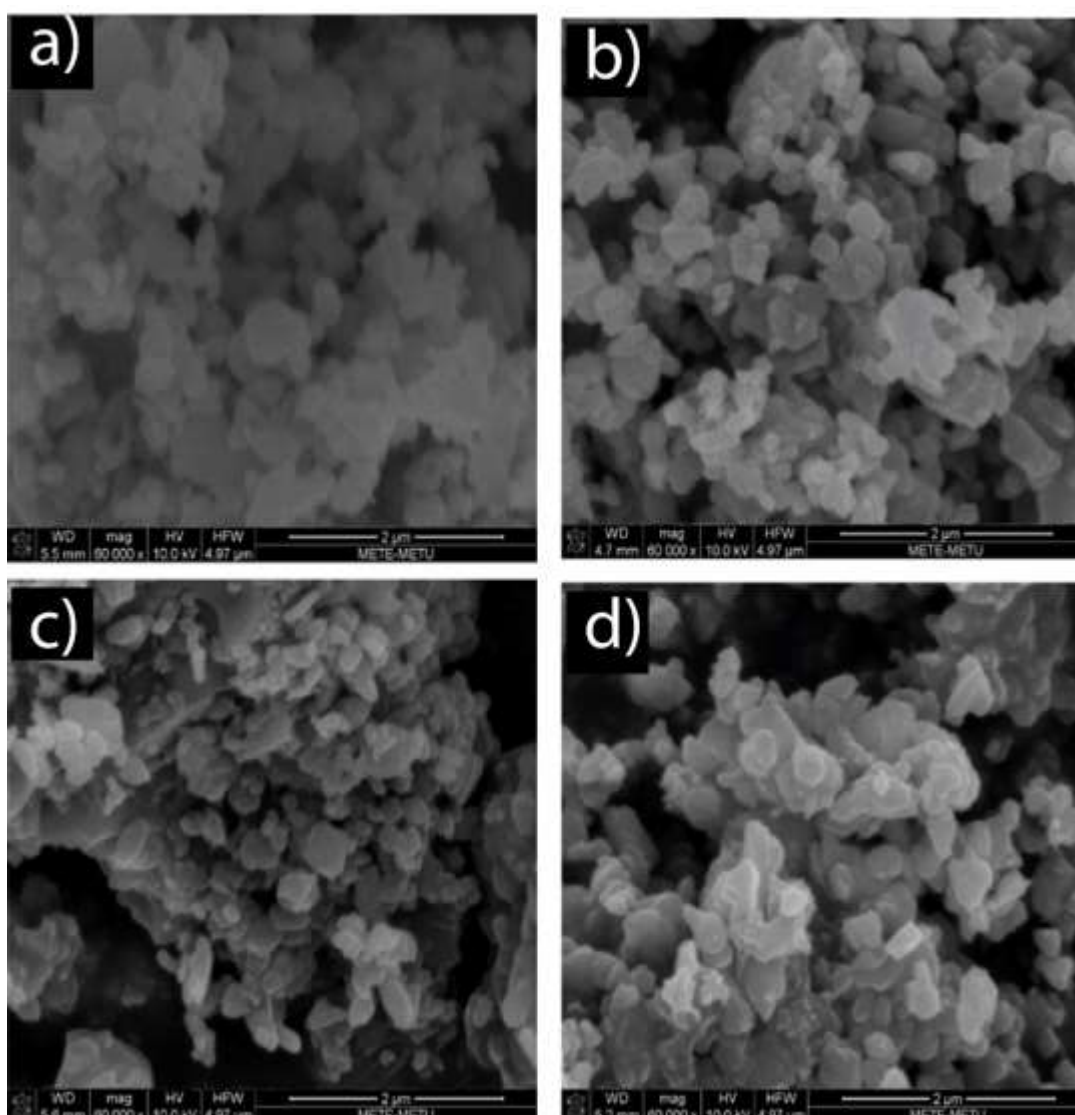
**Figure 4.23.** SEM images of 2La-DCP and GO/2La- DCP samples, a) 2La-DCP, b) 1GO/2La-DCP, c) 2GO/2La-DCP, d) 3GO/2La-DCP.

The TGA studies of the manufactured La-DCP and GO/La-DCP samples are shown in Figure 4.24. TGA curves are exhibiting a continuous low loss in the mass of the on increasing constantly the heat treatment. TGA curves are revealing three regions of mass loss. First gradual weight loss was found in the range of 19-360°C. This loss in the mass was ascribed to the removal of absorbed water from the surface and lattice of the of the sample (Liao et al., 1999). Consequently, second loss in the mass was observed in the region of 360-440°C and this loss can be ascribed to the thermal anhydrous monetite ($CaHPO_4$) to $\gamma$-$Ca_2P_2O_7$ ($2CaHPO_4 \rightarrow \gamma$-$Ca_2P_2O_7 + H_2O$) (Ren et

al., 2016). Finally, third stage loss in the mass (%) was nearly negligible but was assigned to the decomposition of GO (Figure 4.20(d)).
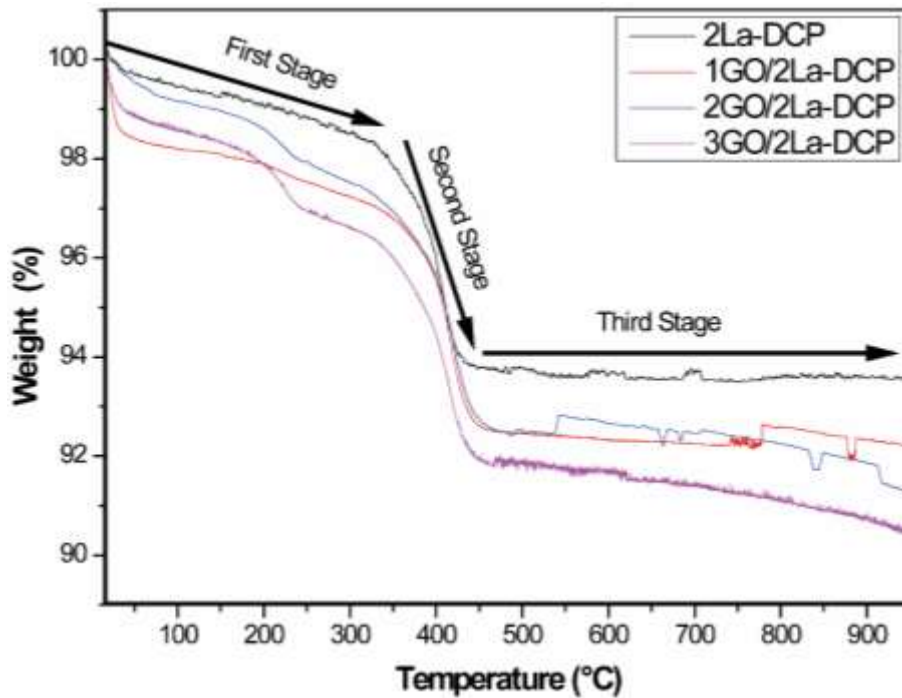


**Figure 4.24.** TGA analysis of 2La-DCP and GO/2La- DCP samples.

UV visible spectroscopy was inducted for the spectroscopic studies and considered as most important for biomedical studies (Samui & Sahu, 2020). UV/Visible spectra of La-DCP and GO/La-DCP cements is presented in Figure 4.24 . The most prominent electronic $\pi \rightarrow \pi^*$ transitions in all GO samples were considered due to common aromatic C=C bonds (Naumov, 2017) or due to nanometre scale $SP^2$ clusters (Lai et al., 2012). In case of GO, electronic transition dominates the transition occurring at ~248 nm (Lai et al., 2012). Moreover, in addition to the $\pi \rightarrow \pi^*$ transition, atypical absorption band (for GO) has an absorption band at ~333 nm. This absorption band was ascribed to $n \rightarrow \pi^*$ transition due to oxygen-containing functional groups (C=O bonds). On seeing the UV/Visible spectrum bands, it was revealed that increased intensity of the absorption bands further confirms the incorporation of GO in the monetite cements.
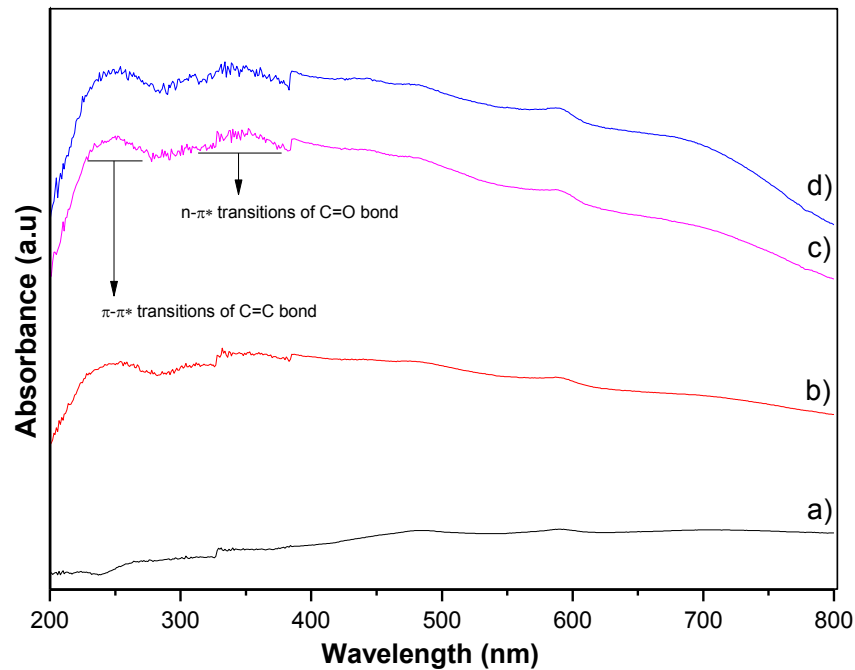
**Figure 4.25.** UV–Vis spectrum of 2La-DCP and GO/2La-DCP cements, a) 2La-DCP, b) 1GO/2La-DCP, c) 2GO/2La-DCP, d) 3GO/2La-DCP.

Regarding bioactive cements' properties, it is critical to prepare clinically appropriate monetite cement having suitable setting time (Jang et al., 2018). During this study, impact of the GO on the 2La-DCP cement setting time was also probed and results have been depicted in the Figure 4.26 (a). Results confirmed initial and final setting time for La-DCP about 9 to 19 min and with a minimum addition of GO (1.5wt.%) in the 2La-DCP significantly decreases down the setting time of the cement to 3.8 min (initial time) and 5 min (final) and similar behaviour was observed with increment of GO amount. However, there are no statistically significant difference between GO-2La-DCP groups. It's well known that the setting time of cement can be manipulated via powder/liquid ratio, higher amount of liquid led to increase in the setting time of cement. This could be explained as addition of GO absorbs some amount of water and decreases the setting time of 2La-DCP cements (Wang et al., 2017). Previous studies have observed same behaviour. Wang et al. deduced that incorporation 0.6 wt.% of Reduced GO is enough to reduce the initial setting time of calcium phosphate cement from 17 to 8 min and the final from 64 to 30 mins (Wang et al., 2017). Furthermore, addition of 2 wt.% of GO signifantly decreased the setting

time of calcium phosphate/calcium sulfate/methylcellulose cements (Oğuz & Ege, 2019).

*In vitro* degradation of $La^{3+}$ ions doped βTCP powders and DCP cements were investigated in this thesis (Figure 4.5 and Figure 4.15). Profound influences were observed in the degradation rate of βTCP powders and DCP cements with the incorporation of $La^{3+}$ ions. Substitution of $La^{3+}$ ions deteriorated the internal structure of the host; as a result, apparent changes were observed in the degradation rate. However, in GO/La-DCP cement composites, the degradation test was not conducted in this study. Some reasons were behind this decision: (i) GO particles were mixed with La-DCP cement in the composite shape. Based on the obtained microstructure results, the addition of GO had a negligible effect on the internal structure of La-DCP cement (Figure 4.23). Therefore, an additional small amount of GO could have no impact on the degradation rate of La-DCP cements, (ii) In previous studies (Nosrati et al., 2020; Tatavarty et al., 2014; Kim et al., 2017), GO was used as an additive to improve the mechanical and biological properties of a wide range of bioactive materials. In the mentioned studies, the researchers did not perform the degradation test, in which the addition of GO could not affect the degradation rate of the host materials. (iii) the degradation of GO is very weak, and in case it is released, probably it will be under the limitation of the ICP-OES device.

In this study, cements with short setting time could be obtained. However, cements with low setting time will further reduce the complication rate, permits earlier wound closure, and decreased operative time (Costantino et al., 2000). Although the setting time may be short and the operation time will not be enough (Ginebra et al., 1994), the surgeon can overcome this issue by careful planning and evaluation of the defect before cement preparation and application (Costantino et al., 2000).

Specimens of 2La-DCP with different contents of GO were prepared to evalute the compressive strength and the results were given in Figure 4.26 (b). The compressive strength of 2La-DCP cement was about 9.6 MPa. With incorporation of GO no

significant change was observed. However, the compressive strength increased gradually with increment of of GO, it was about 10.7 for 3GO/2La-DCP. This improvement in compressive strength attributed to the two-dimensional structure of GO expands the contact zone, hence the load moved through network to GO by shear distortion might be more effective. With the expansion of the load, GO started to withstand the tensile stress, acted as bridges in La-DCP scaffolds (Wang et al., 2017).
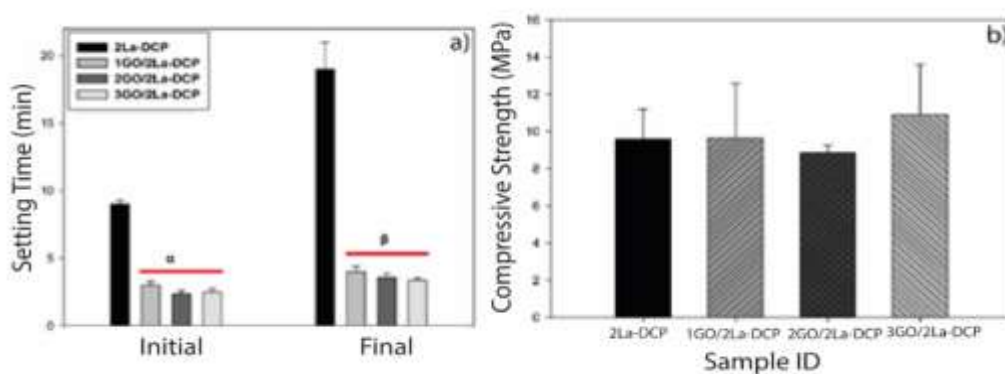


**Figure 4.26.** a) Setting time and b) Compressive strength of 2La-DCP and GO/2La-DCP cement composites. α: Indicates statistically significant difference between results of GO/2La-DPC and 2La-DPC groups (P<0.05). β: Indicates statistically significant difference between results of GO/2La-DPC and 2La-DPC groups (P<0.05).

The results of protein adsorption and desorption test are presented in Figure 4.27. The group, 2La-DCP showed the lowest protein affinity among groups. The presence of GO was observed to improved protein adsorption on 1GO/2La-DCP and 2GO/2La-DCP groups. Group with the highest GO ratio, 3GO/2La-DCP, had the highest protein adsorption level while having the lowest protein desorption amount. After 24 h of incubation in PBS, 3GO/2La-DCP group was able to keep roughly 40% of adsorbed proteins. The main interaction routes of GO with proteins have observed to depend on electrostatic interactions, hydrophobic effects by the hydrophobic aromatic groups on GO and π–π stacking that support spontaneous adsorption of proteins on GO surface. Also, covalent links between epoxide moieties on GO surface and lysine units of proteins can be established to create more stable attachment (Li et al., 2016; Qi et al., 2019). Protein adsorption ability of a material strongly effect

material-cell interaction which determine biocompatibility of the material (Fu et al., 2017). Higher protein adsorption on 3GO/2La-DPC cement group was the result of higher GO concentration which has created more GO aggregation points on cement surface. The improved protein adsorption capacity of GO incorporated cement groups shows that GO can be used to improve biocompatibility of materials and 1GO/2La-DPC, 2GO/2La-DPC, 3GO/2La-DPC groups were expected to sustain better cell-material interaction.
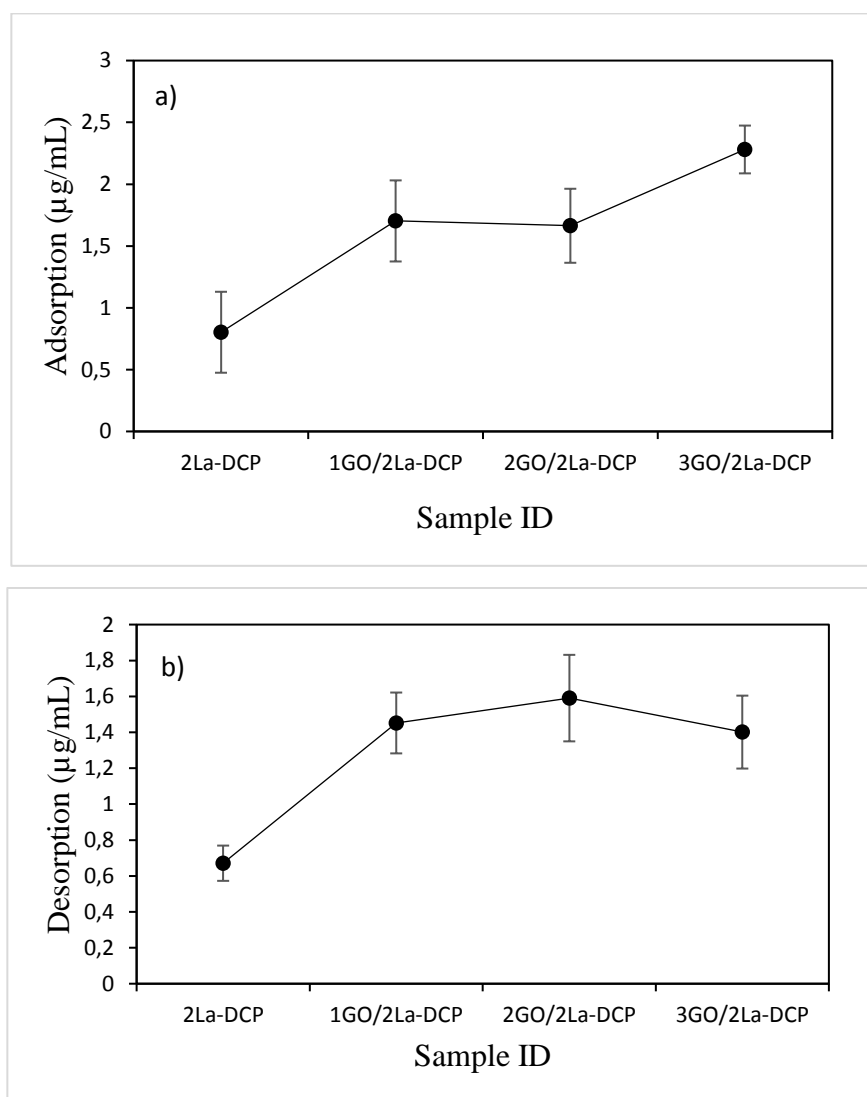


**Figure 4.27.** Amount of protein a) adsorption and b) desorption on/from cement disc groups after 24 h of incubation period.

The study of La doped βTCP have shown that the effect of La on Saos-2 cells is strictly dose dependent and in this study control 2La-DCP groups was prepared accordingly (Motameni et al., 2020). Indirect cell viability of cement groups was studied with different concentrations of the extracts. Extracts were prepared by incubating cements in growth media for 3 days and cell viabilities were determined after 1 and 4 days of incubation (Figure 4.28). After 1 day, the group incubated with 0.2 g/mL concentration of 1GO/2La-DCP cement extract had higher cell viability compared to group incubated in extract of 2La-DCP. At 0.1 g/mL concentration, group incubated with 2GO/2La-DCP showed higher cell viability compared to other groups. After 4 days, groups incubated with lower extract concentrations showed higher cell viabilities compared to groups incubated with higher extract concentrations. The reason of this, is the presence of high concentration of ions released through 3 days of incubation period into the extracts of bone cements. High ion concentration in the media could restrict proliferation of cells and decrease cell viability.

Study of Maeno et al., have reported that number of mouse primary osteoblast cells starts to decrease as the $Ca^{+2}$ concentration in incubation medium is increased above 8 mM for monolayer and 6 mM for 3D cultures (Maeno et al., 2005). GO at higher concentrations, reported to effect cell viability. Study of Ricci et al., have investigated the cytotoxicity of GO nanoribbons on MG-63 osteoblast cell line and reported a decrease in cell viability when GO nanoribbon concentration was higher than 200 µg/mL (Ricci et al., 2017). Suspended GO nanoparticles have reported to enhance Saos-2 cell viability at 20-40 µg/mL concentration while decrease cell viability at 80 µg/mL concentration (Foroutan et al., 2018). In this study 0.2 g/mL concentration represents an extract media which contain total of ion released through 3 days and it is expected to have decreased cell viability in this concentration. Also, in an *in vivo* application where body fluids will continuously wash the cement surrounding, ion over accumulation that could decrease cell viability would be prevented.
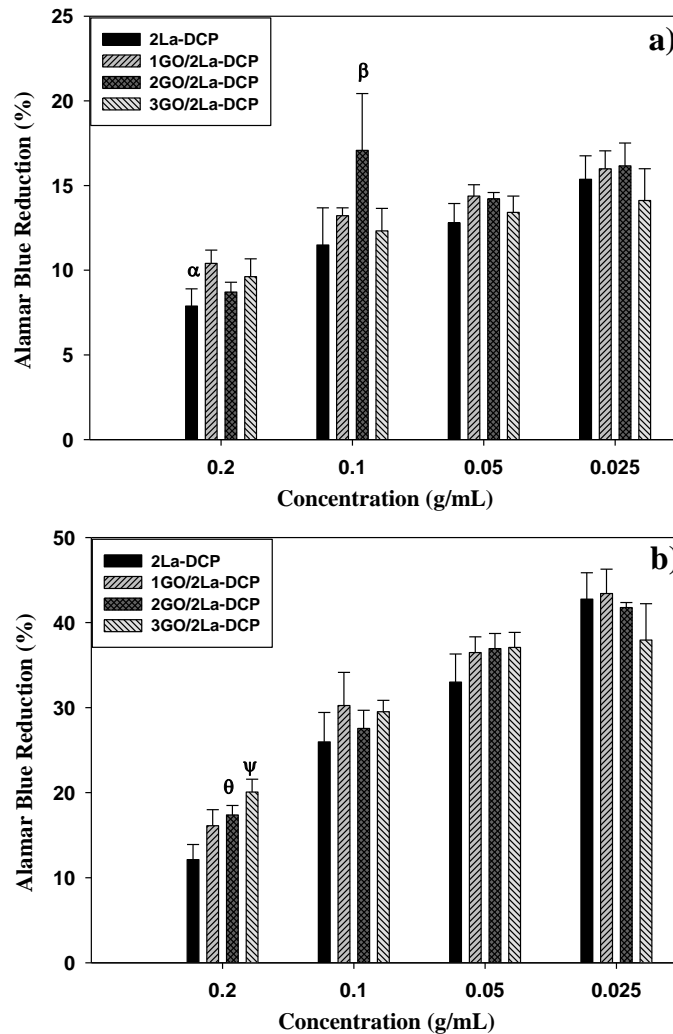
**Figure 4.28.** Percent Alamar Blue reduction of cells result of indirect cell viability study after a) 1 and b) 4 days of incubation. α: Indicates statistically significant difference between results of 1GO/2La-DPC and 2La-DPC groups (P<0.05). β: Indicates statistically significant difference between results of 2GO/2La-DPC and La-DPC groups (P<0.05). θ: Indicates statistically significant difference between results of 2GO/2La-DPC and 2La-DPC groups (P<0.05). Ψ: Indicates statistically significant difference between results of 3GO/La-DPC and 2La-DPC groups (P<0.01).

Viability of Saos-2 cells after direct incubation on cement disc surface (Figure 4.29(a)) showed that cement groups have sustained similar level of cell viability which increased for all groups after 4 days of incubation period. After 4 days of incubation cell viability of 3GO/La-DPC group was slightly lower compared to other groups. Previous studies reported that La incorporated materials can enhance cell viability when cells are treated at certain concentration range. Above a certain

96

concentration La was reported to decrease cell viability (Bai et al., 2018; Liu et al., 2012a; Pagano et al., 2015). In this study, La doping concentration indicated a positive cell response (Motameni et al., 2020). GO is a well identified material that has been reported to enhance bone regeneration by improving cell viability, ALP activity, expression of osteogenic factors and cell attachment/adhesion (Liu et al., 2014a; Purohit et al., 2019).

On the other hand, high GO concentration can lead to decrease in cell viability. Chang et al., have investigated the dose dependent toxic effect on A549 cells and concluded that even though GO is a very safe material to use, it can decrease cell viability at higher concentrations by creating oxidative stress (Chang et al., 2011). This could be the reason of slight decrease in cell viability.

ALP activity of cells incubated with group extracts were compared after 7 and 14 days. Results showed that extracts of 1GO/2La-DPC and 2GO/2La-DPC groups have improved ALP activity of cells compared to 2La-DPC after 7 days of incubation. The ALP activity of the 1GO/2La-DPC group was also higher than 3GO/2La-DPC after 7 days of incubation. Previous studies have shown that La was able to initiate osteogenic differentiation of cells and interaction of La on bone mesenchymal stem cells was reported to be through Wnt/β-catenin signaling pathway that triggers gene expression of ALP, osteocalcin and collagen I (Dang et al., 2019; Hu et al., 2018).
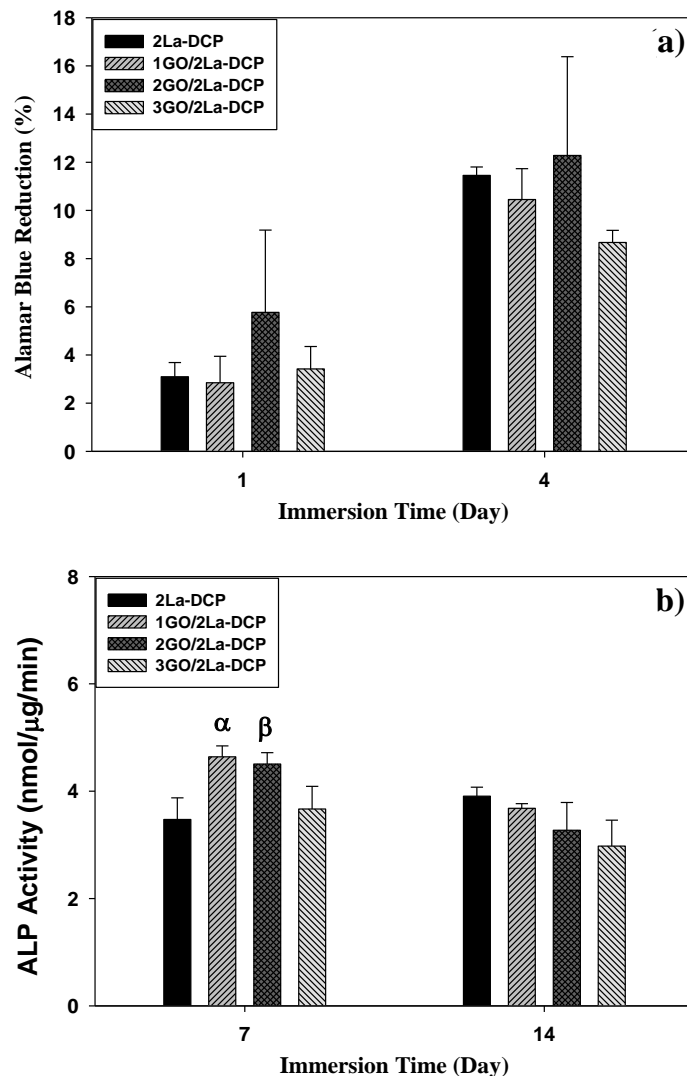
**Figure 4.29.** Percent Alamar Blue reduction of cells result of direct cell viability study after a) 1 and b) 4 days of incubation. α: Indicates statistically significant difference of 1GO/2La-DPC from 3GO/2La-DPC and 2La-DPC groups (P<0.05). β: Indicates statistically significant difference between results of 2GO/2La-DPC and 2La-DPC groups (P<0.05).

In the study of Hermenean et al., GO incorporation into chitosan scaffold was shown to improve osteogenesis by increasing expression of bone morphogenetic protein (BMP) and Runx-2 and at the late stage up-regulating osteopontin and osteocalcin *in vivo* (Hermenean et al., 2017). A recent study used GO to improve cell interaction of brushite bone cement and has reported slight toxicity that caused decrease in cell viability and ALP activity on cells when GO was used above 2% in cement material (Nasrollahi et al., 2019). Similarly, in this study, the group with 3.5 wt.% GO content

(3GO/2La-DPC) showed lower ALP activity compared to groups with 1.5 and 2.5 wt.% GO content. Results show that GO incorporation at specific concentrations in bone cement materials can improve material-cell interactions, osteogenic activity, and bone regeneration.

The ability of Saos-2 cells to interact with cement materials was investigated with SEM images. Cell attachment and morphologies after initial attachment on cement groups can be seen in Figure 4.30. The ability of cells to interact with materials depends on protein adhesion capacity on the material (Che et al., 2019). Protein adsorption study showed that 2La-DPC group had the lowest protein adhesion which was increased by incorporation of GO into the cement structure.

SEM images of cell attachment on all cement groups were successful. However, the attached cells on 2La-DPC group was not fully spread on the material surface and round cell morphologies were observed which shows a poor cell-material interaction (Figure. 4.30(a)). Cell morphology on the group 1GO/2La-DPC was slightly better than that of 2La-DPC group with interacted cell clusters but still there were round cells which fail to fully interact with the surface(Figure. 4.30(b)). Improved cell interaction was observed on 2GO/La-DPC and 3GO/La-DPC cement surfaces with fully spread, flattened cells (Figure 4.30 (c-d)). Presence of GO increases the protein deposition which is one of the major factor that improves cell-material interaction (Dalgic et al., 2018).

The study of Foroutan et al., reported that presence of GO can enhance osteoblast cell attachment and proposed that GO can penetrate into cells and interact with metabolic pathways that increase the expression of gene for cell adhesion markers connexin (Foroutan et al., 2018). GO reinforcement in materials has improved osteoblast cell interaction and initial attachment, which was also connected to improved cell viability by the presence of GO (Girase et al., 2012). Results have shown that 2GO/La-DPC and 3GO/La-DPC cement groups with higher GO content were more cell compatible and sustain better cell-material interaction.
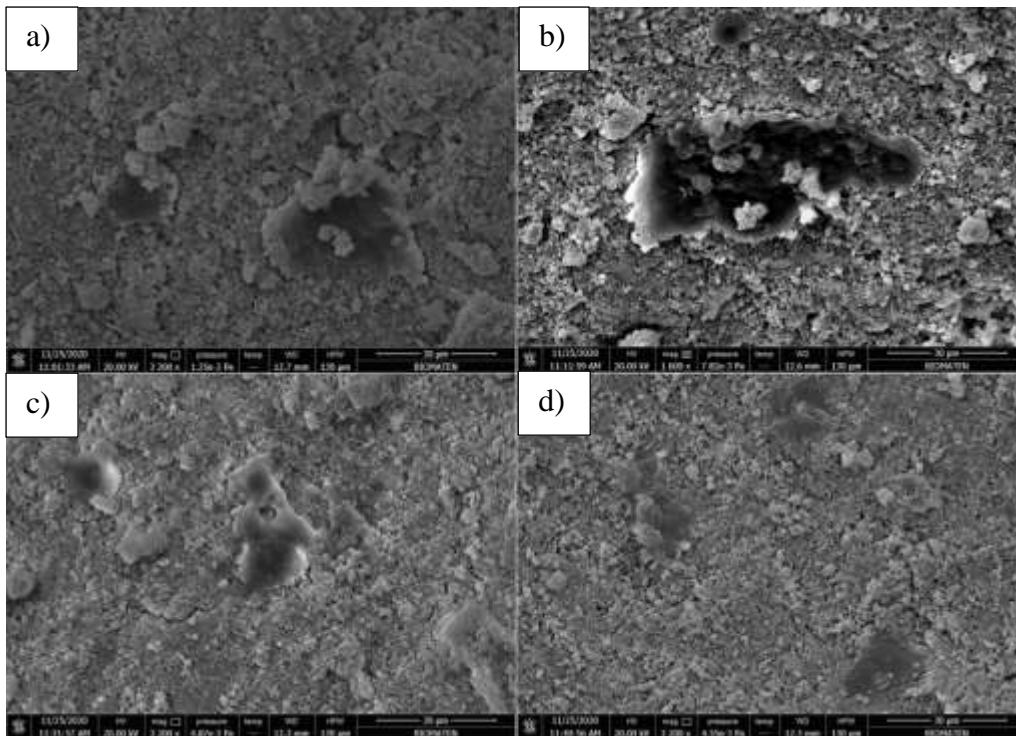
**Figure 4.30.** Cell morphologies, 1 day after initial attachment on cement groups; a) La-DPC, b) 1GO/La-DPC, c) 2GO/La-DPC, d) 3GO/La-DPC. Scale bars on images show 30 µm length.

# CHAPTER 5

## 5. CONCLUSION

Following are the major findings of this thesis:

1. The mesoporous nature of βTCP and La doped βTCP was developed using a wet precipitation method. The findings of this thesis revealed that $La^{3+}$ ions were successfully incorporated into βTCP lattice and caused expansion in lattice parameters and pore size while diminishing the crystallite size and surface area of particles. Similarly, $La^{3+}$ ions' addition displayed sustained release of serum protein over a 24 hour of incubation. The addition of $La^{3+}$ ions decreased the dissolution of βTCP. The Saos-2 cell line incubated with extracts of βTCP and La- βTCP powders. The results showed that the entire prepared materials were cytocompatible. The extract of 3La-βTCP $(Ca_{8.550}La_{0.45}(PO_4)_6)$ powder promoted cell proliferation significantly more than pure βTCP. The effect of La doping on Saos-2 cell viability and ALP activity was observed to be dose dependent. Based on the outcomes, it was concluded that La- βTCP materials have a vast potential to use in bone tissue regeneration.

2. This study focused on the impact of addition of $La^{3+}$ ions to DCP cements as a bone filler. With incorporation and an increasing amount of $La^{3+}$ ions, expansion in lattice parameters of DCP crystals, inhibition in growth size, and the paste phase of cements hardening were achieved. With incorporation of $La^{3+}$ ions (0.225 mole, 2La-DCP), the compressive strength of DCP cements (monetite phase) was improved. The presence of $La^{3+}$ ions in DCP lattice improved the degradation rate of the host materials, and leaching amount of $La^{3+}$ ions were not sufficient to be detected by the ICP-OES device.

Incorporation of La improved the protein adsorption capacity of bone cement groups and 2La-DCP group showed high protein adsorption capacity with the lowest protein desorption. All bone cement groups supported Saos-2 cell viability and adhesion while 2La-DCP bone cement showed the highest cell viability after four and seven days of incubation. 2La-DCP showed a better performance in osteogenic potency in terms of ALP activity.

3. In the last part of this thesis, GO was used as an additive. GO/2La-DCP bone cement composites were successfully prepared in this study. The materials were characterized precisely using XRD, FTIR, and SEM; the presence of GO was confirmed using TGA and UV-Vis. The addition of 3.5 wt.% of GO led (a) decreased the setting time of cements, (b) improved the mechanical properties, (c) improved the loading capacity of 2La-DCP cements, and (d) enhanced proliferation and differentiation properties of Saos-2 cell line.

As a summary, 0.225 mole of La doped DCP mixed with 3.5 wt% of GO (3GO/2La-DCP) might be ideal for bone regeneration, especially when used as a bone void filler or as a synthetic bone graft for non-load bearing applications.

# REFERENCES

Aati, S. (2017). Monetite layer-by-layer coating for bone regeneration application, MSc Thesis, Factuly of Dentistry, McGill University Libraries.

Abdel-Fattah, W.I., Reicha, F.M., Elkhooly, T.A. (2008). Nano-beta-tricalcium phosphates synthesis and biodegradation: 1. Effect of microwave and $SO_4^{2-}$ ions on β-TCP synthesis and its characterization. Biomedical Materials, 3(3), 034121.

Aberg, J., Brisby, H., Henriksson, H., Lindahl, A., Thomsen, P., Engqvist, H., (2010). Premixed acidic calcium phosphate cement: characterization of strength and microstructure. Journal of Biomedical Materials Research Part B: Applied Biomaterials, 93(2), 436-441.

Ahmari, A., (2010). Amélioration Du Ciment Acrylique Osseux Utilisé Lors de Vertébroplasties, MSc Thesis, Université de Sherbrooke.

Aissa, A., Debbabi, M., Gruselle, M., Thouvenot, R., Flambard, A., Gredin, Beaunier, P., Tõnsuaadu, K. (2009). Sorption of tartrate ions to lanthanum (III)-modified calcium fluor- and hydroxyapatite. Journal of Colloid and Interface Science, 330(1), 20-28.

Akram, M., Alshemary, A.Z., Goh, Y.-F., Ibrahim, W.A.W., Lintang, H.O., Hussain, R. (2015). Continuous microwave flow synthesis of mesoporous hydroxyapatite. Materials Science and Engineering: C,56, 356-362.

Alkhraisat, M.H., Moseke, C., Blanco, L., Barralet, J.E., Lopez-Carbacos, E., Gbureck, U. (2008). Strontium modified biocements with zero order release kinetics. Biomaterials, 29(35), 4691-4697.

Alshaaer, M., Cuypers, H., Rahier, H., Wastiels, J. (2011). Production of monetite-based Inorganic Phosphate Cement (M-IPC) using hydrothermal post curing (HTPC). Cement and Concrete Research, 41(1), 30-37.

Alshemary, A.Z., Akram, M., Goh, Y.-F., Kadir, M.R.A., Abdolahi, A., Hussain, R. (2015). Structural characterization, optical properties and *in vitro* bioactivity

of mesoporous erbium-doped hydroxyapatite. Journal of Alloys and Compounds, 645, 478-486.

Alshemary, A.Z., Pazarçeviren, E.A., Dalgic, A.D., Tezcaner, A., Keskin, D., Evis, Z. (2019). Nanocrystalline $Zn^{2+}$ and $SO_4^{2-}$ binary doped fluorohydroxyapatite: A novel biomaterial with enhanced osteoconductive and osteoinconductive properties. Materials Science and Engineering: C, 109884.

Amador, C., Martin de Juan, L. (2016). Chapter 19 - Strategies for structured particulate systems design. In M. Martín, M. R. Eden, N.G. Chemmangattuvalappil (Eds.), Computer Aided Chemical Engineering (Vol. 39, pp. 509-579): Elsevier.

Arora, M., Chan, E.K., Gupta, S., Diwan, A.D. (2013). Polymethylmethacrylate bone cements and additives: A review of the literature. World Journal of Orthopedics, 4(2), 67.

Ascherl, R. (2011). Science of bone cement. Ortho Supersite, Accessed August, 4.

ASTM 266–2008, Standard Test Method for Time of Setting of Hydraulic-Cement Paste by Gillmore Needles.

ASTM F451-2016, Standard Specification for Acrylic Bone Cement.

Bai, H., Li, C., Wang, X., Shi, G. (2010). A pH-sensitive graphene oxide composite hydrogel. Chemical Communications, 46(14), 2376-2378.

Bai, J., Wang, X.-h., Zhang, C.-j., Huang, J., Müller, W.E. (2018). Lanthanum-containing bioparticles are associated with the influence of lanthanum on high phosphate mediated bone marrow stromal cells viability. Biometals, 31(5), 771-784.

Balusamy, B., Taştan, B.E., Ergen, S.F., Uyar, T., Tekinay, T. (2015). Toxicity of lanthanum oxide ($La_2O_3$) nanoparticles in aquatic environments. Environmental Science: Processes & Impacts, 17(7), 1265-1270.

Ban, F., Majid, S., Huang, N., Lim, H. (2012). Graphene oxide and its electrochemical performance. International Journal of Electrochemical Science, 7(5), 4345-4351.

Bannerman, A., Williams, R., Cox, S., Grover, L. (2016). Visualising phase change in a brushite-based calcium phosphate ceramic. Scientific Reports, 6, 32671.

Baradaran, S., Basirun, W.J., Mahmoudian, M.R., Hamdi, M., Alias, Y. (2013). Synthesis and characterization of monetite prepared using a sonochemical method in a mixed solvent system of water/ethylene glycol/N, N-dimethylformamide. Metallurgical and Materials Transactions A, 44(5), 2331-2338.

Barralet, J., Gaunt, T., Wright, A., Gibson, I.R., Knowles, J. (2002). Effect of porosity reduction by compaction on compressive strength and microstructure of calcium phosphate cement. Journal of Biomedical Materials Research, 63(1), 1-9.

Barralet, J., Grover, L., Gbureck, U. (2004). Ionic modification of calcium phosphate cement viscosity. Part II: hypodermic injection and strength improvement of brushite cement. Biomaterials, 25(11), 2197-2203.

Bavnhøj, C.G., Knopp, M.M., Madsen, C.M., Löbmann, K. (2019). The role interplay between mesoporous silica pore volume and surface area and their effect on drug loading capacity. International Journal of Pharmaceutics: X, 1, 100008.

Berzina-Cimdina, L., Borodajenko, N. (2012). Research of calcium phosphates using Fourier transform infrared spectroscopy. Infrared Spectroscopy-Materials Science, Engineering and Technology, 12(7), 251-263.

Bessière, A., Benhamou, R.A., Wallez, G., Lecointre, A., Viana, B. (2012). Site occupancy and mechanisms of thermally stimulated luminescence in $Ca_9Ln(PO_4)_7$ (Ln=lanthanide). Acta Materialia, 60(19), 6641-6649.

Bigi, A., Foresti, E., Gandolfi, M., Gazzano, M., Roveri, N. (1997). Isomorphous substitutions in β-tricalcium phosphate: the different effects of zinc and strontium. Journal of Inorganic Biochemistry, 66(4), 259-265.

Bohner, M., (2010). Design of ceramic-based cements and putties for bone graft substitution. European Cells and Materials, 20(1), 1-12.

Bohner, M., Gbureck, U. (2008). Thermal reactions of brushite cements. Journal of Biomedical Materials Research Part B: Applied Biomaterials: 84(2), 375-385.

Bohner, M., Gbureck, U., Barralet, J. (2005). Technological issues for the development of more efficient calcium phosphate bone cements: a critical assessment. Biomaterials, 26(33), 6423-6429.

Bonfield, W., Best, S., Nobuyuki, A. (1998). Method for coating a calcium phosphate compound onto a metallic material. Patent No: WIPO WO9813539, 3.

Boroujeni, N.M., (2012). Monetite cement composites for orthopedic and dental applications, MSc Thesis, University of Toledo.

Boroujeni, N.M., Zhou, H., Luchini, T.J., Bhaduri, S.B. (2013). Development of multi-walled carbon nanotubes reinforced monetite bionanocomposite cements for orthopedic applications. Materials Science and Engineering: C, 33(7), 4323-4330.

Boroujeni, N.M., Zhou, H., Luchini, T.J., Bhaduri, S.B. (2014). Development of monetite/phosphorylated chitosan composite bone cement. Journal of Biomedical Materials Research Part B: Applied Biomaterials, 102(2), 260-266.

Boushell, M.K., Khanarian, N.T., LeGeros, R.Z., Lu, H.H. (2017). Effect of ceramic calcium–phosphorus ratio on chondrocyte-mediated biosynthesis and mineralization. Journal of Biomedical Materials Research Part A, 105(10), 2694-2702.

Brundavanam, S., Poinern, G.E.J., Fawcett, D. (2014). Growth of flower-like brushite structures on magnesium substrates and their subsequent low temperature transformation to hydroxyapatite. American Journal of Biomedical Engineering, 4(4), 79-87.

Cai, X., Tan, S., Lin, M., Xie, A., Mai, W., Zhang, X., Lin, Z., Wu, T., Liu, Y. (2011). Synergistic antibacterial brilliant blue/reduced graphene oxide/quaternary phosphonium salt composite with excellent water solubility and specific targeting capability. Langmuir, 27(12), 7828-7835.

Cama, G., Barberis, F., Capurro, M., Di Silvio, L., Deb, S. (2011). Tailoring brushite for in situ setting bone cements. Materials Chemistry and Physics, 130(3), 1139-1145.

Cama, G., Gharibi, B., Knowles, J., Romeed, S., DiSilvio, L., Deb, S. (2014). Structural changes and biological responsiveness of an injectable and mouldable monetite bone graft generated by a facile synthetic method. Journal of The Royal Society Interface, 11(101), 20140727.

Cama, G., Gharibi, B., Sait, M.S., Knowles, J., Lagazzo, A., Romeed, S., Di Silvio, L., Deb, S. (2013). A novel method of forming micro-and macroporous monetite cements. Journal of Materials Chemistry B, 1(7), 958-969.

Cama, G., Nkhwa, S., Gharibi, B., Lagazzo, A., Cabella, R., Carbone, C., Dubruel, P., Haugen, H., Di Silvio, L., Deb, S. (2017). The role of new zinc incorporated monetite cements on osteogenic differentiation of human mesenchymal stem cells. Materials Science and Engineering: C, 78, 485-494.

Carrodeguas, R.G., Lasa, B.V., Del Barrio, J.S.R. (2004). Injectable acrylic bone cements for vertebroplasty with improved properties. Journal of Biomedical Materials Research Part B: Applied Biomaterials, 68(1), 94-104.

Chang, Y., Yang, S.-T., Liu, J.-H., Dong, E., Wang, Y., Cao, A., Yuanfang, L., Wang, H. (2011). *In vitro* toxicity evaluation of graphene oxide on A549 cells. Toxicology letters, 200(3), 201-210.

Charnley, J. (1960). Anchorage of the femoral head prosthesis to the shaft of the femur. The Journal of Bone and Joint Surgery, 42(1), 28-30.

Che, Y., Min, S., Wang, M., Rao, M., Quan, C. (2019). Biological activity of hydroxyapatite/poly (methylmethacrylate) bone cement with different surface morphologies and modifications for induced osteogenesis. Journal of Applied Polymer Science, 136(47), 48188.

Chen, C., Sun, X., Pan, W., Hou, Y., Liu, R., Jiang, X., Zhang, L. (2018a). Graphene oxide-templated synthesis of hydroxyapatite nanowhiskers to improve the mechanical and osteoblastic performance of poly (lactic acid) for bone tissue regeneration. ACS Sustainable Chemistry & Engineering, 6(3), 3862-3869.

Chen, G., Luo, G., Yang, L., Xu, J., Sun, Y., Wang, J. (2005). Synthesis and size control of CaHPO4 particles in a two-liquid phase micro-mixing process. Journal of Crystal Growth, 279(3-4), 501-507.

Chen, S., Gururaj, S., Xia, W., Engqvist, H. (2016). Synthesis of Ag doped calcium phosphate particles and their antibacterial effect as additives in dental glass ionomer cements. Journal of Materials Science: Materials in Medicine, 27(11), 172.

Chen, S., Wang, S., Li, H., Forsberg, K. (2018b). $Eu^{3+}$ doped monetite and its use as fluorescent agent for dental restorations. Ceramics International, 44(9), 10510-10516.

Choi, B.G., Park, H., Park, T.J., Yang, M.H., Kim, J.S., Jang, S.-Y., Su Heo, N., Yup Lee, S., Kong, J., Hong, W. H. (2010). Solution chemistry of self-assembled graphene nanohybrids for high-performance flexible biosensors. ACS Nano, 4(5), 2910-2918.

Chow, L.C. (1991). Development of self-setting calcium phosphate cements. Journal of the Ceramic Society of Japan, 99(1154), 954-964.

Chow, L.C. (1999). Calcium phosphate cements: chemistry, properties, and applications. MRS Online Proceedings Library Archive, 599.

Chow, L.C. (2009). Next generation calcium phosphate-based biomaterials. Dental Materials Journal, 28(1), 1-10.

Chow, L.C., Takagi, S. (2001). A natural bone cement—A laboratory novelty led to the development of revolutionary new biomaterials. Journal of Research of the National Institute of Standards and Technology, 106(6), 1029.

Constantz, B.R., Barr, B.M., Ison, I.C., Fulmer, M.T., Baker, J., McKinney, L.,Goodman, S.B., Gunasekaren, S., Delaney, D.C., Ross, J., Poser, R.D., (1998). Histological, chemical, and crystallographic analysis of four calcium phosphate cements in different rabbit osseous sites. Journal of Biomedical Materials Research, 43(4), 451-461.

Costantino, P.D., Chaplin, J.M., Wolpoe, M.E., Catalano, P.J., Sen, C., Bederson, J.B., Govindaraj, S. (2000). Applications of fast-setting hydroxyapatite cement: cranioplasty. Otolaryngology—Head and Neck Surgery, 123(4), 409-412.

Cox, S.C., Patel, S., Gbureck, U., Wright, A.J., Grover, L.M. (2017). A cohesive premixed monetite biocement. Journal of the American Ceramic Society, 100(3), 1241-1249.

da Rocha, D.N., de Oliveira Cruz, L.R., de Campos, J.B., dos Santos, J.L., Marçal, R.L.S.B., Mijares, D.Q., Barbosa, R.M., Coelho, P., da Silva, M.H.P. (2019). Bioactivity of strontium-monetite coatings for biomedical applications. Ceramics International, 45(6), 7568-7579.

da Silva, M.P., Lima, J., Soares, G., Elias, C., De Andrade, M., Best, S., Gibson, I. R. (2001). Transformation of monetite to hydroxyapatite in bioactive coatings on titanium. Surface and Coatings Technology, 137(2-3), 270-276.

Dagang, G., Haoliang, S., Kewei, X., Yong, H. (2007). Long-term variations in mechanical properties and in vivo degradability of CPC/PLGA composite. Journal of Biomedical Materials Research Part B: Applied Biomaterials, 82(2), 533-544.

Dalgic, A.D., Alshemary, A.Z., Tezcaner, A., Keskin, D., Evis, Z. (2018). Silicate-doped nano-hydroxyapatite/graphene oxide composite reinforced fibrous scaffolds for bone tissue engineering. Journal of Biomaterials Applications, 32(10), 1392-1405.

Dang, W., Ma, B., Huan, Z., Lin, R., Wang, X., Li, T., Wu, J.F., Ma, N., Chang, J., Wu, C. (2019). $LaB_6$ surface chemistry-reinforced scaffolds for treating bone tumors and bone defects. Applied Materials Today, 16, 42-55.

Dawei, Z., Jinchao, Z., Yao, C., Mengsu, Y., Xinsheng, Y. (2007). Effects of lanthanum and gadolinium on proliferation and differentiation of primary osteoblasts. Progress in Natural Science, 17(5), 618-623.

Deb, S., (2006). Orthopedic bone cement. Wiley Encyclopedia of Biomedical Engineering, 118-146.

Desai, T.R., Bhaduri, S.B., Tas, A.C. (2007). A self-setting, monetite ($CaHPO_4$) cement for skeletal repair. Paper presented at the Ceramic Engineering and Science proceedings.

Destainville, A., Champion, E., Bernache-Assollant, D., Laborde, E. (2003). Synthesis, characterization and thermal behavior of apatitic tricalcium phosphate. Materials Chemistry and Physics, 80(1), 269-277.

Dikin, D.A., Stankovich, S., Zimney, E.J., Piner, R.D., Dommett, G.H., Evmenenko, G., SonBinh T,N., Ruoff, R.S. (2007). Preparation and characterization of graphene oxide paper. Nature, 448(7152), 457-460.

Dorozhkin, S.V. (2008). Calcium orthophosphate cements for biomedical application. Journal of Materials Science, 43(9), 3028-3057.

Dorozhkin, S.V. (2013). Self-setting calcium orthophosphate formulations. Journal of Functional Biomaterials, 4(4), 209-311.

Dorozhkin, S.V. (2016). Multiphasic calcium orthophosphate ($CaPO_4$) bioceramics and their biomedical applications. Ceramics International, 42(6), 6529-6554.

Dorozhkin, S.V., Epple, M. (2002). Biological and medical significance of calcium phosphates. Angewandte Chemie International Edition, 41(17), 3130-3146.

Dosen, A., Giese, R.F. (2011). Thermal decomposition of brushite, $CaHPO_4 \cdot 2H_2O$ to monetite $CaHPO_4$ and the formation of an amorphous phase. American Mineralogist, 96(2-3), 368-373.

110

Driessens, F., Planell, J., Boltong, M., Khairoun, I., Ginebra, M. (1998). Osteotransductive bone cements. Proceedings of the Institution of Mechanical Engineers, Part H: Journal of Engineering in Medicine, 212(6), 427-435.

Drouet, C. (2013). Apatite formation: why it may not work as planned, and how to conclusively identify apatite compounds. BioMed Research International, 2013 (4):490946.

Duncan, J., MacDonald, J.F., Hanna, J.V., Shirosaki, Y., Hayakawa, S., Osaka, A., Skakle, J.M.S., Gibson, I. R. (2014). The role of the chemical composition of monetite on the synthesis and properties of α-tricalcium phosphate. Materials Science and Engineering: C, 34, 123-129.

Eliaz, N., Metoki, N. (2017). Calcium phosphate bioceramics: a review of their history, structure, properties, coating technologies and biomedical applications. Materials, 10(4), 334.

Ellingsen, J., Pinholt, E. (1995). Pretreatment of titanium implants with lanthanum ions alters the bone reaction. Journal of Materials Science: Materials in Medicine, 6(3), 125-129.

Elliott, J. (1994). Hydroxyapatite and nonstoichiometric apatites. Structure and chemistry of the apatites and other calcium orthophosphates, Publisher: Elsevier.

Enderle, R., Götz-Neunhoeffer, F., Göbbels, M., Müller, F.A., Greil, P. (2005). Influence of magnesium doping on the phase transformation temperature of β-TCP ceramics examined by Rietveld refinement. Biomaterials, 26(17), 3379-3384.

Engstrand, J., Persson, C., Engqvist, H. (2014). The effect of composition on mechanical properties of brushite cements. Journal of the Mechanical Behavior of Biomedical Materials, 29, 81-90.

Engstrand Unosson, J., Persson, C., Engqvist, H. (2015). An evaluation of methods to determine the porosity of calcium phosphate cements. Journal of Biomedical Materials Research Part B: Applied Biomaterials, 103(1), 62-71.

Ergun, C., Liu, H., Webster, T.J. (2009). Osteoblast adhesion on novel machinable calcium phosphate/lanthanum phosphate composites for orthopedic applications. Journal of Biomedical Materials Research Part A, 89(3), 727-733.

Feig, V.R., Tran, H., Bao, Z. (2018). Biodegradable polymeric materials in degradable electronic devices. ACS Central Science, 4(3), 337-348.

Felgueiras, H.P., Antunes, J.C., Martins, M.C.L., Barbosa, M.A. (2018). Fundamentals of protein and cell interactions in biomaterials. In M.A. Barbosa & M.C.L. Martins (Eds.), Peptides and Proteins as Biomaterials for Tissue Regeneration and Repair (pp. 1-27): Woodhead Publishing.

Ferna, E., Gil, F., Ginebra, M., Driessens, F., Planell, J., Best, S. (1999). Calcium phosphate bone cements for clinical applications. Part I: solution chemistry. Journal of Materials Science: Materials in Medicine, 10(3), 169-176.

Foroutan, T., Nazemi, N., Tavana, M., Kassaee, M.Z., Motamedi, E., Sonieshargh, S., Zare Zardini, H. (2018). Suspended graphene oxide nanoparticle for accelerated multilayer osteoblast attachment. Journal of Biomedical Materials Research Part A, 106(1), 293-303.

Francis, A., Rahman, M.A. (2016). The environmental sustainability of calcined calcium phosphates production from the milling of eggshell wastes and phosphoric acid. Journal of Cleaner Production, 137, 1432-1438.

Fu, C., Bai, H., Zhu, J., Niu, Z., Wang, Y., Li, J., Yang, X., Bai, Y. (2017). Enhanced cell proliferation and osteogenic differentiation in electrospun PLGA/hydroxyapatite nanofibre scaffolds incorporated with graphene oxide. PLOS ONE, 12(11), 0188352.

Fu, Q., Saiz, E., Rahaman, M.N., Tomsia, A.P. (2013). Toward strong and tough glass and ceramic scaffolds for bone repair. Advanced Functional Materials, 23(44), 5461-5476.

Galakhov, A., Kutsev, S., Kryuchkov, V., Prokof'ev, A., Litvinov, I. (1993). Effect of compaction pressure on the sinterability of submicron powders of tetragonal zirconium dioxide. Refractories, 34(1-2), 70-81.

Gallinetti, S., Canal, C., Ginebra, M.P. (2014). Development and characterization of biphasic hydroxyapatite/β-TCP cements. Journal of the American Ceramic Society, 97(4), 1065-1073.

Gamal, G., Al-Mufadi, F., Said, A. (2013). Effect of iron additives on the microstructure of hydroxyapatite. Engineering, Technology & Applied Science Research, 3(6), 532-539.

Gbureck, U., Hölzel, T., Klammert, U., Wuerzler, K., Mueller, F.A., Barralet, J. E. (2007). Resorbable dicalcium phosphate bone substitutes prepared by 3D powder printing. Advanced Functional Materials, 17(18), 3940-3945.

Gencalp Irizalp, S., Saklakoglu, N. (2017). Laser Peening of Metallic Materials. In M.S.J. Hashmi (Ed.), Comprehensive Materials Finishing (pp.408-440). Oxford: Elsevier.

Geng, Z., Cui, Z., Li, Z., Zhu, S., Liang, Y., Liu, Y., Li, X., He, X., Yu, X., Wang, R., Yang, X. (2016). Strontium incorporation to optimize the antibacterial and biological characteristics of silver-substituted hydroxyapatite coating. Materials Science and Engineering: C, 58, 467-477.

Gerber, L.C., Moser, N., Luechinger, N.A., Stark, W.J., Grass, R.N. (2012). Phosphate starvation as an antimicrobial strategy: the controllable toxicity of lanthanum oxide nanoparticles. Chemical Communications, 48(32), 3869-3871.

Ghosh, R., Sarkar, R., Paul, S. (2016). Development of machinable hydroxyapatite-lanthanum phosphate composite for biomedical applications. Materials & Design, 106, 161-169.

Gibson, I.R., Bonfield, W. (2002). Novel synthesis and characterization of an AB-type carbonate-substituted hydroxyapatite. Journal of Biomedical Materials Research, 59(4), 697-708.

Ginebra, M.-P., Traykova, T., Planell, J.A. (2006). Calcium phosphate cements as bone drug delivery systems: a review. Journal of Controlled Release, 113(2), 102-110.

Ginebra, M., Fernández, E., Boltong, M., Bermúdez, O., Planell, J., Driessens, F. (1994). Compliance of an apatitic calcium phosphate cement with the short-term clinical requirements in bone surgery, orthopaedics and dentistry. Clinical Materials, 17(2), 99-104.

Girase, B., Shah, J.S., Misra, R.D.K. (2012). Cellular mechanics of modulated osteoblasts functions in graphene oxide reinforced elastomers. Advanced Engineering Materials, 14(4), B101-B111.

Goh, Y.-F., Alshemary, A.Z., Akram, M., Kadir, M.R.A., Hussain, R. (2014). *In-vitro* characterization of antibacterial bioactive glass containing ceria. Ceramics International, 40(1), 729-737.

Graziani, G., Boi, M., Bianchi, M. (2018). A review on ionic substitutions in hydroxyapatite thin films: Towards complete biomimetism. Coatings, 8(8)

Gunatillake, P., Adhikari, R. (2016). Nondegradable synthetic polymers for medical devices and implants. In Biosynthetic Polymers for Medical Applications (pp. 33-62): Elsevier.

Guo, D., Wang, A., Han, Y., Xu, K. (2009). Characterization, physicochemical properties and biocompatibility of La-incorporated apatites. Acta Biomaterialia, 5(9), 3512-3523.

Habraken, W., Habibovic, P., Epple, M., Bohner, M. (2016). Calcium phosphates in biomedical applications: materials for the future?. Materials Today, 19(2), 69-87.

Heini, P.F., Berlemann, U., Kaufmann, M., Lippuner, K., Fankhauser, C., van Landuyt, P. (2001). Augmentation of mechanical properties in osteoporotic vertebral bones–a biomechanical investigation of vertebroplasty efficacy with different bone cements. European Spine Journal, 10(2), 164-171.

Hench, L.L., Polak, J.M. (2002). Third-generation biomedical materials. Science, 295(5557), 1014-1017.

Henrichsen, E., Jansen, K., Krogh-Poulsen, W. (1952). Experimental investigation of the tissue reaction to acrylic plastics. Acta Orthopaedica Scandinavica, 22(1-4), 141-146.

Hermenean, A., Codreanu, A., Herman, H., Balta, C., Rosu, M., Mihali, C.V., Ivan, A., Dinescu, S., Ionita, M., Costache, M. (2017). Chitosan-graphene oxide 3D scaffolds as promising tools for bone regeneration in critical-size mouse calvarial defects. Scientific Reports, 7(1), 1-12.

Higuita, L.P., Vargas, A.F., Gil, M.J., Giraldo, L.F. (2016). Synthesis and characterization of nanocomposite based on hydroxyapatite and monetite. Materials Letters, 175, 169-172.

Hofmann, M., Nazhat, S., Gbureck, U., Barralet, J. (2006). Real-time monitoring of the setting reaction of brushite-forming cement using isothermal differential scanning calorimetry. Journal of Biomedical Materials Research Part B: Applied Biomaterials, 79(2), 360-364.

Hong, M., Kim, S., Lee, Y. (2017). Mechanical and biological properties of biphasic calcium phosphate scaffold depending on different nanoparticle fabrication methods. Journal of Ceramic Science and Technology, 8(4), 541-545.

Honkanen, P., Kellomäki, M., Lehtimäki, M., Törmälä, P., Mäkelä, S., Lehto, M. (2003). Bioreconstructive joint scaffold implant arthroplasty in metacarpophalangeal joints: short-term results of a new treatment concept in rheumatoid arthritis patients. Tissue Engineering, 9(5), 957-965.

Hsiao, M.-C., Liao, S.-H., Yen, M.-Y., Liu, P.-I., Pu, N.-W., Wang, C.-A., Ma, C.-C. M. (2010). Preparation of covalently functionalized graphene using residual oxygen-containing functional groups. ACS Applied Materials & Interfaces, 2(11), 3092-3099.

Hu, H., Wang, X., Wang, J., Wan, L., Liu, F., Zheng, H., Chen, R., Xu, C. (2010). Preparation and properties of graphene nanosheets–polystyrene nanocomposites via in situ emulsion polymerization. Chemical Physics Letters, 484(4-6), 247-253.

Hu, H., Zhao, P., Liu, J., Ke, Q., Zhang, C., Guo, Y., Ding, H. (2018). Lanthanum phosphate/chitosan scaffolds enhance cytocompatibility and osteogenic efficiency via the Wnt/β-catenin pathway. Journal of Nanobiotechnology, 16(1), 98.

Huan, Z., Chang, J. (2009). Novel bioactive composite bone cements based on the β-tricalcium phosphate–monocalcium phosphate monohydrate composite cement system. Acta Biomaterialia, 5(4), 1253-1264.

Huang, M., Li, T., Zhao, N., Yao, Y., Yang, H., Du, C., Wang, Y. (2014). Doping strontium in tricalcium phosphate microspheres using yeast-based biotemplate. Materials Chemistry and Physics, 147(3), 540-544.

Iacoboni, I., Perrozzi, F., Macera, L., Taglieri, G., Ottaviano, L., Fioravanti, G. (2019). In situ syntheses of hydroxyapatite-grafted graphene oxide composites. Journal of Biomedical Materials Research Part A, 107(9), 2026-2039.

Idowu, B., Cama, G., Deb, S., Di Silvio, L. (2014). *In vitro* osteoinductive potential of porous monetite for bone tissue engineering. Journal of Tissue Engineering, 5, 2041731414536572.

Ishigami, M., Chen, J., Cullen, W., Fuhrer, M., Williams, E. (2007). Atomic structure of graphene on $SiO_2$. Nano Letters, 7(6), 1643-1648.

Ito, A., Kawamura, H., Otsuka, M., Ikeuchi, M., Ohgushi, H., Ishikawa, K., Onuma, K., Kanzaki, N., Sogo, Y., Ichinose, N. (2002). Zinc-releasing calcium phosphate for stimulating bone formation. Materials Science and Engineering: C, 22(1), 21-25.

Jaber, H.L., Hammood, A.S., Parvin, N. (2018). Synthesis and characterization of hydroxyapatite powder from natural Camelus bone. Journal of the Australian Ceramic Society, 54(1), 1-10.

Jadalannagari, S., Deshmukh, K., Verma, A.K., Kowshik, R.V., Ramanan, M., Roy, S. (2014). Lanthanum-doped hydroxyapatite nanoparticles as biocompatible fluorescent probes for cellular internalization and biolabeling. Science of Advanced Materials, 6(2), 312-319.

Jang, J.-H., Shin, S., Kim, H.-J., Jeong, J., Jin, H.-E., Desai, M. S., Lee, S-W., Kim, S.-Y. (2018). Improvement of physical properties of calcium phosphate cement by elastin-like polypeptide supplementation. Scientific Reports, 8(1), 1-11.

Jokić, B., Mitrić, M., Radmilović, V., Drmanić, S., Petrović, R., Janaćković, D. (2011). Synthesis and characterization of monetite and hydroxyapatite whiskers obtained by a hydrothermal method. Ceramics International, 37(1), 167-173.

Kannan, S., Goetz-Neunhoeffer, F., Neubauer, J., Ferreira, J.M. (2011). Cosubstitution of zinc and strontium in β-tricalcium phosphate: synthesis and characterization. Journal of the American Ceramic Society, 94(1), 230-235.

Karimi, M., Ramsheh, M.R., Ahmadi, S.M., Madani, M.R. (2017). One-step and low-temperature synthesis of monetite nanoparticles in an all-in-one system (reactant, solvent, and template) based on calcium chloride-choline chloride deep eutectic medium. Ceramics International, 43(2), 2046-2050.

Kawabata, K., Yamamoto, T., Kitada, A. (2011). Substitution mechanism of Zn ions in β-tricalcium phosphate. Physica B: Condensed Matter, 406(4), 890-894.

Kaygili, O., Tatar, C., Keser, S., Bulut, N. (2017). Preparation and characterization of monetites co-doped with Ni/Al, Ni/Mn and Al/Mn. Materials Letters, 201, 39-42.

Kellomäki, M., Niiranen, H., Puumanen, K., Ashammakhi, N., Waris, T., Törmälä, P. (2000). Bioabsorbable scaffolds for guided bone regeneration and generation. Biomaterials, 21(24), 2495-2505.

Kharaziha, M., Fathi, M. (2010). Improvement of mechanical properties and biocompatibility of forsterite bioceramic addressed to bone tissue engineering materials. Journal of the Mechanical Behavior of Biomedical Materials, 3(7), 530-537.

Khashaba, R.M., Moussa, M.M., Mettenburg, D.J., Rueggeberg, F.A., Chutkan, N. B., Borke, J.L. (2010). Polymeric-calcium phosphate cement composites-

material properties: *in vitro* and in vivo investigations. International Journal of Biomaterials, 2010: 691452.

Khor, E. (2014). Chapter 3 - Taking Academic Biomedical Research Beyond the Lab Bench. In E. Khor (Ed.), From Academia to Entrepreneur (pp. 45-73). Amsterdam: Academic Press.

Khoshsima, S., Alshemary, A.Z., Tezcaner, A., Surdem, S., Evis, Z. (2018). Impact of $B_2O_3$ and $La_2O_3$ addition on structural, mechanical and biological properties of hydroxyapatite. Processing and Application of Ceramics, 12(2), 143-152.

Khoshsima, S., Yilmaz, B., Tezcaner, A., Evis, Z. (2016). Structural, mechanical and biological properties of hydroxyapatite-zirconia-lanthanum oxide composites. Ceramics International, 42(14), 15773-15779.

Kim, D.H., Yoon, S.Y., Park, H.C. (2014). Dispersion stability of hydroxyapatite-calcium phosphate glass ceramic-tertiary butyl alcohol system. Advanced Materials Research, 941–944, 505–508.

Kim, J.H., Oh, J.H., Han, I., Kim, H.-S., Chung, S.W. (2011). Grafting using injectable calcium sulfate in bone tumor surgery: comparison with demineralized bone matrix-based grafting. Clinics in Orthopedic Surgery, 3(3), 191-201.

Kim, J.-W., Shin, Y.C., Lee, J.-J., Bae, E.-B., Jeon, Y.-C., Jeong, C.-M., Yun, M.-J., Lee, S.-H., Han, D.-W., Huh, J.-B. (2017). The effect of reduced graphene oxide-coated biphasic calcium phosphate bone graft material on osteogenesis, International Journal of Molecular Sciences, 18(8), 1725.

Klammert, U., Reuther, T., Jahn, C., Kraski, B., Kübler, A., Gbureck, U. (2009). Cytocompatibility of brushite and monetite cell culture scaffolds made by three-dimensional powder printing. Acta Biomaterialia, 5(2), 727-734.

Koju, N., Sikder, P., Gaihre, B., Bhaduri, S. (2018). Smart injectable self-setting monetite based bioceramics for orthopedic applications. Materials, 11(7), 1258.

118

Komath, M., Varma, H., Sivakumar, R. (2000). On the development of an apatitic calcium phosphate bone cement. Bulletin of Materials Science, 23(2), 135-140.

Kong, X.-D., Sun, X.-D., Lu, J.-B., Cui, F.-Z. (2005). Mineralization of calcium phosphate in reverse microemulsion. Current Applied Physics, 5(5), 519-521.

Kraus, T., Fischerauer, S.F., Hänzi, A.C., Uggowitzer, P.J., Löffler, J. F., Weinberg, A. M. (2012). Magnesium alloys for temporary implants in osteosynthesis: in vivo studies of their degradation and interaction with bone. Acta Biomaterialia, 8(3), 1230-1238.

Kruppke, B., Farack, J., Wagner, A.-S., Beckmann, S., Heinemann, C., Glenske, K., Rößler, S., Wiesmann, H-S., Wenisch, S., Hanke, T. (2016). Gelatine modified monetite as a bone substitute material: an *in vitro* assessment of bone biocompatibility. Acta Biomaterialia, 32, 275-285.

Kuehn, K.-D., Ege, W., Gopp, U. (2005). Acrylic bone cements: composition and properties. Orthopedic Clinics, 36(1), 17-28.

Kühn, K.-D. (2005). What is bone cement? The well-cemented total hip arthroplasty (pp. 52-59): Springer.

Lai, Q., Zhu, S., Luo, X., Zou, M., Huang, S. (2012). Ultraviolet-visible spectroscopy of graphene oxides. AIP Advances, 2(3), 032146.

Lee, J., Kim, J., Kim, S., Min, D.-H. (2016). Biosensors based on graphene oxide and its biomedical application. Advanced Drug Delivery Reviews, 105, 275-287.

LeGeros, R.Z. (2002). Properties of osteoconductive biomaterials: calcium phosphates. Clinical Orthopaedics and Related Research, 395, 81-98.

Lemaitre, J., Mirtchi, A., Mortier, A. (1987). Calcium phosphate cements for medical use: state of the art and perspectives of development. Silicates Industry Ceramic Science Technology, 52(9-10), 141-146.

Li, H., Fierens, K., Zhang, Z., Vanparijs, N., Schuijs, M.J., Van Steendam, K., Feiner Gracia, N., De Rycke, R., De Beer., T., De Beuckelaer, A. De Koker, S., Deforce, D., Albertazzi, L., Grooten, J., Lambrecht, B., De Gees, B-G., (2016). Spontaneous protein adsorption on graphene oxide nanosheets allowing efficient intracellular vaccine protein delivery. ACS Applied Materials & Interfaces, 8(2), 1147-1155.

Li, M., Liu, Q., Jia, Z., Xu, X., Cheng, Y., Zheng, Y., Xi, T., Wei, S. (2014a). Graphene oxide/hydroxyapatite composite coatings fabricated by electrophoretic nanotechnology for biological applications. Carbon, 67, 185-197.

Li, X., Ito, A., Sogo, Y., Wang, X., LeGeros, R. (2009). Solubility of Mg-containing β-tricalcium phosphate at 25 C. Acta Biomaterialia, 5(1), 508-517.

Li, Y., Liu, C., Zhai, H., Zhu, G., Pan, H., Xu, X., Tang, R. (2014b). Biomimetic graphene oxide–hydroxyapatite composites via in situ mineralization and hierarchical assembly. Royal Society of Chemistry Advances, 4(48), 25398-25403.

Liang, G., Neophytou, N., Lundstrom, M.S., Nikonov, D.E. (2008). Contact effects in graphene nanoribbon transistors. Nano Letters, 8(7), 1819-1824.

Liao, C.-J., Lin, F.-H., Chen, K.-S., Sun, J.-S. (1999). Thermal decomposition and reconstitution of hydroxyapatite in air atmosphere. Biomaterials, 20(19), 1807-1813.

Lin, B., Zhou, H., Leaman, D.W., Goel, V.K., Agarwal, A.K., Bhaduri, S.B. (2014). Sustained release of small molecules from carbon nanotube-reinforced monetite calcium phosphate cement. Materials Science and Engineering: C, 43, 92-96.

Lindahl, H., Malchau, H., Herberts, P., Garellick, G. (2005). Periprosthetic femoral fractures: classification and demographics of 1049 periprosthetic femoral fractures from the Swedish National Hip Arthroplasty Register. The Journal of Arthroplasty, 20(7), 857-865.

Ling-Ling, E., Xu, L.-L., Wu, X., Wang, D.-S., Lv, Y., Wang, J.-Z., Liu, H.-C. (2010). The interactions between rat-adipose-derived stromal cells, recombinant human bone morphogenetic protein-2, and beta-tricalcium phosphate play an important role in bone tissue engineering. Tissue Engineering Part A, 16(9), 2927.

Liu, D., Ge, K., Sun, J., Chen, S., Jia, G., Zhang, J. (2015). Lanthanum breaks the balance between osteogenesis and adipogenesis of mesenchymal stem cells through phosphorylation of Smad1/5/8. Royal Society of Chemistry Advances, 5(53), 42233-42241.

Liu, D., Zhang, J., Wang, G., Liu, X., Wang, S., Yang, M. (2012). The dual-effects of $LaCl_3$ on the proliferation, osteogenic differentiation, and mineralization of $MC_3T_3-E_1$ cells. Biological Trace Element Research, 150(1-3), 433-440.

Liu, H., Cheng, J., Chen, F., Bai, D., Shao, C., Wang, J., Xi, P., Zeng, Z. (2014). Gelatin functionalized graphene oxide for mineralization of hydroxyapatite: biomimetic and *in vitro* evaluation. Nanoscale, 6(10), 5315-5322.

Lou, W., Dong, Y., Zhang, H., Jin, Y., Hu, X., Ma, J., Liu, J.,Wu, G. (2015). Preparation and characterization of lanthanum-incorporated hydroxyapatite coatings on titanium substrates. International Journal of Molecular Sciences, 16(9), 21070-21086.

Lu, J., Do, I., Drzal, L. T., Worden, R.M., Lee, I. (2008). Nanometal-decorated exfoliated graphite nanoplatelet based glucose biosensors with high sensitivity and fast response. ACS Nano, 2(9), 1825-1832.

Luchini, T.J.F. (2012). Development of high strength dicalcium phosphate anhydrous cement with nanosilica sol, MSc Thesis, University of Toledo,

Luo, J., Martinez-Casado, F.J., Balmes, O., Yang, J., Persson, C., Engqvist, H., Xia, W. (2017). In situ synchrotron X-ray diffraction analysis of the setting process of brushite cement: reaction and crystal growth. ACS Applied Materials & Interfaces, 9(41), 36392-36399.

Ma, M.-G., Zhu, Y.-J., Chang, J. (2006). Monetite formed in mixed solvents of water and ethylene glycol and its transformation to hydroxyapatite. The Journal of Physical Chemistry B, 110(29), 14226-14230.

Marcano, D.C., Kosynkin, D.V., Berlin, J.M., Sinitskii, A., Sun, Z., Slesarev, A., Alemany, L.B., Lu, W., Tour, J.M. (2010). Improved synthesis of graphene oxide. American Chemical Society Nano. 24;4(8):4806-14..

Maeno, S., Niki, Y., Matsumoto, H., Morioka, H., Yatabe, T., Funayama, A., Toyama, Y., Taguchi,T., Tanaka, J. (2005). The effect of calcium ion concentration on osteoblast viability, proliferation and differentiation in monolayer and 3D culture. Biomaterials, 26(23), 4847-4855.

Matsumoto, N., Yoshida, K., Hashimoto, K., Toda, Y. (2010). Dissolution mechanisms of β-tricalcium phosphate doped with monovalent metal ions. Journal of the Ceramic Society of Japan, 118(1378), 451-457.

Medvecky, L., Stulajterova, R., Giretova, M., Mincik, J., Vojtko, M., Balko, J., Briancin, J. (2018). Effect of tetracalcium phosphate/monetite toothpaste on dentin remineralization and tubule occlusion *in vitro*. Dental Materials, 34(3), 442-451.

Meenambal, R., Singh, R.K., Kumar, P.N., Kannan, S. (2014). Synthesis, structure, thermal stability, mechanical and antibacterial behaviour of lanthanum ($La^{3+}$) substitutions in β-tricalciumphosphate. Materials Science and Engineering: C, 43, 598-606.

Meng, N., Zhang, S.-Q., Zhou, N.-L., Shen, J. (2010). Biopolymer-modified graphite oxide nanocomposite films based on benzalkonium chloride–heparin intercalated in graphite oxide. Nanotechnology, 21(18), 185101.

Mestres, G., Ginebra, M.-P. (2011). Novel magnesium phosphate cements with high early strength and antibacterial properties. Acta Biomaterialia, 7(4), 1853-1861.

Middleton, J.C., Tipton, A.J. (2000). Synthetic biodegradable polymers as orthopedic devices. Biomaterials, 21(23), 2335-2346.

Mirtchi, A.A., Lemaitre, J., Terao, N. (1989). Calcium phosphate cements: study of the β-tricalcium phosphate—monocalcium phosphate system. Biomaterials, 10(7), 475-480.

Motameni, A., Dalgic, A.D., Alshemary, A.Z., Keskin, D., Evis, Z. (2020). Structural and biological analysis of mesoporous lanthanum doped βTCP for potential use as bone graft material. Materials Today Communications, 101151

Müller, F.A., Gbureck, U., Kasuga, T., Mizutani, Y., Barralet, J.E., Lohbauer, U. (2007). Whisker-reinforced calcium phosphate cements. Journal of the American Ceramic Society, 90(11), 3694-3697.

Mulongo-Masamba, R., El Kassri, T., Khachani, M., Arsalane, S., Halim, M., El Hamidi, A. (2016). Synthesis and thermal dehydroxylation kinetic of anhydrous calcium phosphate monetite $CaHPO_4$. Journal of Thermal Analysis and Calorimetry, 124(1), 171-180.

Nasrollahi, N., Dehkordi, A.N., Jamshidizad, A., Chehelgerdi, M. (2019). Preparation of brushite cements with improved properties by adding graphene oxide. International Journal of Nanomedicine, 14, 3785.

Naumov, A.V. (2017). Optical properties of graphene oxide. In Graphene Oxide-Fundamentals Appl. (pp. 147-174): Wiley Online Library.

Nien, Y.H., Huang, C.L. (2010). The mechanical study of acrylic bone cement reinforced with carbon nanotube. Materials Science and Engineering: B, 169(1-3), 134-137.

Nilsson, H., Dragomir, A., Ahlander, A., Ljungkvist, M., Roomans, G.M. (2006). A modified technique for the impregnation of lanthanum tracer to study the integrity of tight junctions on cells grown on a permeable substrate. Microscopy Research and Technique, 69(10), 776-783.

Nishad, K., Sureshbabu, S., Komath, M., Unnikrishnan, G. (2017). Synthesis and characterization of low dimensional bioactive monetite by solvent exchange method. Materials Letters, 209, 19-22.

Nosrati, H., Sarraf-Mamoory, R., Le, D.Q.S., Emameh, R.Z., Perez, M.C., Bünger, C.E., (2020). Improving the mechanical behavior of reduced graphene oxide/hydroxyapatite nanocomposites using gas injection into powders synthesis autoclave, Scientific Reports,10(1), 1-13.

Nottrott, M. (2010). Acrylic bone cements: influence of time and environment on physical properties. Acta Orthopaedica, 81(341), 1-27.

O'Neill, R., McCarthy, H.O., Montufar, E.B., Ginebra, M.-P., Wilson, D., Lennon, A., Dunne, N. (2017). Critical review: Injectability of calcium phosphate pastes and cements. Acta Biomaterialia, 50, 1-19.

Ofudje, E.A., Adeogun, A.I., Idowu, M.A., Kareem, S.O. (2019). Synthesis and characterization of Zn-Doped hydroxyapatite: scaffold application, antibacterial and bioactivity studies. Heliyon, 5(5), e01716.

Oguchi, H., Ishikawa, K., Mizoue, K., Seto, K., Eguchi, G. (1995). Long-term histological evaluation of hydroxyapatite ceramics in humans. Biomaterials, 16(1), 33-38.

Oğuz, Ö.D., Ege, D. (2019). Preparation of graphene oxide-reinforced calcium phosphate/calcium sulfate/methylcellulose-based injectable bone substitutes. Materials Research Society Communications, 9(4), 1174-1180.

Okada, M. (2002). Chemical syntheses of biodegradable polymers. Progress in Polymer Science, 27(1), 87-133.

Oktar, F.N., Ozyegin, L.S., Meydanoglu, O., Aydin, H., Agathopoulos, S., Rocha, G., Sennaroglu, B., Kayali, E.S. (2006). Sintering effect on mechanical properties of composites of hydroxyapatite lanthanum oxide (HA-La2O3). Key Engineering Materials, 101–104.

Ossonon, B.D., Bélanger, D. (2017). Synthesis and characterization of sulfophenyl-functionalized reduced graphene oxide sheets. Royal Society of Chemistry Advances, 7(44), 27224-27234.

Ouerfelli, N., Zid, M. (2016). New polymorph of $CaHPO_4$ (monetite): synthesis and crystal structure. Journal of Structural Chemistry, 57(3), 628-631.

Ovesen, J., Møller-Madsen, B., Thomsen, J.S., Danscher, G., Mosekilde, L. (2001). The positive effects of zinc on skeletal strength in growing rats. Bone, 29(6), 565-570.

Pagano, G., Guida, M., Tommasi, F., Oral, R. (2015). Health effects and toxicity mechanisms of rare earth elements—Knowledge gaps and research prospects. Ecotoxicology and Environmental Safety, 115, 40-48.

Pazarlioglu, S., Salman, S. (2019). Effect of lanthanum oxide additive on the sinterability, physical/mechanical, and bioactivity properties of hydroxyapatite-alumina composite. Journal of the Australian Ceramic Society, 55(4), 1195-1209.

Peng, X.-Y., Hu, M., Liao, F., Yang, F., Ke, Q.-F., Guo, Y.-P., Zhu, Z.-H. (2019). La-Doped mesoporous calcium silicate/chitosan scaffolds for bone tissue engineering. Biomaterials Science, 7(4), 1565-1573.

Pham Minh, D., Galera Martínez, M., Nzihou, A., Sharrock, P. (2013). Thermal behavior of apatitic calcium phosphates synthesized from calcium carbonate and orthophosphoric acid or potassium dihydrogen orthophosphate. Journal of Thermal Analysis and Calorimetry, 112(3), 1145-1155.

Pillai, C. (2014). Recent advances in biodegradable polymeric materials. Materials Science and Technology, 30(5), 558-566.

Purohit, S.D., Bhaskar, R., Singh, H., Yadav, I., Gupta, M.K., Mishra, N.C. (2019). Development of a nanocomposite scaffold of gelatin–alginate–graphene oxide for bone tissue engineering. International Journal of Biological Macromolecules, 133, 592-602.

Qazi, R.A., Martin, K.J. (2008). Calcium, phosphorus, renal bone disease, and calciphylaxis. In Therapy in Nephrology & Hypertension (pp. 765-772): Elsevier.

Qi, Y., Chen, W., Liu, F., Liu, J., Zhang, T., Chen, W. (2019). Aggregation morphology is a key factor determining protein adsorption on graphene oxide and reduced graphene oxide nanomaterials. Environmental Science: Nano, 6(5), 1303-1309.

Qiao Y, Zhang W, Tian P, Meng F, Zhu H, Jiang X, Liu X, Chu PK.(2014) Stimulation of bone growth following zinc incorporation into biomaterials. Biomaterials, 35(25):6882-97.

Ren, D., Ruan, Q., Tao, J., Lo, J., Nutt, S., Moradian-Oldak, J. (2016). Amelogenin affects brushite crystal morphology and promotes its phase transformation to monetite. Crystal Growth & Design, 16(9), 4981-4990.

Ricci, R., Leite, N.C.S., da-Silva, N.S., Pacheco-Soares, C., Canevari, R.A., Marciano, FR., Webster, T.J., Lobo, A.O., (2017) Graphene oxide nanoribbons as nanomaterial for bone regeneration: Effects on cytotoxicity, gene expression and bactericidal effect. Materials Science and Engineering: C, 78:341-348.

Romieu, G., Garric, X., Munier, S., Vert, M., Boudeville, P. (2010). Calcium–strontium mixed phosphate as novel injectable and radio-opaque hydraulic cement. Acta Biomaterialia, 6(8), 3208-3215.

Roy, M., DeVoe, K., Bandyopadhyay, A., Bose, S. (2012). Mechanical property and *in vitro* biocompatibility of brushite cement modified by polyethylene glycol. Materials Science and Engineering: C, 32(8), 2145-2152.

Sabir, M.I., Xu, X., Li, L. (2009). A review on biodegradable polymeric materials for bone tissue engineering applications. Journal of Materials Science, 44(21), 5713-5724.

Sahin, E. (2018). Cement based materials, calcium phosphate bone cements., (pp.191-219): Intech Open.

Sahin, E., Çiftçioğlu, M. (2014). Monetite promoting effect of citric acid on brushite cement setting kinetics. Materials Research Innovations, 18(3), 138-145.

Saleh, A.T., Ling, L.S., Hussain, R. (2016). Injectable magnesium-doped brushite cement for controlled drug release application. Journal of Materials Science, 51(16), 7427-7439.

Samui, A., Sahu, S.K. (2020). Characterizations of MOFs for biomedical application. In Metal-Organic Frameworks for Biomedical Applications (pp. 277-295): Elsevier.

Schaad, P., Gramain, P., Gorce, F., Voegel, J. (1994). Dissolution of synthetic hydroxyapatite in the presence of lanthanum ions. Journal of the Chemical Society, Faraday Transactions, 90(22), 3405-3408.

Senamaud, N., Bernache-Assollant, D., Champion, E., Heughebaert, M., Rey, C. (1997). Calcination and sintering of hydroxyfluorapatite powders. Solid State Ionics, 101, 1357-1362.

Serodre, T., Oliveira, N.A., Miquita, D.R., Ferreira, M.P., Santos, A.P., Resende, V.G., Furtado, C.A. (2019). Surface silanization of graphene oxide under mild reaction conditions. Journal of the Brazilian Chemical Society, 30(11), 2488-2499.

Serret, A., Cabanas, M.V., Vallet-Regi, M. (2000). Stabilization of calcium oxyapatites with lanthanum (III)-created anionic vacancies. Chemistry of Materials, 12(12), 3836-3841.

Sharma, N., Sharma, V., Jain, Y., Kumari, M., Gupta, R., Sharma, S., Sachdev, K. (2017). Synthesis and characterization of graphene oxide (GO) and reduced graphene oxide (rGO) for gas sensing application. Macromolecular Symposia, 376 (1):1700006

Sheikh, Z., Zhang, Y.L., Tamimi, F., Barralet, J. (2017). Effect of processing conditions of dicalcium phosphate cements on graft resorption and bone formation. Acta Biomaterialia, 53, 526-535.

Shen, C., Wu, L., Chen, Y., Li, S., Rashid, S., Gao, Y., Liu, J. (2016). Efficient removal of fluoride from drinking water using well-dispersed monetite bundles inlaid in chitosan beads. Chemical Engineering Journal, 303, 391-400.

Shin-Ike, M., Tsutsui, J., Tanaka, A., Murayama, S., Fujita, A. (1989). Attempts to improve the strength of sintered lanthanum-containing hydroxyapatites. Journal of Osaka Dental University, 52, 854-861.

Smolen, D., Chudoba, T., Malka, I., Kedzierska, A., Lojkowski, W., Swieszkowski, W., Kurzydlowski K.J. , Kolodziejczyk-Mierzynska M., Lewandowska-Szumiel, M. (2013). Highly biocompatible, nanocrystalline hydroxyapatite synthesized in a solvothermal process driven by high energy density microwave radiation. International Journal of Nanomedicine, 8, 653.

Song, R., Murphy, M., Li, C., Ting, K., Soo, C., Zheng, Z. (2018). Current development of biodegradable polymeric materials for biomedical applications. Drug design, Development and Therapy, 12, 3117.

Stulajterova, R., Medvecky, L., Giretova, M., Sopcak, T., Kovalcikova, A. (2017). Effect of bioglass 45S5 addition on properties, microstructure and cellular response of tetracalcium phosphate/monetite cements. Materials Characterization, 126, 104-115.

Subramaniam, A., Sethuraman, S. (2014). Biomedical applications of nondegradable polymers. In Natural and Synthetic Biomedical Polymers (pp. 301-308): Elsevier.

Suchanek, W., Yoshimura, M. (1998). Processing and properties of hydroxyapatite-based biomaterials for use as hard tissue replacement implants. Journal of Materials Research, 13(1), 94-117.

Švecová, M., Bartůněk, V. (2018). Facile synthesis of monetite nanoparticles from basic raw materials. Ceramics International, 44(13), 16079-16082.

Sych, E., Pinchuk, N., Tovstonog, A., Golovkova, M., Kotlyarchuk, A., Evich, Y.I., Skorokhod, V., Savkova, I. (2014). The structure and properties of calcium phosphate ceramics produced from monetite and biogenic hydroxyapatite. Powder Metallurgy and Metal Ceramics, 53(7-8), 423-430.

Sych, O.Y., Pinchuk, N., Pasichnyi, V., Ostapenko, S., Kotlyarchuk, A., Tovstonog, G., Yevich, Y.I. (2015). Structure and properties of ceramics based on

monetite and nanodispersed silica. Powder Metallurgy and Metal Ceramics, 54(3-4), 175-182.

Taha, A., Akram, M., Jawad, Z., Alshemary, A.Z., Hussain, R. (2017). Strontium doped injectable bone cement for potential drug delivery applications. Materials Science and Engineering: C, 80, 93-101.

Tamimi, F., Kumarasami, B., Doillon, C., Gbureck, U., Le Nihouannen, D., Cabarcos, E.L., Barralet, J. E. (2008a). Brushite–collagen composites for bone regeneration. Acta Biomaterialia, 4(5), 1315-1321.

Tamimi, F., Le Nihouannen, D., Eimar, H., Sheikh, Z., Komarova, S., Barralet, J. (2012a). The effect of autoclaving on the physical and biological properties of dicalcium phosphate dihydrate bioceramics: brushite vs. monetite. Acta Biomaterialia, 8(8), 3161-3169.

Tamimi, F., Sheikh, Z., Barralet, J. (2012b). Dicalcium phosphate cements: Brushite and monetite. Acta Biomaterialia, 8(2), 474-487.

Tamimi, F., Torres, J., Al-Abedalla, K., Lopez-Cabarcos, E., Alkhraisat, M.H., Bassett, D.C., Gbureck, U., Barralet, J.E., (2014). Osseointegration of dental implants in 3D-printed synthetic onlay grafts customized according to bone metabolic activity in recipient site. Biomaterials, 35(21):5436-45.

Tamimi, F., Torres, J., Bassett, D., Barralet, J., Cabarcos, E.L. (2010). Resorption of monetite granules in alveolar bone defects in human patients. Biomaterials, 31(10), 2762-2769.

Tamimi, F., Torres, J., Kathan, C., Baca, R., Clemente, C., Blanco, L., Cabarcos, E. L. (2008b). Bone regeneration in rabbit calvaria with novel monetite granules. Journal of Biomedical Materials Research Part A, 87(4), 980-985.

Tamimi, F.M., Torres, J., Tresguerres, I., Clemente, C., López-Cabarcos, E., Blanco, L.J., (2006) Bone augmentation in rabbit calvariae: comparative study between Bio-Oss and a novel beta-TCP/DCPD granulate. Journal of Clinical Periodontology, 33(12), 922-928.

Tas, A.C. (2008). Preparation of porous apatite granules from calcium phosphate cement. Journal of Materials Science: Materials in Medicine, 19(5), 2231-2239.

Tas, A.C. (2009). Monetite ($CaHPO_4$) synthesis in ethanol at room temperature. Journal of the American Ceramic Society, 92(12), 2907-2912.

Tatavarty, R., Ding, H., Lu, G., Taylor, R.J., Bi, X., (2014). Synergistic acceleration in the osteogenesis of human mesenchymal stem cells by graphene oxide–calcium phosphate nanocomposites, Chemical Communications, 50(62), 8484-8487.

Theiss, F., Apelt, D., Brand, B., Kutter, A., Zlinszky, K., Bohner, M., Matter, S., Frei, C., Auer, J.A., Von Rechenberg, B., (2005). Biocompatibility and resorption of a brushite calcium phosphate cement. Biomaterials. 26(21), 4383-94.

Tokuoka, Y., Ito, Y., Kitahara, K., Niikura, Y., Ochiai, A., Kawashima, N. (2006). Preparation of monetite ($CaHPO_4$) with hexagonally packed mesoporous structure by a sol–gel method using cationic surfactant aggregates as a template. Chemistry Letters, 35(11), 1220-1221.

Torres, J., Tamimi, I., Cabrejos-Azama, J., Tresguerres, I., Alkhraisat, M., López-Cabarcos, E., Hernández, G., Tamimi, F., (2015). Monetite granules versus particulate autologous bone in bone regeneration. Annals of Anatomy, 200, 126-33.

Tortet, L., Gavarri, J., Nihoul, G., Dianoux, A. (1997). Study of protonic mobility in $CaHPO_4 \cdot 2H_2O$ (brushite) and $CaHPO_4$ (monetite) by infrared spectroscopy and neutron scattering. Journal of Solid State Chemistry, 132(1), 6-16.

Toshima, T., Hamai, R., Tafu, M., Takemura, Y., Fujita, S., Chohji, T., Tanda, S., Li, S., Qin, G. W. (2014). Morphology control of brushite prepared by aqueous solution synthesis. Journal of Asian Ceramic Societies, 2(1), 52-56.

Touny, A., Saleh, M. (2018). Fabrication of biphasic calcium phosphates nanowhiskers by reflux approach. Ceramics International, 44(14), 16543-16547.

Touny, A.H., Bhaduri, S.B. (2010). A reactive electrospinning approach for nanoporous PLA/monetite nanocomposite fibers. Materials Science and Engineering: C, 30(8), 1304-1312.

Tsukimura, N., Yamada, M., Aita, H., Hori, N., Yoshino, F., Chang Lee, M., Kimoto, K., Jewett, A., Ogawa, T., (2009). N-acetyl cysteine (NAC)-mediated detoxification and functionalization of poly(methyl methacrylate) bone cement. Biomaterials, 30(20):3378-89.

Urrutia, J., Bono, C.M., Mery, P., Rojas, C. (2008). Early histologic changes following polymethylmethacrylate injection (vertebroplasty) in rabbit lumbar vertebrae. Spine, 33(8), 877-882.

Vahabzadeh, S., Bandyopadhyay, A., Bose, S., Mandal, R., Nandi, S.K. (2015a). IGF-loaded silicon and zinc doped brushite cement: physico-mechanical characterization and in vivo osteogenesis evaluation. Integrative Biology, 7(12), 1561-1573.

Vahabzadeh, S., Roy, M., Bose, S. (2015b). Effects of silicon on osteoclast cell mediated degradation, in vivo osteogenesis and vasculogenesis of brushite cement. Journal of Materials Chemistry B, 3(46), 8973-8982.

Vedakumari, S.W., Jayalakshmi, R., Sanjayan, C., Jayavardhini, B., Arya, K., Murugesan, R. (2020). Fabrication of microcomposites based on silk sericin and monetite for bone tissue engineering. Polymer Bulletin, 77(1), 475-481.

Von Rosenberg, S., Wehr, U. (2012). Lanthanum salts improve bone formation in a small animal model of post-menopausal osteoporosis. Journal of Animal Physiology and Animal Nutrition, 96(5), 885-894.

Wang, J., Chen, Y., Zhu, X., Yuan, T., Tan, Y., Fan, Y., Zhang, X. (2014). Effect of phase composition on protein adsorption and osteoinduction of porous calcium phosphate ceramics in mice. Journal of Biomedical Materials Research Part A, 102(12), 4234-4243.

Wang, S., Zhang, S., Wang, Y., Sun, X., Sun, K. (2017). Reduced graphene oxide/carbon nanotubes reinforced calcium phosphate cement. Ceramics International, 43(16), 13083-13088.

Wang, X., Ye, J., Wang, Y., Chen, L. (2007). Reinforcement of calcium phosphate cement by bio-mineralized carbon nanotube. Journal of the American Ceramic Society, 90(3), 962-964.

Waugh, W. (2012). John Charnley: the man and the hip: Springer Science & Business Media.

Wei, K., Lai, C., Wang, Y. (2007). Formation of monetite nanoparticles and nanofibers in reverse micelles. Journal of Materials Science, 42(14), 5340-5346.

Wijesinghe, W.P.S.L., Mantilaka, P., Rajapakse, R., Peiris, T.A.N., Premachandra, T., Herath, H., Raja, R., Wijayantha, K., Pitawala, H.M.T.G. (2018). Preparation and characterization of mesoporous hydroxyapatite with non-cytotoxicity and heavy metal adsorption capacity. New Journal of Chemistry, 42(12), 10271-10278.

Willbold, E., Gu, X., Albert, D., Kalla, K., Bobe, K., Brauneis, M.,Tillmann, W. (2015). Effect of the addition of low rare earth elements (lanthanum, neodymium, cerium) on the biodegradation and biocompatibility of magnesium. Acta Biomaterialia, 11, 554-562.

Xu, C., Wang, X., Zhu, J. (2008). Graphene−metal particle nanocomposites. The Journal of Physical Chemistry C, 112(50), 19841-19845.

Xu, H.H., Simon Jr, C.G. (2004). Self-hardening calcium phosphate cement–mesh composite: Reinforcement, macropores, and cell response. Journal of Biomedical Materials Research Part A, 69(2), 267-278.

Xu, H.H., Weir, M.D., Burguera, E.F., Fraser, A.M. (2006). Injectable and macroporous calcium phosphate cement scaffold. Biomaterials, 27(24), 4279-4287.

Xu, N., Ye, X., Wei, D., Zhong, J., Chen, Y., Xu, G., He, D. (2014). 3D artificial bones for bone repair prepared by computed tomography-guided fused deposition modeling for bone repair. ACS Applied Materials & Interfaces, 6(17), 14952-14963.

Yoshikawa, H., Myoui, A. (2005). Bone tissue engineering with porous hydroxyapatite ceramics. Journal of Artificial Organs, 8(3), 131-136.

Yousefi, A.-M., Oudadesse, H., Akbarzadeh, R., Wers, E., Lucas-Girot, A. (2014). Physical and biological characteristics of nanohydroxyapatite and bioactive glasses used for bone tissue engineering. Nanotechnology Reviews, 3(6), 527-552.

Yu, C., Gong, J., Yin, F.-l., Huang, J., Zhang, T.-l., Wang, K. (2017). Influences of LaCl$_3$ on the mineral phase transformation during osteoblast mineralization *in vitro*. Journal of Environmental Sciences, 51, 88-96.

Yu, Q., Chen, H. (2015). Interaction of switchable biomaterials surfaces with proteins. In Switchable and Responsive Surfaces and Materials for Biomedical Applications (pp. 167-188): Elsevier.

Zeng, Y., Pei, X., Yang, S., Qin, H., Cai, H., Hu, S., Sui, L., Wan, Q., Wang, J., (2015). Graphene oxide/hydroxyapatite composite coatings fabricated by electrochemical deposition. Surface and Coatings Technology, 286, 72-79.

Zhang, J., Xu, S., Wang, K., Yu, S. (2003). Effects of the rare earth ions on bone resorbing function of rabbit mature osteoclasts i*n vitro*. Chinese Science Bulletin, 48(20), 2170-2175.

Zhou, H., Luchini, T.J., Boroujeni, N.M., Agarwal, A.K., Goel, V.K., Bhaduri, S.B. (2015). Development of nanosilica bonded monetite cement from egg shells. Materials Science and Engineering: C, 50, 45-51.

Zhou, N., Meng, N., Ma, Y., Liao, X., Zhang, J., Li, L., Shen, J. (2009). Evaluation of antithrombogenic and antibacterial activities of a graphite oxide/heparin–benzalkonium chloride composite. Carbon, 47(5), 1343-1350.

CURRICULUM VITAE

**PERSONAL INFORMATION**

Surname, Name: Motameni, Ali
Nationality: Turkish (TC)
Date and Place of Birth: 26 January1985, Tabriz
Marital Status: Married
 email: ali.motameni@raymaklab.com

**EDUCATION**

| Degree | Institution | Year of Graduation |
|---|---|---|
| MS | METU Metallurgical & Materials Engineering | 2011 |
| BS | METU Metallurgical & Materials Engineering | 2014 |
| High School | Pajuhesh, Tabriz | 2003 |

**WORK EXPERIENCE**

| Year | Place | Enrollment |
|---|---|---|
| 2011-Present | METU Metallurgical & Materials Engineering | Testing Engineer |

**FOREIGN LANGUAGES**

Advanced English

**PUBLICATIONS**

1. Alipour Ghasabi, A., Motameni, A. & Kadioglu, S. ''Fatigue Precracking Time Estimates for Three-Point Bending Specimens'', J Fail. Anal. and Preven. 19**,** 1275–1285 (2019)

2. Motameni, A., Dalgic, A.D., Alshemary, A.Z., Keskin, D., Evis, Z. ''Structural and biological analysis of mesoporous lanthanum doped $\beta$TCP for potential use as bone graft material'', Materials Today Communications, 101151(2020).

3. Turhan, Ş.Ö., Motameni, A. & Gürbüz, R. Fatigue Behavior of Welded API 5L X70 Steel Used in Pipelines. J Fail. Anal. and Preven. 20, 1554–1567 (2020).

4. Motameni, A., Alshemary, A.Z., Dalgic, A.D., Keskin, D., Evis, Z., ''Lanthanum doped dicalcium phosphate bone cements for potential use as filler for bone defects'', Materials Today Communications,Volume 26, 101774, 2352-4928 (2021)

5. Motameni, A., Alshemary, A.Z., Evis, Z., ''A review of synthesis methods, properties and use of monetite cements as filler for bone defects'', Ceramics International, Volume 47, Issue 10, Part A, (2021)

6. Alshemary, A.Z, Bilgin, S,. Işık, G., Motameni, A., Tezcaner, A., Evis, Z., ''Biomechanical Evaluation of an Injectable Alginate / Dicalcium Phosphate Cement Composites for Bone Tissue Engineering'', J Mech Behav Biomed Mater (2021)